The Dissertation Committee for Paula Sharon Kulis Certifies that this is the approved version of the following dissertation:

Modeling a Gravity Current in a Shallow Fluid System

Committee:

Ben R. Hodges, Supervisor

David Maidment

Lynn Katz

Danny Reible

Venkat Raman

Modeling a Gravity Current in a Shallow Fluid System

by

Paula Sharon Kulis, B.S.; M.S.

Dissertation

Presented to the Faculty of the Graduate School of

The University of Texas at Austin

in Partial Fulfillment

of the Requirements

for the Degree of

Doctor of Philosophy

The University of Texas at Austin

December 2011

Dedication

This dissertation is dedicated to my husband, Brian Kulis. I love you.

Acknowledgements

There are too many people who have helped me with this endeavor, both professionally and personally. First, thanks to my advisor, Ben Hodges, for sticking with me even when I left the state – I can't tell you how much I appreciate your patience. And of course, thanks to my committee: David Maidment, Lynn Katz, Danny Reible and Venkat Raman. Ernest To, Shahidul Islam, Dharhas Pothina, Cedric David, Omer Kose, Jordan Furnans and Bridget Wadzuk were all wonderful sources of ideas and feedback. The WATERS Testbed members have all contributed to insights, feedback, and ideas introduced or built on in this dissertation. Lauren Nance and Andrew Brouwer both contributed to the work discussed here as well. Camp, Dresser & McKee has also funded a large portion of this research, and the staff in the Walnut Creek office has been a source of support in the last couple of years.

Shipeng Fu, my lab mate and close friend, has really been a source of inspiration through this whole process. Lily Chen's friendship has been invaluable to me, and I will cherish it always. Becky Teasley has been a support and an inspiration. We all held each other together in graduate school, and I am very thankful for such wonderful friends. My family's support has been invaluable. My parents have been inspiring me for my whole life. My mom, Anne Deardon, has taught me to always find a way to do what I love, and to be passionate. My dad, Ken Deardon, has been a rock of support and love. My Aunt, Jean Olson, has provided unwavering support as I have tried to finish this degree remotely, and I can never thank her enough.

It goes without saying that my husband Brian has been more than a rock; he has been a dishwasher, housecleaner, grocery shopper, overall care taker, and reminder to

enjoy life, at least a little bit, even when I am under stress. It says something about a relationship when going through a stressful time just brings you closer. And finishing a PhD, remotely, certainly qualifies!

Modeling a Gravity Current in a Shallow Fluid System

Paula Sharon Kulis, Ph. D.

The University of Texas at Austin, 2011

Supervisor: Ben R. Hodges

Corpus Christi Bay in Texas is a wind driven system, and under most conditions winds over the bay mix the water column vertically. However, seasonal, episodic, bottom-water hypoxia has been observed in the bay in conjunction with vertical salinity stratification. This stratification may be caused by dense gravity currents entering the bay.

Understanding and modeling the mechanisms that result in stratification in Corpus Christi Bay may help predict hypoxia, and for this reason that is the focus of this dissertation. An evaluation of existing gravity current modeling techniques shows that most currently available models are designed to capture *either* phenomena local to a gravity current, such as gravity current entrainment and spreading, *or* larger scale phenomena such as wind mixing and large-scale circulation, but not both.

Because gravity current mixing in Corpus Christi Bay is enhanced by wind-induced turbulence, both local gravity current physics and wind mixing effects are critical elements governing gravity current propagation in Corpus Christi Bay. As existing models do not represent gravity current entrainment and wind mixing together, this dissertation develops a coupled model system that accounts *explicitly* for turbulent wind mixing of a bottom-boundary layer, in addition to representing other local features of dense gravity current propagation such as entrainment and spreading. The coupled model

system consists of a 2D depth-averaged hydrodynamic model that calculates gravity current mixing and spreading, coupled with a 3D hydrodynamic model whose domain includes a lighter ambient fluid surrounding the gravity current. The coupled models have flexible boundary conditions that allow fluid exchange to represent mixing from both gravity current entrainment and wind mixing.

The coupled model system's development, verification and application in Corpus Christi Bay advances understanding of gravity current mechanisms, and contributes to our scientific understanding of hypoxia in Corpus Christi Bay. This modeling technique has the flexibility to be applied to other density-stratified systems that are shallow and potentially wind-driven, such as shallow desalination brine disposal sites.

Table of Contents

List of Tables

List of Figures

Chapter 1: Introduction

1.1 Motivational Setting: Hypoxia, Gravity Currents and Corpus Christi Bay

Density influences fluid circulation in almost all environmental systems. The sinking of cold water in the North Atlantic Ocean drives global ocean circulation. Coastal breezes result from colder air over the ocean rushing in during the day to displace lighter, warmer air over land. These are examples of gravity currents, or dense fluid flows along the bottom boundary of a larger, less dense fluid system. Gravity currents, also called dense underflows, are found on various scales throughout natural and engineered environments: in the atmosphere, oceans, lakes, industrial processes, and even in drafty houses. The dynamics of gravity currents spreading and mixing in the environment can impact water quality by affecting the physical transport of nutrients, pollutants and microorganisms.

In the case of Corpus Christi Bay in Texas (Figure 1.1), gravity currents may be controlling the transport and fate of dissolved oxygen. The vertical and horizontal mixing and spreading processes that characterize gravity current transport in a system such as Corpus Christi Bay are therefore of scientific interest. Low levels of dissolved oxygen (DO), or hypoxia, are frequently observed in the bottom waters of Corpus Christi Bay. This hypoxia occurs primarily in the mid-to-late summer, and has a negative impact on sedimentary infauna (Ritter and Montagna 1999; Montagna and Froeschke 2009, Nelson and Montagna 2009). The hypoxia is also statistically related to water column stratification (Ritter and Montagna 1999; Hodges et al 2011) that may originate from a dense gravity current; the possibility of a causal relationship between stratification and hypoxia motivates us to understand the mechanisms of stratification in fluid systems like Corpus Christi Bay.

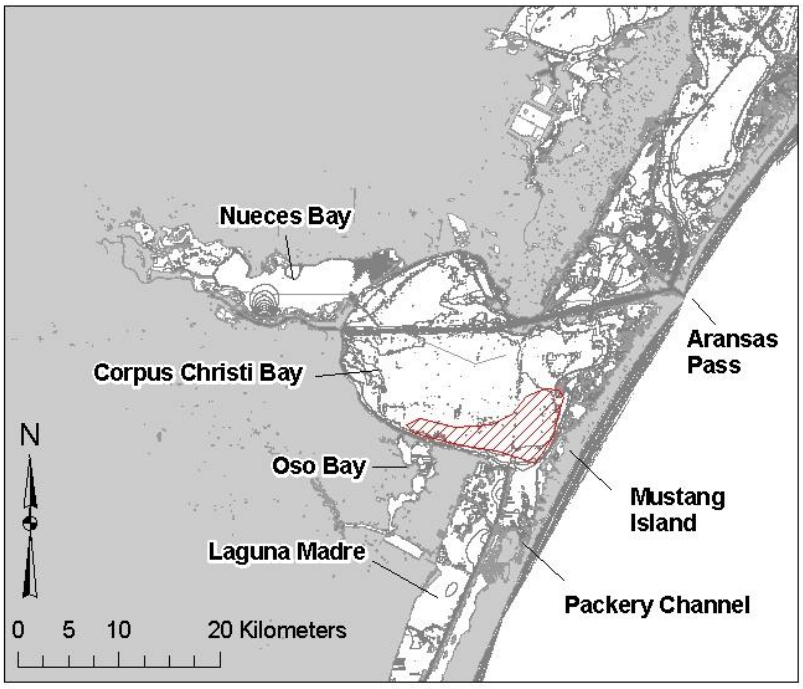

Figure 1.1: Corpus Christi Bay. The red hatched region indicates the extent of hypoxia approximated from Nelson and Montagna (2009). Grey lines are 1 m contours.

Corpus Christi Bay is located along the coast of the Gulf of Mexico (the Gulf Coast). Mustang Island limits exchanges between Corpus Christi Bay and the Gulf to a 400 m wide ship channel and the Packery Channel in Laguna Madre. Due to Corpus Christi Bay's isolation from the Gulf and shallow depth (mean depth is ~3.5 m), high regional summertime evaporation rates (10 cm/month, Ward 1997) can result in inverse estuarine conditions, where salinity concentrations are higher in the bay than in the Gulf. Typical summertime salinities in Corpus Christi Bay are approximately 35 practical salinity units (psu), compared with a typical oceanographic salinity of 33 psu.

Oso Bay and Laguna Madre, two shallow side embayments with mean depths below 1 m, connect to the southern side of Corpus Christi Bay (Figure 1.1). Due to the

side bays' shallow bathymetry and isolation from the Gulf, both Oso Bay and Laguna Madre typically have salinities upwards of 50 psu in the summertime.

When wind or currents introduce dense hypersaline water from the shallow side embayments Laguna Madre or Oso Bay into Corpus Christi Bay, the heavy water sinks below the lighter ambient Corpus Christi Bay water in the form of a gravity current (To and Maidment 2009, Hodges et al 2011). If the wind cannot immediately mix the water column, the heavy water stays on the bottom of the bay until large-scale circulations move it away or mix it throughout the water column. As the heavy water stays on the bottom of the bay, the DO in the water is consumed by the benthos as a sediment oxygen demand (SOD). Without DO replenishment, hypoxia may result.

Figure 1.2 shows the relationship between DO depletion and density stratification. The regions where bottom-water hypoxia has been documented in Corpus Christi Bay are just north of Laguna Madre and Oso Bay (Figure 1.1), and field measurements show vertical salinity stratification in these areas that is consistent with a dense underflow exiting the side bays (Hodges et al 2011, Hodges et al 2006, Minsker et al 2007).

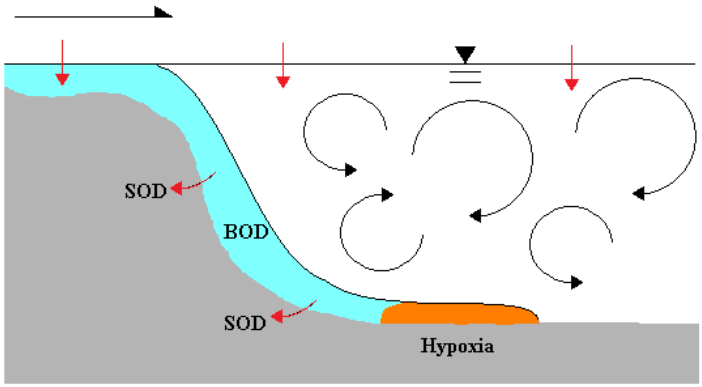

Figure 1.2 Schematic of the relationship between dissolved oxygen and density stratification. As dense water (blue) sinks and remains isolated from atmospheric DO replenishment, oxygen is depleted by local BOD and SOD. Eventually the water may become hypoxic (orange).

Modeling Gravity Currents in Corpus Christi Bay

Gravity currents in water bodies are commonly observed in the environment at a range of scales, from driving circulation in the Atlantic Ocean Basin, to salt wedges in estuaries, to episodic currents resulting from differential heating and cooling in wetlands and lakes. Gravity currents can also be on varied scales relative to the larger fluid system in which they are flowing; in a shallow wetland, gravity currents driven by differential heating and cooling can drive the large-scale circulation in the wetland (Oldham and Sturman 2001). Gravity currents can also play more minor roles in fluid systems; for instance, turbidity currents (sediment-laden gravity currents) flowing down continental shelfs do not drive regional ocean circulation.

Because gravity currents occur on such varied scales relative to the fluid systems containing them, they are difficult to model. The sharp horizontal and vertical density gradients are easily diffused by coarse grid resolution (Winton et al 1998, Kulis and Hodges 2005, 2006, Danabasoglu et al 2010, Legg et al 2009, e.g.). Resolving vertical density gradients in 3D models that are also designed to represent larger, basin-scale circulation can be computationally expensive. Because the scales of gravity currents and ambient water bodies can be different, removing the gravity current into a separate, coupled model is a technique that can be useful for estimating gravity current fate and transport in the environment (Killworth and Edwards 1999, Dallimore et al 2001, Holland 2010).

Corpus Christi Bay is shallow enough that it is typically characterized as a well-mixed, one-layer system with little to no stratification (Matsumoto et al 1997, Ward 1997, Islam et al 2010). Where gravity currents have been observed, the density profile vertically above the gravity current is uniform (Hodges et al 2011, Hodges and Furnans 2007, Hodges et al 2006). This characterization suggests that wind mixing extends

throughout the depth of the Bay, exposing any gravity currents that are flowing along the bed to wind-induced turbulence.

Most aqueous field-scale gravity currents that have been studied have been flowing in deep water bodies, so that the gravity current has not been exposed to the turbulence present in the wind-mixed layer (Ilicak et al 2011, Dallimore et al 2001, Danabasoglu et al 2010, e.g.). In these systems, ambient turbulence is generally low compared with the turbulence generated by the gravity current itself, and is often neglected (bo Pedersen 1986). However, as is discussed further in Chapter 2, in Corpus Christi Bay we find that wind mixing and ambient turbulence cannot be considered negligible.

Research Questions

Research questions that result from examination of hypoxia in Corpus Christi Bay and existing modeling techniques for dense bottom plumes, that motivate this dissertation, include:

1. **What are the physical processes governing vertical mixing and plume spreading in Corpus Christi Bay?** Field data and analysis indicates that although underflow entrainment plays a significant role in mixing the underflow, plumes tend to persist on the order of days in Corpus Christi Bay, which is consistent with time scales estimated for wind mixing. A numerical model that includes representation of both entrainment and wind mixing would both confirm the role of entrainment and wind mixing, and it would also provide more quantified estimates of mixing timescales.
2. **How can the mass exchange and displacement associated with a gravity current in a shallow fluid system be represented in a numerical model?**

Existing numerical models are either overly diffusive, or are developed for systems with different dominating processes than those present in shallow bays. Developing a numerical model that reflects the physical processes present in shallow bays will improve analysis of gravity current fate and transport in Corpus Christi Bay.

This dissertation develops a numerical model that captures gravity current mixing and spreading, and also represents gravity current interaction with basin-scale circulation. The following sections outline specific research objectives, methodologies, and research benefits and contributions.

1.2 RESEARCH OBJECTIVES

This dissertation's goal is to develop a methodology for quantifying wind mixing effects on gravity current spreading in shallow water. This goal is accomplished via the following objectives:

Objective 1: Develop a methodology capturing dense underflow spreading within a 3D hydrodynamic model. In the literature, spreading processes for environmental-scale gravity currents are largely examined for systems with sloping or channel-like conditions in which the underflow has a clear path, rather than systems such as Corpus Christi Bay that are relatively flat and experience lateral spreading (Iliak et al 2011, Ozgokmen et al 2003, Dallimore et al 2001, e.g.). This dissertation examines field-scale lateral spreading and provides an estimate of the spatial extent for the plumes observed in Corpus Christi Bay.

Objective 2: Develop a set of numerical algorithms that represent dense underflow mixing in shallow fluid systems. Existing gravity current studies quantify entrainment of ambient fluid into a gravity current due to turbulence existing within the underflow (Ellison and Turner 1959, bo Pedersen 1986, Dallimore et al 2001, e.g.), but do not quantify entrainment of underflow fluid into an ambient fluid. Models of wind-mixed layer deepening provide insights into entrainment of dense fluid into a lighter region above (Hodges et al 2000, Spigel et al 1986, Nielsen et al 2005, e.g.), and by combining these entrainment laws we can obtain an accurate model of a gravity current in the presence of ambient turbulence.

Objective 3: Demonstrate model performance through model application on a gravity current entering Corpus Christi Bay from Oso Bay. Hypoxia results in Corpus Christi Bay if the time scale associated with DO depletion is shorter than the time scale for disintegration of the stratification isolating DO demands from DO sources (Hodges et al 2011). Relating gravity current fate and transport to hypoxia formation helps quantify the impacts that mixing and spreading have on the entire bay system.

Characterization of plume spreading, plume mixing and conditions that may lead to hypoxia in Corpus Christi Bay may guide future field studies in examining the physical and biological processes associated with hypoxia in the bay, and may potentially be used to inform desalination brine studies in the future.

1.3 METHODS

The objectives are accomplished through model development that is loosely guided by scales observed in field studies (Hodges et al 2006, 2011). Field data provides a mechanism for comparing mixing and spreading scales with DO demands, and modeling studies allow a spatially and temporally comprehensive examination of fluid processes under various conditions.

To quantify both spreading and mixing, we develop a modeling system that captures the physics affecting shallow bays containing gravity currents. The sharp gradients associated with thin gravity currents are difficult to resolve in a 3D hydrodynamic model that is designed to compute basin-scale currents (Danabasoglu et al 2010). Mixing artificially weakens gradients due to poor grid resolution and inappropriate turbulence representation. Solutions that have been developed in the literature maintain the density gradient, but do not model mixing in a manner that reflects wind mixing (Beckman and Doscher 1997, Dallimore et al 2003, Holland 2011, e.g.).

This dissertation develops a Coupled Model System (CMS) that is designed to maintain the sharp gradient between a gravity current and an ambient fluid; the CMS models mixing based on the appropriate physical processes. Like existing gravity current modeling systems in the literature (Dallimore et al 2001, Holland 2011, Killworth and Edwards 1999, e.g.), the CMS consists of two separate models: a 3D model similar to a traditional 3D representation of a fluid system, and a depth-integrated 2D model representing the dense gravity current. In this way, the underflow is removed from the 3D model's domain. This configuration allows parameterization of fluid exchanges between the two models, and also allows the gravity current to spread without being diffused with ambient fluid. The CMS differs from existing gravity current models in its treatment of both mixing and the ambient model's domain delineation; mixing into and

out of the underflow is accounted for in the CMS, allowing wind mixing to erode the underflow. The CMS also allows the underflow to displace ambient fluid even though the fluids are contained in separate models; the underflow defines the ambient model's bottom boundary at every timestep. The separation of the model domains is depicted in Figure 1.3.

Figure 1.3: CMS model domains. Denser fluid is represented with a darker blue. The underflow model domain (a) is separated from the 3D model representing the rest of the basin (b).

Both 2D and 3D CMS models are based on the ELCIRC code (Zhang et al 2004); because the models share the same basic grid, governing equations and solution method, model coupling is arguably simpler and more robust than a creating a separate underflow model. This method for model coupling could be applied to virtually any 3D hydrodynamic model. The method could also be used to develop coupled systems containing more than 2 independent models.

1.4 CONTRIBUTION TO SCIENCE AND ENGINEERING

The contributions to science and engineering from this dissertation include:

1. A conceptual model describing vertical gravity current mixing in the presence of significant ambient turbulence. Existing gravity current conceptual models do not include ambient turbulence and resulting underflow mixing out into the ambient

fluid. The inclusion of ambient turbulence in a conceptual underflow model is a contribution to gravity current conceptual representation.

2. A new numerical method for developing coupled model systems. The inclusion is mass balance and displacement of ambient fluid on a field-scale model application is unique, and improves model representation of physical processes in shallow water bodies.
3. Developing an underflow model as a 2D representation of a 3D model is a technique that facilitates numerical issues associated with model grid coupling, and also sets the foundation for coupling multiple 2D layered models together. This technique can be applied to other numerical models.

1.5 RESEARCH BENEFITS

Three uses for the model developed in this dissertation are of particular interest: 1) the model developed to capture gravity current circulation can be used to understand hypoxia in the Bay and to guide future field work, 2) the model can be used to estimate fate of shallow desalination brine discharges, and 3) the model development documents a framework for model coupling that is useful for many modeling applications.

1.5.1 Potential to Inform other Studies on CCB

There has been much progress on collecting, disseminating and analyzing data in Corpus Christi Bay in the last several years. Extensive observational data monitoring systems have been developed (Islam et al 2011a, b). Field collection has also been conducted to enable studies to examine the statistical relationship between hypoxia and salinity, temperature, and wind (Coopersmith et al 2011), and also to quantify the impacts

of low dissolved oxygen in Corpus Christi Bay on benthic community biodiversity and general health (Montagna and Froeschke 2009). Data shows trends of increasing free surface temperature in the Bay, along with decreasing benthic dissolved oxygen (Applebaum and Montagna 2005), and lowered biodiversity in areas frequently exposed to hypoxic conditions (Montagna and Froeschke 2009).

This dissertation is motivated by the possibility of aiding field data collection systems, which in turn will improve data analysis and our understanding of the phenomena in Corpus Christi Bay. Gaining insight to the relative scales of underflow transport, mixing and DO depletion can improve data collection systems, and potentially help guide planning-level decisions.

1.5.2 Desalination Brine Mixing

As desalination becomes more common practice in arid regions of the world, disposal of dense brine in larger water bodies and coastal areas is becoming a more common practice. The Texas 2007 state water plan's water management strategies include up to 313,000 AFY of desalinated water by 2060, present in 8 out of the state's 16 planning regions. For example, the Laguna Madre Water District is pursuing construction alternatives for a 1 million gallon per day (mgd) desalination plant that would take water from the Gulf of Mexico (TWDB 2007).

Studies suggest that brine discharges close to the coast may not fully mix with ambient water, creating water quality concerns (Purnama and Al-Barwani 2006, Fernàndez-Torquemada et al 2005, Voutchkov 2011, e.g.). In some cases, these concerns include dissolved oxygen deficiencies similar to those observed in Corpus Christi Bay (Voutchkov, 2011, Peters and Pinto, 2008, e.g.). Desalination plants with ocean outfalls exist around the world, for example in Singapore, Australia, the United States, Spain, and

various countries in the Middle East (Voutchkov 2011). Studying the environmental impacts of dense brine disposal requires tools that accurately capture features of gravity currents as they interact with larger scale currents and ambient turbulence.

1.5.3 Model Coupling Methodology

This dissertation presents a methodology that is simple and robust, and could easily be exported to other models of stratified fluid systems. The underflow model uses a modified version of the 3D ELCIRC code, which simplifies model coupling and develops a framework for multiple fluid layers modeled as separate, coupled models.

1.6 DISSERTATION STRUCTURE

Chapter 2 provides background information documenting: mechanisms for bottom water hypoxia, Corpus Christi Bay characteristics, a Corpus Christi Bay field study conducted in August 2005, existing modeling techniques for dense underflows, and mixing parameterizations developed in the literature. Chapter 3 presents the conceptual model of the CMS, and algorithms associated with the transport, spreading and plunging of an underflow, as well as the displacement of ambient fluid which results from gravity current spreading. Chapter 4 presents the mixing algorithms associated both with entrainment into the underflow, and wind-induced mixing into the ambient fluid. Chapter 5 presents a preliminary application of the underflow model to the bathymetry of Corpus Christi Bay. Gravity current spreading, and eventual mixing in the presence of a moderate wind, is examined in comparison with 3D ELCIRC. Chapter 6 discusses conclusions and future work.

Chapter 2: Background

2.1 INTRODUCTION

This chapter lays the foundation for the model developed in this dissertation. First the need for the model is established by reviewing mechanisms for hypoxia development in general and in Corpus Christi Bay. A summary of a field data collection exercise provides insight into the relationship between hypoxia and gravity currents in Corpus Christi Bay. Existing techniques used in the literature to capture gravity currents in numerical models are discussed, along with limitations and advantages for applying them to Corpus Christi Bay. The following chapters draw on the modeling techniques and physics discussed in this chapter to develop a unique model that is tailored to the physics governing vertical mixing of gravity currents in shallow, wind-driven systems.

2.2 HYPOXIA MECHANISMS

2.2.1 Hypoxia in the Environment

Typical water body sinks and sources of dissolved oxygen (DO) are depicted in Figure 2.1 for an unstratified system. Sources include atmospheric replenishment and in situ primary production, while sinks include water column biological oxygen demand (BOD) and sediment oxygen demand (SOD). Hypoxia occurs in water bodies when DO sinks exceed DO sources for a sufficient time interval. This phenomenon can occur due to either natural or anthropogenic influences. In lakes, hypoxia is commonly a result of eutrophication, a process that is accelerated by nitrogen and phosphorus loading. Nutrient loading increases primary production, which results in increased biomass in the waterbody. Biomass decay increases BOD such that demand may exceed supply for

extended periods, resulting in hypoxia (Master, 1997). A typical example of eutrophication is seen in small ponds that are often found adjacent to sporting fields. These ponds often have green surface films, which is an indication of a eutrophic water body.

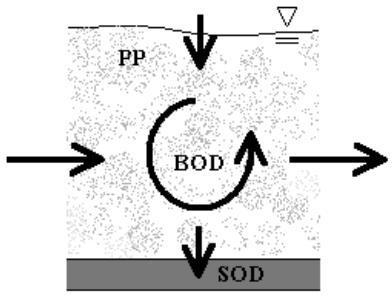

Figure 2.1: Schematic of DO transport in an unstratified water column. Arrows represent DO fluxes. Sources include primary production (PP) and gray coloration indicates oxygen sinks (BOD and SOD). Fluxes include diffusion from the atmosphere and advection to (and from) other parts of the water body.

In coastal areas, such as enclosed bays and more open continental shelves, hypoxia can occur when rivers or other sources introduce an influx of water rich in nutrients and organic matter. River water slows down when it joins a larger water body, and subsequently particulate organic matter begins to settle below the wind-mixed, oxygen-rich layer of the water body. Sinking organic matter increases the DO demand in deeper water. This phenomenon is observed annually at the Mississippi River outfall into the Gulf of Mexico, resulting in one of the most extensive patches of coastal hypoxia in the world (Murrell and Lehrter 2011, Rabalais 2011).

2.2.2 Stable Stratification and Hypoxia

Water bodies are stably stratified when a monotonic vertical density gradient is present, such that denser fluid lies below lighter fluid. The energy required to displace fluid in the water column inhibits turbulent vertical mixing (Kundu and Cohen 2002, Fernando 2002). While there are many forms of stable vertical density stratification in water bodies, coastal areas are often characterized by a halocline that vertically separates a less dense, wind-mixed surface layer from a denser bottom layer that is separated from wind effects and the atmosphere (bo Pedersen 1986, Fischer et al 1979).

Stratification can contribute to hypoxia development by altering DO sources and transport (Master, 1997, Verity et al 2006, Lin et al 2006, Melrose et al 2001, Hagy and Murrell 2007, e.g.). Figure 2.2 is a schematic of the DO sources and sinks in a salinity-stratified water column. Above the halocline, wind mixes the water column, and therefore density and water quality constituents such as DO are vertically uniform in the wind-mixed layer. Below the thermocline, water is exposed to both an SOD, and a BOD in the form of sinking biological and organic matter. In a significantly stratified system such as that depicted in the figure, transport between oxygen-rich surface waters and oxygen poor deeper waters can be limited (bo Pedersen 1986). The deeper layer's local DO consumption may exceed production, resulting in hypoxia. Density stratification enhancing bottom water hypoxia is a concern for coastal systems with natural density stratification (Hagy and Murrel 2007, Bleninger and Jirka 2008).

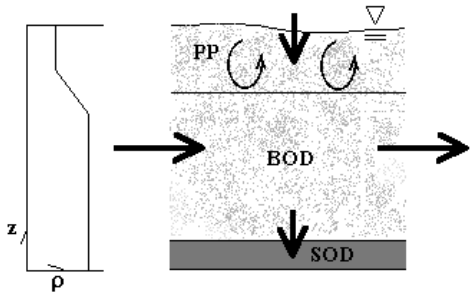

Figure 2.2: Schematic of DO transport in a stratified water column. Arrows represent DO fluxes and wind mixing. Sources include primary production (PP) and gray coloration indicates oxygen sinks (BOD and SOD). Fluxes include diffusion from the atmosphere and advection to (and from) other parts of the water body. The gradient zone in the density profile to the left indicates a halocline separating bottom waters from the atmosphere.

2.2.3 Historical Hypoxia in Corpus Christi Bay

In the mid to late summer, episodic, isolated bottom water hypoxic events are frequently documented in the south and southwest of Corpus Christi Bay (Figure 2.3) (Ritter and Montagna 1999; Applebaum et al 2005, Montagna and Ritter 2006, Hodges et al 2011, Islam et al 2011a e.g.). The hypoxia was first documented in 1988 (Montagna and Kalke 1992), and has been found virtually every summer thereafter (Martin and Montagna 1995; Ritter and Montagna 1999, 2001; Applebaum et al 2005; Islam et al 2011a; Hodges et al 2011; e.g.). Hypoxic events most commonly occur in July and August, and typically persist for a duration on the order of several days (Ritter and Montagna, 2001; Morehead et al, 2002; Morehead and Montagna 2003, 2004). They have been shown to impact benthic organisms in the bay (Ritter and Montagna, 1999), and have been statistically linked with episodic salinity stratification (Coopersmith et al 2011, To and Maidment 2009). Episodic stratification may be a necessary precursor for hypoxia in Corpus Christi Bay.

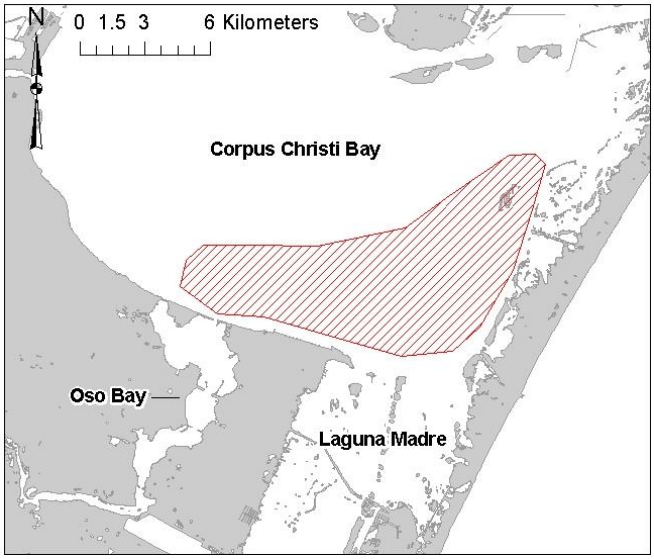

Figure 2.3: Corpus Christi Bay. The hatched region indicates the extent of hypoxia (Nelson and Montagna 2009).

2.3 CORPUS CHRISTI BAY

2.3.1 Bay Morphology and Circulation

Corpus Christi Bay is a large (~ 400 km^2), flat, shallow bay. It has a mean depth of only 3.6 meters and its shape has been compared to a frying pan (Ward, 1997). Within a kilometer of the southern shore, the bathymetry slopes at a rate of 1/400; farther offshore, the bathymetry of the bay slopes much more gradually, at 1/3000 (see contours in Figure 2.4). Ship channels run through the Bay east-west and north-south.

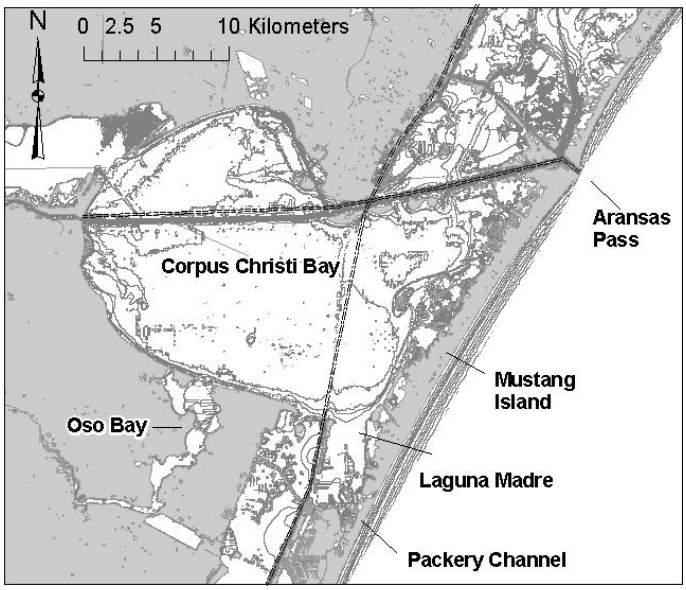

Figure 2.4: Corpus Christi Bay System. Grey lines refer to 1-m depth contours. Dashed black lines represent shipping channels.

Mustang Island, situated between the Bay and the Gulf of Mexico (Figure 2.4), is a typical example of the barrier islands that dampen tidal influences in coastal areas in the Gulf of Mexico. A string of similar barrier islands extends along the Gulf Coast from Mexico all the way to the Florida Panhandle. Corpus Christi Bay is connected to several shallower bays: Nueces Bay to the northwest, Oso Bay to the south, Laguna Madre to the southeast and Redfish Bay to the northeast. Laguna Madre and Oso Bay are both as flat as Corpus Christi Bay, as can be seen in Figure 2.4. Oso Bay and Laguna Madre have mean depths on the order of 0.2 meters, and are characterized by salinities upwards of 60 psu in the summer months (Hodges et al 2011, Islam et al 2011b). This creates a salinity gradient between Corpus Christi Bay and its adjacent Bays of as much as 25 psu, or a density gradient of approximately 19 kg/m^3.

The Corpus Christi Bay National Estuary Project (CCBNEP) and other organizations have conducted studies of the bay including 2D modeling (Matsumoto

1997, Dawson et al 2001, Furnans 2004, Islam and Bonner 2006). Ward (1997) provides a thorough description of the processes in the bay and its geological and anthropogenic history. Real-time and historical weather and tidal data on the bay is disseminated through the Texas Coast Online Observation Network (TCOON; http://www.lighthouse.tamu.edu). Stationary ADCP measurements support 2D modeling results suggesting an overall counter clockwise along-shore circulation (Ojo et al 2006). In the absence of salinity stratification, Corpus Christi is a wind driven, well mixed water body (Islam et al 2010, Islam et al 2011a, b).

2.3.2 Exchange Flows

The Corpus Christi Bay ship channel connects the port of Corpus Christi to the Gulf of Mexico via the Aransas Pass (Figure 2.4). The channel is fourteen meters deep and cuts across the otherwise shallow Corpus Christi Bay east-west, and it is suspected that flows in the deeper portions of the ship channel are largely tidally driven (Pothina 2009).

The Aransas Pass is the only outlet connecting Corpus Christi Bay with the Gulf of Mexico aside from the Packery Channel in Laguna Madre. Tidal signatures in the entire bay system have only approximately 40% that of the Gulf of Mexico, and the response dampens with both distance from the Aransas Pass and depth; typical tidal oscillations are on the order of tens of centimeters. Despite this, the limited exchanges with the Gulf result in very strong currents in the ship channel, reaching 1 m/s at peak flood (Ward 1997).

The Nueces River watershed contributed an average of 77 percent of the freshwater inflows among Corpus Christi Bay (including Oso Bay), Laguna Madre,

Redfish Bay and Nueces Bay between 1968 and 1990 (Ward 1997). Oso Creek flows are generally less than five percent of Nueces River flows.

2.3.3 Hydroclimatology

Ward (1997) provides descriptions of weather patterns along the Texas Coastal Bend, from which we draw much of the following discussion. The entire Corpus Christi Bay System can be described as an episodically inverse estuary, as evaporation rates can exceed freshwater inflows. In these cases, salinities exceed those in the Gulf of Mexico. There is a net evaporation deficit in Laguna Madre on an annual basis, and the average evaporation rate in Corpus Christi Bay in July and August typically exceeds 10 inches/month. While salinities in Corpus Christi Bay itself tend to be above ocean water salinities in the summer time, the most extreme high salinities are observed in the shallower side bays, Laguna Madre and Oso Bay.

Predominant winds in Corpus Christi Bay are from the southwest in the summer months at 4-6 m/s, and shift to the North-Northeast in the winter months (Ward 1997). Sustained winds can reach up to 12 m/s in the late afternoon to early evening in the summer, and typically diminish during the night and into the early morning.

2.3.4 Oso Bay Characteristics

Oso Bay is a small, flat, shallow bay whose north edge joins Corpus Christi Bay. It has a mean depth of only 0.2 meters, a surface area of only about 3 km^2 (Ward 1997, Taylor et al 2008), and a volume of 2 x 10^6 m^3. Total inflows into Oso Bay from 2000 through 2005 are on the order of 1 x 10^6 m^3/d, giving water in the bay a typical residence time on the order of a half a day. Total flows include base streamflows in Oso Creek, four wastewater treatment plants (WWTPs, Robstown WWTP, Greenwood WWTP, Greenwood WWTP2, and Oso WWTP), and the Barney Davis Power Plant. The BDP

takes in water from Laguna Madre as cooling water and discharges it into Oso Bay. Locations of these anthropogenic inputs to the bay are depicted in Figure 2.5.

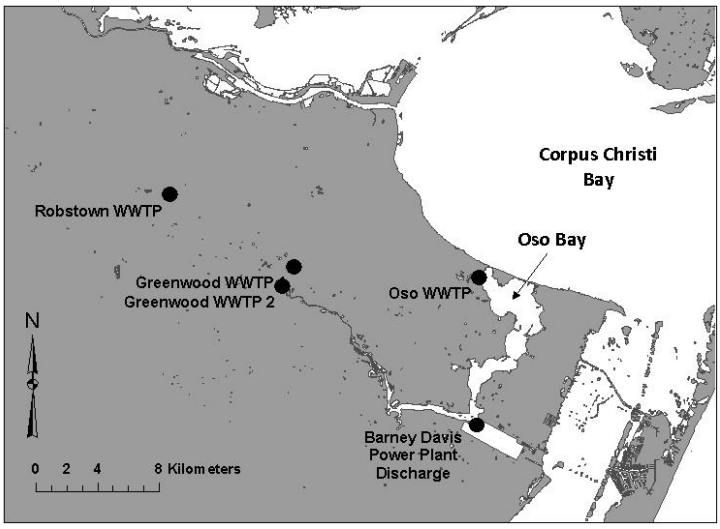

Figure 2.5: Waste water treatment plant and power plant discharges entering Oso Bay.

The base stream flows into Oso Bay are an order of magnitude smaller than the WWTP flows and the Barney Davis discharges, except during periods of heavy rain (typically in the fall) (Figure 2.6). Median stream flows are on the order of 8×10^3 m^3/d, while median total wastewater treatment plant flows are on the order of 6×10^4 m^3/d, and Barney Davis median flows are on the order of 1×10^6 m^3/d. A time history of monthly flows dating from 2000 through 2006 shows the consistency of these median flows (Figure 2.6).

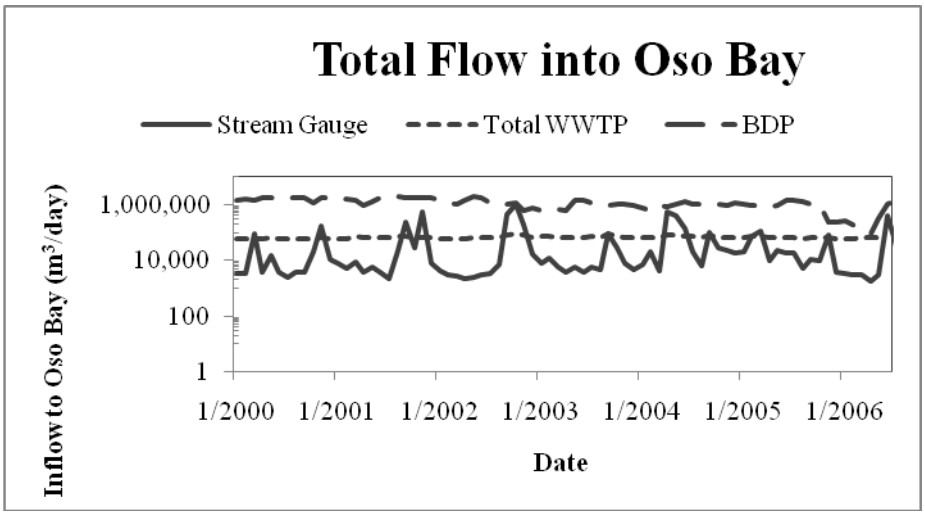

Figure 2.6: Monthly total flows (m3/day) entering Oso Bay from Oso Creek, WWTPs, and the BDP. Plant flow data was provided by plant operators. Streamflow data was obtained from USGS streamgage 08211520.

Flows from the WWTP account for approximately 5% of the total flows entering Oso Bay on average. Water coming from the Barney Davis Plant is taken initially from Laguna Madre, which in the mid to late summer is typically hypersaline (TPWD 2002, Ward 1997). The water passes through a cooling pond and is discharged into Oso Bay. Historical salinities in Oso Bay are low upstream of the power plant's discharge, and are higher downstream of the discharge (Ward 1997); we have observed salinities in the bay between 45 and 50 psu (Hodges et al 2011).

2.3.5 Field Testing At the Nexus of Oso Bay and Corpus Christi Bay

Hodges et al 2011 (hereafter referred to as HFK11) documents and analyzes field data collected in August 2005 at the nexus of Oso Bay and Corpus Christi Bay. This field study supplies a basis for gravity current scale estimates in Corpus Christi Bay that influences CMS model features. The field observations are also used for model comparisons in Chapter 5. This section discusses some of the key insights from HFK11

that are particularly relevant to this dissertation. Further details on sampling methods and analysis can be found in the publication itself, and are not repeated here.

Sampling Methodology

Profile data was collected over a transect of 10 sampling locations shown in Figure 2.7. DO, salininity and temperature data were collected at several depths at each sampling station over the course of a 48-hour sampling period. The depth profile of the transect is shown in Figure 2.8, along with the typical vertical resolution of sampling depths. In addition to water quality data along the transect, another boat was used to measure fluxes into and out of Oso Bay.

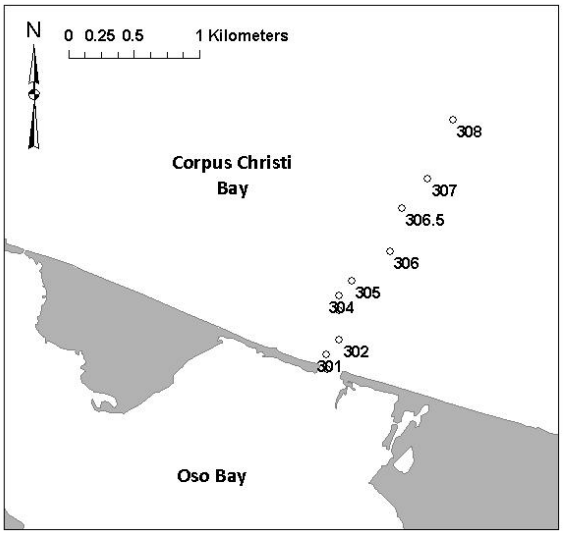

Figure 2.7: Sampling Sites for Oso Bay field study.

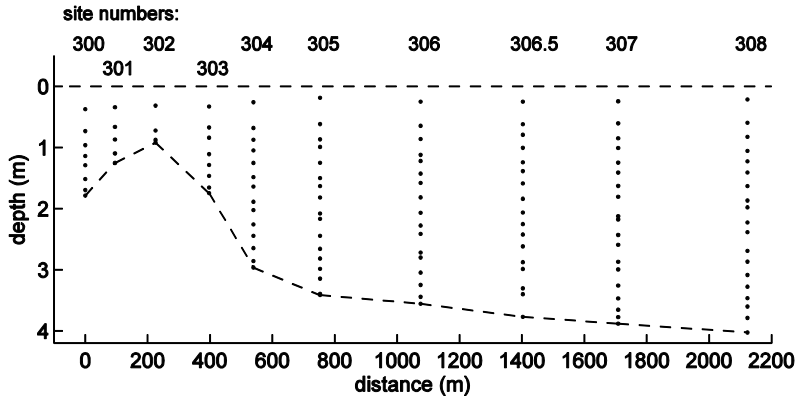

Figure 2.8: Sampling along a typical study transect. Each dot represents a sample position in transect T14. Distance is measured from Site 300 at nexus of Oso Bay and Corpus Christi Bay (Reprinted from Fig. 3 of HFK11).

Data and Analysis

Field data allows clear identification of three principal outflow events from Oso Bay into Corpus Christi Bay, each transporting hypersaline water (between 45 and 50 psu) into Corpus Christi Bay. During each event, the hypersaline fluid plunged to follow the sloping bed of Corpus Christi Bay in the form of a gravity current. Typical profile data obtained from these outflow events is shown in Figure 2.9. Outflow fluxes are estimated at 20 m^3/s, and tend to correspond to tidal oscillations. Strong density stratification was observed to persist in the bottom 20 – 30 cm of Corpus Christi Bay on the order of days. The field data show that after approximately 9-12 hours of isolation time from the free surface, the plume was hypoxic. This isolation time corresponds to a transport distance of approximately 1-1.5 km from the mouth of Oso Bay.

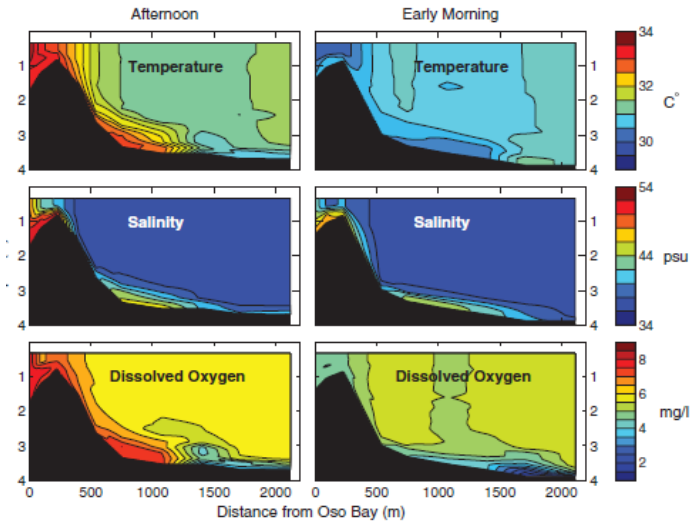

Figure 2.9: Typical results from field collection along transect (Reprinted from Fig. 6 of HFK11).

Analysis shows that entrainment into the gravity current is the dominant form of mixing along the steeper slope and is a lesser factor in the flatter portions of the transect. In these flatter portions of the transect (>750 m offshore), wind mixing may play a significant role in gravity current mixing. However, the field results also suggest that wind mixing occurs slowly relative to gravity current spreading and hypoxia development; a scaling analysis confirms that the winds observed over the bay during the field exercise were too low to mix the water column during the time period of observations.

The field data presented in HFK11 provides insight into the dominant physics that may be driving gravity current spreading and mixing in Corpus Christi Bay. The observed connection between stratification and hypoxia in Corpus Christi Bay establishes the need to capture stratification in numerical models. Modeling gravity current fate and transport in the bay could help inform field data collection and confirm and expand on our understanding of mechanisms for hypoxia in Corpus Christi Bay and other shallow

systems. Throughout this dissertation, gravity currents scaled on observations from the August 2005 field study are modeled and compared qualitatively with this field data.

2.4 NUMERICAL GRAVITY CURRENT MODELING

2.4.1 Overview

Gravity currents have been modeled extensively at both laboratory and field scales. Modeling techniques vary in terms of both governing equations and numerical sophistication from Direct Numerical Simulations (DNS), to 2D models solving the Reynolds-Averaged Navier Stokes Equations (RANS), to simple parameterized and analytical models. This section reviews approaches for modeling field-scale and laboratory gravity currents (Sections 2.3.2 and 2.3.3, respectively). Laboratory-scale gravity current model domains are often limited to the dimensions of the gravity current itself, such that model domain discretization can be optimized for resolving the gravity current. In larger physical systems, model domains can be vertically and horizontally larger than the gravity current. This competition of scales can require a sacrifice of accuracy for efficiency. Field scale models that parameterize gravity current characteristics allow calculation of gravity current propagation in a more grid-independent way, and Section 2.3.4 discusses aspects of existing parameterized models that are applicable to modeling gravity currents in shallow water bodies.

2.4.2 Multi-Scale Approaches in the literature

Many environmental density current model applications involve using a 3D hydrodynamic model to represent the physical system containing the current, as other, larger-scale circulation phenomena are often also of interest (Legg et al 2006, Ilicak et al 2011, Chung et al 2009, Ozgokmen et al 2003, Laanaia et al 2010, e.g.). The physical scale of the larger system is often much larger than the scale of the gravity current, both

vertically and horizontally. The gravity current existing Oso Bay in HFK11 was ~20 cm thick and ~2 km long, in a Bay 3 m deep and 20 km wide. As a more extreme example, general circulation models (GCMs) have difficulty representing North Atlantic deep water formation from gravity currents on the order of meters thick in the North Atlantic Ocean basin (Danabasoglu et al 2010).

Modeling studies of systems containing gravity currents include applications of z-coordinate models, where the vertical layers are fixed and are orthogonal to the x-y plane, and also sigma-coordinate models, in which the vertical grid is terrain-following (with the x-y plane fixed). Although sigma-coordinate models resolve the bottom boundary well, and therefore lend themselves to modeling bottom boundary-following phenomena such as gravity currents, they are also subject to issues of increased error propagation where the total water column depth varies sharply over the computational domain. Advantages and limitations in capturing gravity currents using grid configurations have are discussed in detail below.

Z-Coordinate Models

For z-coordinate models, the stair-stepping effect can result in artificial entrainment (Danabasoglu et al 2010, Winton et al 1998). The difficulties associated with modeling gravity currents in z-coordinate models are demonstrated visually for a 2D example basin in Figure 2.10.

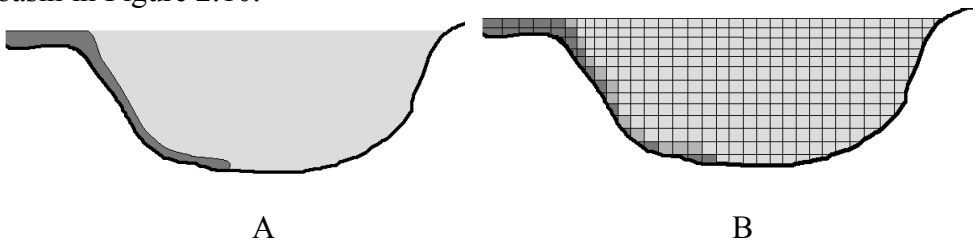

Figure 2.10: Stair-stepping impact on modeled entrainment. (A) a gravity current in a basin, (B) a discretized representation. (B) has a less sharp density gradient.

Many large-basin (i.e. oceanographic) modeling studies involving gravity currents explore criterion for the minimum grid resolution that will allow a model to maintain a gravity current's vertical stratification (Winton et al 1998, Tseng and Dietrich 2006, Laanaia et al 2010, e.g.). Winton et al (1998) identifies the horizontal grid spacing criterion of:

$$\Delta x < \frac{h}{\tan(\theta)} \qquad 2\text{-}1$$

and a vertical criterion of:

$$\Delta z < h \qquad 2\text{-}2$$

where Δx is the horizontal grid size, h is the local gravity current thickness, θ is the bed slope, and Δz is the vertical grid size. Following this criteria, Ezer and Mellor (2004) uses one to two vertical layers to resolve the underflow. However, Tseng and Dietrich (2006) find that refining both of the above criteria by at least a factor of 2 was required to achieve good gravity current representation, and use 5 to 6 grid cells to establish "benchmark" test case. For smaller than oceanographic scale applications, (reservoirs and embayments, for example), where more refined resolution is possible, additional grid layers are used to resolve underflows. Chung et al (2009) uses 20-30 vertical grid layers to resolve an underflow in the Daechong Reservoir (Korea). Malcangio and Petrillo (2010) simulate potential desalination brine outfalls off the coast of Southern Italy using 2-m vertical layers to simulate fate of effluent released approximately 20 m above the bed. Yeates et al (2006) uses 0.5-m vertical layers to simulate desalination brine fate released in the bottom grid layer.

Sigma-Coordinate Models

For grid-independent modeled gravity current entrainment in a sigma-coordinate model, the test configuration in Kulis and Hodges (2006) requires 10 to 15 grid cells

vertically resolving the underflow, with approximately 5-10 grid cells being sufficient to represent bulk gravity current properties. Laanaia et al (2010) finds that using a vertical grid resolution with at least 5 grid cells in an underflow improve modeled gravity current propagation. Rennau and Burchard (2011) also find that increased vertical grid resolution in vertical regions of stratification reduces numerical mixing. However, most field-scale model applications use grid with less than 5 vertical layers in an underflow. The Regional Ocean Modeling System (ROMS) has been applied to large-scale gravity currents such as the Red Sea outfall (Iliak et al 2011), using 30 total vertical grid layers in the entire water column, with more refined resolution toward the bottom of the domain where the gravity current was located. Modifications to ROMS are also being made to improve representation of sub grid scale density stratification (Hetland and DiMarco 2008).

2.4.3 Model Applications with Fine Vertical Grid Resolution

In cases where and an underflow is not being modeled within a much larger fluid system, sufficient resolution is more easily provided to capture underflow dynamics. Such systems are sometimes modeled with a 2D model representation, allowing more refined vertical grid. Choi and Garcia (2002) use 200 vertical cells for a 2 meter-deep tank, corresponding to a range of 20 to 40 cells in the underflow. Bonometti et al 2011 use resolutions of 160 cells in the underflow. Georgoulas et al (2010) uses a grid with a bottom layer that is 2 mm thick, expanding at a 1.05 growth rate, to simulate a lock exchange in a basin 40 cm deep (so that the bottom grid layer represents 0.5% of the total water depth). Other modeling techniques applied to laboratory-scale gravity currents include multi-phase modeling (Felix 2001, Gerber et al 2011), adaptable meshes (Hiester

et al 2011), and large eddy simulation (LES, Kirpatrick and Armfield 2005, Ozgokmen et al 2009, Berselli et al 2011).

2.4.4 Depth-Integrated Field-scale Gravity Current Models

Because the grid resolution needed to resolve gravity currents can be prohibitive whether using a sigma-coordinate model or a z-coordinate model, solutions have been developed to remove the underflow from a 3D model. One approach used in oceanographic models is to alter the way in which the bottom grid layer is modeled in x-coordinate models, allowing fluid exchange among the bottom cells in each cell column. This makes the bottom grid cells bottom-boundary following, without accounting for along-slope gravitational forcings (Beckman and Doscher 1997). Another technique used in the oceanographic community is to create a bottom boundary layer model in the bottom grid cells (Killworth and Edwards 1999). While these modeling techniques address issues associated with stair-step models, they force an underflow to the vertical thickness of the bottom model layer. These techniques also do not prevent numerical horizontal diffusion from eroding the shock wave associated with a gravity current front.

Integral models have also been developed to improve modeled underflow representation. Integral models treat the gravity current as a vertically uniform "slab", and use parameterized models of gravity current entrainment (Holland 2011, Dallimore et al 2003, Bradford and Katapodes 1999, e.g.). Underflows are often inserted back into 3D models as a flow source when underflow plumes have either entrained enough fluid to be fully resolved in a 3D model (Dallimore et al 2003), or have reached their neutrally buoyant depth (Holland 2011). Because underflows are excluded from the ambient model domain until inserted as a flow source, this approach is limited to physical systems

where down-slope gravity current propagation has a negligible impact on larger-scale ambient currents.

Most integral models in the literature do not transfer forces such as ambient free surface pressure gradients to the underflow momentum solution, they are limited to fluid systems where the underflow is much thinner than the total water column (Bradford and Katapodes, 1999). They are also designed for systems where the gravity current is well below the wind-mixed layer, and ambient currents and TKE can be considered negligible compared with the motion of the gravity current (so that all mixing occurs *into* the gravity current as entrainment; Dallimore et al 2003, Holland 2011). An exception is the underflow model developed by Killworth and Edwards (1999), which allows for detrainment.

Potential Application to Corpus Christi Bay

The vertical grid-independence of integral underflow representation is desirable for application to Corpus Christi Bay, where horizontal and vertical scales are larger than the underflows that have been observed. However, the shallow depth of Corpus Christi Bay exposes underflows to additional forcings that are not observed in deep systems, and should be included in an integral model to improve gravity current representation in Corpus Christi Bay.

In shallow fluid systems, dense underflow can drive basin-scale circulation (Wells and Sherman 2001, Wells and Wettlaufer 2005, Oldham and Sturman 2001). Although density currents do not likely drive large-scale circulation in Corpus Christi Bay, they may have a locally significant influence on ambient currents. Density currents exiting Laguna Madre can be as much a 1 m thick (30% of the water column), and therefore locally displace non-negligible volumes of ambient fluid (Hodges et al 2006). As

discussed above, most existing integral slab underflow models are designed for deep fluid systems and do not represent this type of coupled interaction between ambient and underflow fluids.

In addition to ambient fluid displacement, existing integral models also do not allow wind mixing to erode an underflow surface. Observations and analyses from HFK11 indicate that wind forcings are non-negligible in calculating gravity current fate. This forcing also needs to be included in an underflow model applied to Corpus Christi Bay.

This dissertation builds on existing slab-representations of gravity currents and modifies them to reflect the characteristics of shallow systems. We couple a 2D slab gravity current model with the 3D ELCIRC model (Zhang et al 2004). Modifications necessary to represent shallow system characteristics include: allowing the underflow's propagation to influence the ambient fluid's circulation and mass balance, and allowing wind mixing in the ambient fluid to penetrate into the gravity current and erode it. Parameterizations for both entrainment and wind mixing are discussed below, and the configuration of this coupled model system (CMS) is discussed in chapters 3 and 4.

2.5 STRATIFICATION AND MIXING

2.5.1 Richardson Number and Turbulent Kinetic Energy

Two common types of mixing are important to gravity current movement in shallow bays: entrainment and wind mixing. Gravity currents in the environment and in the laboratory mix with the ambient fluid surrounding them as they spread. This mixing, or entrainment, is often mostly uni-directional *into* the gravity current (bo Pedersen 1986, Sherman et al 1978), and plays an important role in gravity current fate and transport. Wind mixing occurs in most drnsity-stratified systems that are exposed to wind (bo

Pedersen 1986, Fischer et al 1979). Wind energy generally penetrates through the wind-mixed layer, and slowly erodes the deeper, denser layer below. A typical halocline depth is on the order of 10 m deep (bo Pedersen 1986), and it is therefore generally accepted that shallow water columns on the order of meters deep would be vertically mixed under sustained moderate winds in the absence of a buoyancy flux (Ojo et al 2006, Islam et al 2010). Field data (HFK11) confirms that in the absence of the gravity current exiting Oso Bay, this is the case. Other field data (Islam et al 2010, 2011a, b) also support this conventional scaling argument. However, stratification introduced by gravity currents entering Corpus Christi Bay can tip the balance of wind energy and negative buoyancy.

Richardson Number

Without stratification, mixing occurs when velocity shear produces turbulent eddies, increasing the surface exchange area for molecular diffusive transport of scalars and momentum. For a homogeneous density fluid, the potential energy required to lift a particle is exactly the same as the potential energy lost by an equivalent falling particle, so a turbulent eddy can be thought of as potential energy neutral. However, for mixing to occur within a stratified fluid, the turbulent eddy must lift the heavier fluid into the lighter fluid, which is requires more potential energy than is lost by the lighter fluid moving down into the heavy fluid. This potential energy requirement is a function of the density gradient between the layers, whereas the shear production is a function of the velocity shear between the fluids. A common parameter to assess the balance between the energy due to shear and the strength of the stratification is the Gradient Richardson number:

$$\mathrm{Ri}_g = \frac{g\frac{d\rho}{dz}}{\rho\left(\frac{du}{dz}\right)^2} \qquad 2\text{-}3$$

where u is the local velocity parallel to the density interface, ρ is the density, and g is the acceleration due to gravity. A full derivation of this ratio is beyond the scope of this discussion, but can be found in Kundu and Cohen (2002).

As mentioned above, we can think of Ri_g as buoyancy versus shear, or even as potential energy versus kinetic energy. Studies have found that when Ri_g is sufficiently small, overturning will occur because the shear is sufficient to overcome both the density stratification and viscous dissipation. The threshold for overturning varies in the literature, but is generally approximately 0.25 (Monismith and Fong 1996). Ri_g has previously been used to improve turbulence modeling for stratified flows; for example, the Galperin et al (1988) modification of the Mellor-Yamada 2.5 turbulence closure (1982, also applied in ELCIRC) includes an Ri_g mixing threshold. Similarly, most entrainment laws for gravity currents are often parameterized on either Ri_g or the related bulk Richardson Number, Ri_b:

$$\mathrm{Ri_b} = \frac{\mathrm{g'\,h}}{\mathrm{v^2}} cos\,\theta \qquad 2\text{-}4$$

where v is the depth-averaged along-slope gravity current velocity, g' is the depth-averaged gravity current reduced gravity term, h it the gravity current thickness, and θ is the bed slope (Ellison and Turner 1973, Baines 2005, Parker et al 1987, Dallimore et al 2001).

Turbulent Kinetic Energy

Most analyses of stratified flow begin with a turbulent kinetic energy (TKE, or k) budget. Turbulent kinetic energy is transported as:

$$\frac{\mathrm{Dk}}{\mathrm{Dt}} = \frac{\partial \mathrm{T_j}}{\partial \mathrm{t}} - \mathrm{P} - \mathrm{B} - \varepsilon \qquad 2\text{-}5$$

where

$$T_j = \overline{u_j k} + \frac{\overline{p u_j}}{\rho} + \overline{u_i \nu \left(\frac{\partial u_i}{\partial x_j} + \frac{\partial u_j}{\partial x_i} \right)} \qquad 2\text{-}6$$

$$P = \overline{u_i u_j \frac{\partial U_i}{\partial x_j}} \qquad 2\text{-}7$$

$$B = g \rho u_3 \qquad 2\text{-}8$$

$$\varepsilon = \nu \overline{\left(\frac{\partial u_i}{\partial x_j} \right)^2} \qquad 2\text{-}9$$

In the above equations U is the time-averaged flow; ν is the kinematic viscosity; and italicized terms, *u*, *p*, and *ρ*, are turbulent fluctuations of velocity, pressure, and density, respectively. The overbar indicates time averaging, and the operator $\frac{D}{Dt}$ represents the material derivative. P is the production term, T is the turbulent transport term (or "leakage" term) and ε is the energy dissipation term. The buoyancy-shear balance in the Richardson number is a parameterization of equation (2-5).

The buoyancy term, B, is only present in stratified flows. This term accounts for turbulent kinetic energy losses to the potential energy increase associated with vertical mixing. The presence of B in the TKE equation relates the TKE budget to mixing and entrainment in stratified flows such as gravity currents. It is this relationship that motivates our discussion of TKE budgets here, as we will develop a TKE budget appropriate to Corpus Christi Bay in our conceptual model. A buoyancy flux obtained from a TKE balance will help us to calculate mixing in the gravity current. A full explanation of the physical meaning and derivation of equation (2-5) can be found in Bernard and Wallace (2002), and is beyond the scope of our discussion.

A TKE budget is developed by integrating equation (2-5) over a water column (or a section of the water column), and parameterizing the resultant terms. This parameterization helps identify the TKE available for conversion to a buoyancy flux, or

vertical mixing of dense fluid. Wind mixed layer deepening is often scaled in this way, and the CMS mixing algorithm (Chapter 4) therefore builds on ideas presented in this section. Gravity current entrainment laws applied in the literature and in the CMS are also parameterizations of the TKE equation.

2.5.2 Gravity Current Entrainment Laws

Mixing into a gravity current is often discussed in terms of an entrainment rate, E, which is a bulk parameter reflecting all sources of TKE within the underflow (i.e. bed shear and interfacial shear). The entrainment rate is defined as the ratio of the net vertical velocity into the current from the ambient fluid (i.e. the entrainment velocity, w_e) to the gravity current's mean flow velocity

$$E = \frac{w_e}{v}. \qquad 2\text{-}10$$

This definition of entrainment is robust and has been used extensively in the literature (Ellison and Turner 1959; Bradfod and Katapodes 1999; Garcia 1993, 1994; Dallimore et al 2001; Ozgokmen et al 2003, e.g.).

Empirical relationships have been developed in the literature for entrainment rates, and most are based on Ri_b. Ellison and Turner (1973) derive the following relationship from the momentum equation:

$$E = \frac{S_2 Ri \tan\theta - C_D}{1 + \frac{1}{2} S_1 Ri} \qquad 2\text{-}11$$

where S_1 and S_2 are profile shape factors, C_D is the bottom drag coefficient and θ is the bed slope. Various relationships based on Ri_b^{-1} exist in the literature (Baines 2005, Parker et al 1987). Dallimore et al (2001) form the equation:

$$E = \frac{-h}{S'_{max}} \frac{\partial S_{max}}{\partial x} \qquad 2\text{-}12$$

and Bo Pedersen (1986) establish a simple relationship based on slope:

$$E = 0.072\sin(\theta) \qquad 2\text{-}13$$

HFK11 shows that for Corpus Christi Bay, Bo Pedersen (E_{BP}), Dallimore (E_D), and measured mass balances (E_α) are all on the same order (Table 2.1). Because of this finding, along with the indication from field data that entrainment along the flat part of the slope is negligible in Corpus Christi Bay, the Bo Pedersen entrainment relationship is used in the model developed for this dissertation. Nielsen et al (2005) also used equation (2-13) to parameterize entrainment into an underflow in a basin with similar dimensions and forcings to Corpus Christi Bay. It should be noted, however, that this may be a limitation of the CMS – the Bo Pedersen is a highly empirical entrainment law, and may not be ideal for every system.

Table 2.1: Entrainment rate observations of the Oso Bay Outfall in August 2005. From HFK11. For site locations in Corpus Christi Bay see Figure 2.7.

	E_{BP}	E_α	E_D
Site 300-306: ΔV_B	1.4×10^{-4}	1.9×10^{-4}	1.2×10^{-4}
Site 300-306: ΔV_C	1.4×10^{-4}	1.7×10^{-4}	1.8×10^{-4}
Site 306-308: ΔV_B	2.6×10^{-5}	2.5×10^{-5}	5.9×10^{-5}
Site 306-308: ΔV_C	2.6×10^{-5}	1.1×10^{-5}	4.3×10^{-5}

2.5.3 Water Column Mixing

Mixed layer deepening algorithms have been developed in the literature parameterizing mixing in the wind-mixed layer (Spigel, 1981, Kraus and Turner 1967, Atkinson and Harleman 1987, Hodges et al 2000, e.g.). Similar to entrainment parameterizations, wind-mixed layer deepening scaling and analyses are based on the approximation that TKE in the upper, mixed layer is much larger than TKE in the lower layer (Spigel 1986).

Spigel (1986) scales TKE production P from wind shear as:

$$P = \frac{1}{2}\rho\left(C_N u_*\right)^3 \qquad 2\text{-}14$$

where C_N is an empirical coefficient; commonly the value of 1.33 is used (Spigel 1986, Hodges et al 2000), and u_* is the wind shear velocity:

$$u_* = U_W\sqrt{C_D\frac{\rho_{air}}{\rho_{water}}} \qquad 2\text{-}15$$

where U_W is the wind speed above the boundary layer (typically 10 m above the water surface), ρ_{air} is the density of the air and ρ_{water} is the density of the water at the free surface (Kraus and Turner 1967).

Because the wind mixed layer is assumed to be constantly mixed, any buoyancy flux from deepening the mixed layer instantly mixes throughout the water column thickness H_a. The depth-integrated buoyancy flux B from deepening the wind mixed layer can then be parameterized as (Hodges et al 2000, 2011):

$$B = -\frac{1}{C_m} g\Delta\rho H_a \frac{dH}{dt} \qquad 2\text{-}16$$

Where C_m is a coefficient accounting for losses in conversion from TKE to potential energy, or dissipation (typically between 0.2 and 0.25), $\Delta\rho$ is the density difference between the wind mixed layer and the underflow, H_a is the thickness of the wind mixed layer, and $\frac{dH}{dt}$ is the rate of mixed layer deepening. For systems where:

1. Other sources of TKE are small compared to wind production (or are balanced by unaccounted for dissipation),

2. All available TKE is used for wind mixing (i.e. equation [2-5] is at steady state),

3. TKE leakage is negligible,

Wind mixed layer deepening (wind-induced erosion of the underflow) can be parameterized as:

$$\frac{dH}{dt} = -C_m C_N^3 \left(C_D \frac{\rho_{air}}{\rho_{water}} \right)^{3/2} \frac{U_W^3}{H_a g'} \quad 2\text{-}17$$

The CMS developed in this dissertation uses this parameterization to incorporate wind mixing into modeled underflow and ambient fluid dynamics and mass balances. A similar parameterization is used by Nielsen et al (2005) for a box model of a shallow (~6m deep) wind-driven, estuarine system. Data has not determined that wind-mixed layer deepening scaling arguments are applicable to bottom boundary-following underflows, however. It is possible that wall effects may influence turbulent mixing; field and laboratory studies are needed to determine the applicability of this scaling.

2.6 CONCLUSIONS

Hypoxia in Corpus Christi Bay impacts the biota in the Bay, and density stratification is likely a necessary pre-cursor to hypoxia. This chapter establishes the need to develop a model that can capture the strong stratification observed in field data, and also demonstrates the difficulties associated with using currently available tools for modeling gravity currents in shallow systems. In Corpus Christi Bay and other shallow fluid systems, mass balances and ambient fluid displacement from underflow motions cannot always be neglected. Wind mixing can also be important in determining underflow fluid fate and transport.

This chapter established modifications that can be made to existing models to improve their representation of the phenomena in Corpus Christi Bay. There are several field-scale models that use a "slab" representation of gravity currents spreading in larger water bodies. However, most field-scale models do not allow gravity currents to either

influence ambient fluid circulation, or be eroded by wind mixing. This dissertation introduces a mixing model that takes gravity current entrainment, spreading, and wind-mixing into account in gravity current transport. In shallow fluid systems where wind may play a significant role in gravity current mixing, this accurate representation of mixing improves transport estimates of key water quality constituents such as dissolved oxygen. The combination of wind mixed layer deepening and underflow entrainment into a single conceptual mixing model has not been done. This combination of scaling and conceptual models is a contribution to the study of stratified flows.

Chapter 3: Displacement Model Architecture, Algorithms and Verification

3.1 INTRODUCTION

This chapter presents the displacement and spreading components of a Coupled Model System (CMS) developed for this dissertation. The CMS includes both a 3D hydrodynamic model that simulates circulation in an arbitrary water body, and a 2D model representation with the same bed elevations and horizontal grid information as the 3D model. The 2D model simulates circulation of a dense underflow following the bed in the water body. The CMS allows these two models to exchange boundary condition information at each timestep.

The chapter presents the conceptual model that governs all algorithms and parameterizations made in the CMS. It also develops the model architecture, including communication between models. Algorithms for model communication are discussed. Test cases are presented to demonstrate model features.

Mixing between the underflow and ambient models is not included in this chapter; Chapter 4 discusses the conceptual mixing model, numerical algorithms and test cases. The coupled model presented in this chapter does not include turbulent mixing, but molecular diffusion and viscous shear across model boundaries is modeled.

3.2 CONCEPTUAL MODEL AND GOVERNING EQUATIONS

3.2.1 Coupled Model System

The Coupled Model System (CMS) is designed to represent the physics felt by a shallow, wide basin exposed to moderate to high winds. The basin contains an arbitrary volume of negatively buoyant fluid along a portion of its bottom boundary, though the

dense fluid may in places extend up to the free surface. This fluid will be referred to as the "underflow", while the less dense fluid in the rest of the basin will be referred to as the "ambient fluid". The underflow may also be associated with an inflow of arbitrary volume flux at a basin boundary (see, for example, Figure 3.1). In locations where the dense fluid extends to the free surface, the fluid is still included in the "underflow" in the conceptual model. The basin's free surface is exposed to a moderate to high wind. A 2D representation of the conceptual model is shown in Figure 3.1.

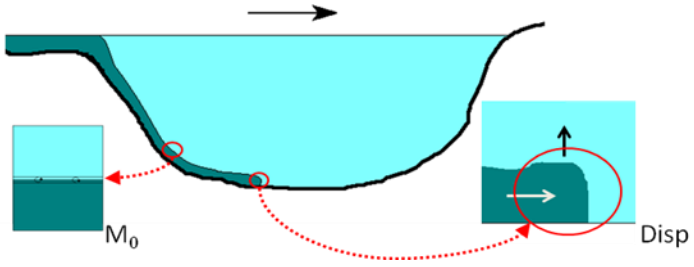

Figure 3.1: A typical basin represented by the conceptual model. Dense fluid contained in the underflow model is represented with darker blue. Interactions between dense and light fluids that are represented in the conceptual model include molecular diffusive and viscous effects (process "M_0") and vertical displacement (process "Disp").

The conceptual model's governing equations define the motions of the underflow and ambient fluid. The ambient and underflow fluids are separated into two conceptual models that are necessarily interdependent. The surface of the underflow is therefore defined the ambient fluid's bottom boundary. The boundary condition at the interface between models is defined in part by shear between the two fluids. If the underflow is not at rest, ambient fluid is vertically displaced as the underflow spreads along the basin's bottom.

3.2.2 Ambient Conceptual Model

The ambient fluid fills the generic basin described by the CMS conceptual model. Vertical and horizontal velocity, salinity and temperature gradients may exist within the ambient fluid. However, vertical density gradients within the ambient fluid are assumed to be small enough that they do not limit wind energy penetration into the water column; the entire ambient water column must be within the wind mixed layer. The domain of the ambient fluid extends from the underflow surface to the basin free surface. Forces acting on the ambient fluid include barotropic and baroclinic pressure gradients, Coriolis forces, and tidal potential, diffusion and viscous effects. The conceptual model applies the hydrostatic approximation and Reynolds Averaging to solve the momentum equations:

$$\frac{Du_{amb}}{Dt} = f\, v_{amb} - \frac{\partial}{\partial x}\left[g(\eta_{amb} - \alpha\hat{\psi}) + \frac{P_a}{\rho_0} \right] - \frac{g}{\rho_0}\int_z^{\eta+msl} \frac{\partial \rho_{amb}}{\partial x} dz + \frac{\partial}{\partial z}\left(K_{mv,amb} \frac{\partial u_{amb}}{\partial z} \right) + F_{mx,amb} \qquad 3\text{-}1$$

$$\frac{Dv_{amb}}{Dt} = -f\, u_{amb} - \frac{\partial}{\partial y}\left[g(\eta_{amb} - \alpha\hat{\psi}) + \frac{P_a}{\rho_0} \right] - \frac{g}{\rho_0}\int_z^{\eta+msl} \frac{\partial \rho_{amb}}{\partial y} dz + \frac{\partial}{\partial z}\left(K_{mv,amb} \frac{\partial v_{amb}}{\partial z} \right) + F_{my,amb} \qquad 3\text{-}2$$

The conceptual model is also governed by the local and depth-integrated continuity equations:

$$\frac{\partial u_{amb}}{\partial x} + \frac{\partial v_{amb}}{\partial y} + \frac{\partial w_{amb}}{\partial z} = 0 \qquad 3\text{-}3$$

$$\frac{\partial \eta_{amb}}{\partial t} + \int_{H_R - h}^{H_R + \eta} u_{amb}\, dz + \int_{H_R - h}^{H_R + \eta} v_{amb}\, dz = 0 \qquad 3\text{-}4$$

and salt and heat conservation:

$$\frac{DS_{amb}}{Dt} = \frac{\partial}{\partial z}\left(K_{sv,amb} \frac{\partial S_{amb}}{\partial z} \right) + F_{s,amb} \qquad 3\text{-}5$$

$$\frac{DT_{amb}}{Dt} = \frac{\partial}{\partial z}\left(K_{hv,amb} \frac{\partial T_{amb}}{\partial z} \right) + \frac{\dot{Q}_{amb}}{\rho_0 C_p} + F_{h,amb}\,. \qquad 3\text{-}6$$

In the above equations, u_{amb}, v_{amb} and w_{amb} are the velocity vectors in the x, y and z directions, respectively; *f* is the Coriolis factor; g is gravitational acceleration; η_{amb} is the free-surface elevation relative to mean sea level; α is the earth elasticity factor; Ψ is the tidal potential; P_a is atmospheric pressure; ρ_{amb} is the density of water; ρ_0 is the reference density of water (taken as 1025 kg/m^3 by default, unless altered in the code); $K_{mv,amb}$, $K_{sv,amb}$, and $K_{hv,amb}$ are vertical eddy viscosity, diffusivity of salt, and diffusivity of heat, respectively; $F_{mx,amb}$, $F_{my,amb}$, $F_{s,amb}$, and $F_{h,amb}$ are horizontal diffusion quantities for the momentum and transport equations; msl is mean sea level (or the free surface elevation at rest); z_0 is the local bed elevation; S_{amb} is salinity and T_{amb} is temperature; $\dot{Q}_{amb}$ is the rate of solar radiation absorption; and C_p is the specific heat of water. The conceptual and numerical models developed in this chapter are based on the ELCIRC model (Zhang et al 2004, discussed in Chapter 2).

Bottom Boundary Condition

As ambient fluid is displaced by underflow movement, the ambient water column shifts vertically up or down. This influences the bed elevation z_0, the free surface elevation η, and the ambient water column's vertical velocity w. Because the ambient bed elevation is exactly the same as the underflow surface elevation, vertical displacement experienced by the ambient fluid is exactly equal to shifts in surface elevation of the underflow below.

Viscous effects are imposed on the interface between the underflow and ambient models. However, the ambient fluid that is not above underflow fluid experiences ELCIRC's traditional no-slip drag boundary conditions.

3.2.3 Underflow Conceptual Model

The underflow is treated as a vertically uniform "slab", which is a common approach in the literature, as discussed in Chapter 2. The slab extends vertically from the location of the maximum density gradient down to the bed. The underflow may not be present in the water column everywhere in the basin. The shallow water approximation is used to describe underflow motions.

The conceptual model coordinate system is shifted so that the underflow lies on a flat bed. This transformation allows the model to follow the bottom boundary exactly, as shown in Figure 3.2.

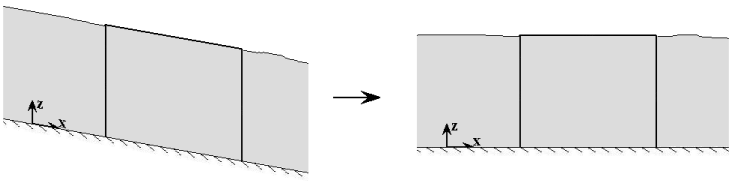

Figure 3.2: Coordinate transformation of underflow model.

Because the underflow model is separated from the ambient fluid completely, all influences from the ambient fluid are treated as boundary conditions and external forcings. The forces acting on the underflow fluid include body forces, baroclinic pressure gradient forces posed by horizontal gradients in the underflow surface location, barotropic pressure gradient forces posed by the ambient fluid free surface gradients, shear stresses at the underflow surface between the underflow and ambient fluids, Coriolis forces and the earth potential.

Because the underflow model is a 2D application of ELCIRC, equations governing the underflow model are similar to the ambient model's governing equations. Differences include the replacement of internal baroclinic forces with the baroclinic pressure gradient imposed by the underflow surface gradients, and changes resulting from

the coordinate system transformation. The coordinate transformation influences any terms in the governing equations that include gravitational acceleration. The resulting governing equations are:

$$\frac{Du_{und}}{Dt} = fv_{und} - \frac{\partial}{\partial x}\left[g'\left(\eta_{und}\cos\theta_x - \alpha\hat{\psi}\right) + \frac{P_{amb}}{\rho_0} \right] + \frac{\partial}{\partial z}\left(K_{mv,und}\frac{\partial u_{und}}{\partial z} \right) + F_{mx,und} + g'\sin\theta_x \quad 3\text{-}7$$

$$\frac{Dv_{und}}{Dt} = -fu_{und} - \frac{\partial}{\partial y}\left[g'\left(\eta_{und}\cos\theta_y - \alpha\hat{\psi}\right) + \frac{P_{amb}}{\rho_0} \right] + \frac{\partial}{\partial z}\left(K_{mv,und}\frac{\partial v_{und}}{\partial z} \right) + F_{my,und} + g'\sin\theta_y \quad 3\text{-}8$$

$$\frac{\partial \eta_{und}}{\partial t} + \int_{H_R-h}^{H_R+\eta} u_{und}\,dz\cos\theta_x + \int_{H_R-h}^{H_R+\eta} v_{und}\,dz\,cos\,\theta_y = 0 \quad 3\text{-}9$$

$$\frac{DS_{und}}{Dt} = \frac{\partial}{\partial z}\left(K_{sv,und}\frac{\partial S_{und}}{\partial z} \right) + F_{s,und} \quad 3\text{-}10$$

$$\frac{DT_{und}}{Dt} = \frac{\partial}{\partial z}\left(K_{hv,und}\frac{\partial T_{und}}{\partial z} \right) + \frac{\dot{Q}_{und}}{\rho_0 C_p} + F_{h,und}, \quad 3\text{-}11$$

where

$$g' = g\frac{\rho_{und} - \rho_{amb}}{\rho_{amb}} \quad 3\text{-}12$$

is the reduced gravity term, and θ is the bed slope. The underflow transport and heat exchange equations are unchanged from the ambient conceptual model. In the underflow governing equations, η_{und} is the interface between the underflow and the ambient fluid. The term P_{amb}, is used to represent the ambient model's barotropic pressure gradient. For clarity, the pressure gradient derived from η_{und} will be referred to as the "underflow baroclinic pressure gradient" and the term derived from P_{amb} as the "ambient barotropic pressure gradient". Because this model is designed to represent shallow systems where wind mixing is strong, ambient fluid vertical stratification is assumed to be small compared with the underflow-ambient density gradient. The ambient model's internal

barotropic pressure gradients are therefore not included in the underflow momentum equation. Atmospheric pressure gradients are also not included in the underflow governing equations, which is another model limitation.

3.3 NUMERICAL MODEL ARCHITECTURE

3.3.1 ELCIRC Structure

The numerical implementation of the CMS developed in this dissertation is based on ELCIRC. The ELCIRC code is used as a basis for both the ambient and underflow models, and is modified as needed to accommodate underflow features and coupling algorithms. ELCIRC is a 3D finite-volume/finite-difference hydrodynamic model (Zhang et al 2004, Baptista et al 2005).

The solution method for ELCIRC uses the International Equation of State for Sea Water in calculating water density. While this method is only appropriate for salinities up to 42 psu, there is no other accepted method for density calculation that is calibrated to higher salinities, and thus we do not alter this in the CMS.

Grid Structure and Variable Storage

ELCIRC uses an unstructured grid comprised of nodes (p_i though p_{i+2} in Figure 3.3), sides (side centers denoted with s_j though s_{j+2} in Figure 3.3), and elements (point e in Figure 3.3). Surface elevations η are stored at element centers, as are vertical velocities w. Velocities are solved and stored as velocity components normal to element sides (u) and components tangential to element sides (v). Salinities and temperatures (S, T in the figure) are stored at both nodes and element sides.

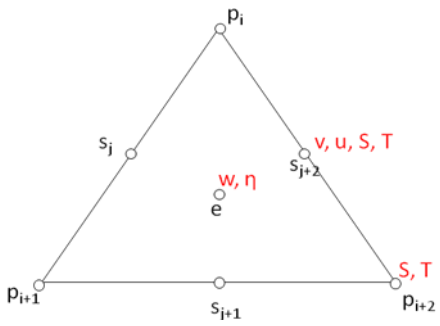

Figure 3.3: Example ELCIRC grid element in plan view. Black text indicates grid components (p for nodes, s for element sides and e for the element center). Red text indicates variables stored at designated locations (surface elevation η, vertical velocity w, normal and tangential velocities u and v respectively, salinity S and temperature T).

ELCIRC's vertical discretization uses a z-coordinate grid to represent a vertical column of grid elements (Figure 3.4). Each layer has a vertical thickness that is fixed throughout the grid, with the exception of the top and bottom layer in each element column. Top and bottom layer thicknesses include only vertical space filled with water. Bottom elevations are read in at nodes (dp_i through dp_{i+2} in Figure 3.4) at the beginning of a simulation, and are interpolated to bottom edges of element sides (dps_j through dps_{j+2} in Figure 3.4) and element centers (dpe in Figure 3.4). Top layer dimensions are re-calculated at every timestep to account for changes in η.

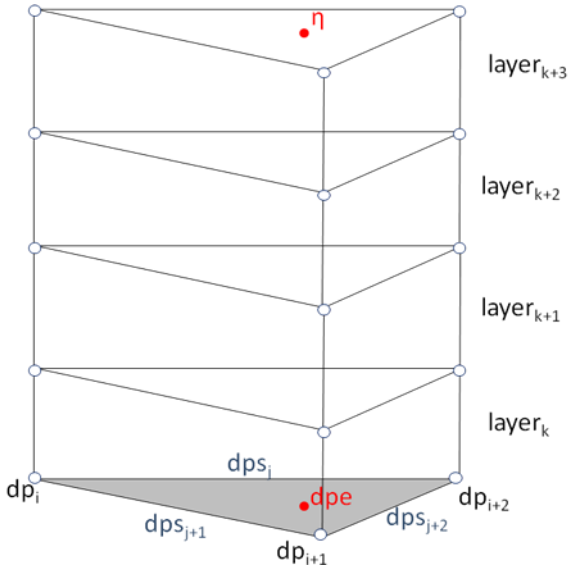

Figure 3.4: Example ELCIRC water column discretized into layers k through k+3. Bed elevations are stored at nodes (dp_i through dp_{i+2}), and are interpolated to element edges (dps_j through dps_{j+2}) and element centers (dpe).

Solution Method

The ELCIRC algorithm is semi-implicit. In the momentum equations, the barotropic term is given an implicitness factor θ that is user-defined but varying between 0.5 and 1. The vertical viscosity and bottom boundary conditions are treated fully implicitly, and all other terms are treated explicitly. Using local coordinate systems allows simple solution of the x-and y-momentum equations on an unstructured grid; the normal component of velocity at an element side becomes the x-axis, while the tangential component becomes the y-axis.

The general algorithm for momentum and continuity equation solutions is as follows:

1. Solve the explicit portions of equations (3-1) and (3-2) for each side and invert the resulting matrices.

2. Insert the inverted matrices from equations (3-1) and (3-2) into equation (3-4) and solve.
3. Use the solution of equation (3-4) to solve the implicit portions of (3-1) and (3-2).
4. Solve equation (3-3) for vertical velocities.
5. Solve equations (3-5) and (3-6).

3.3.2 Coupled Model Architecture

Rather than develop a new model entirely from scratch, or take an existing underflow model and make it compatible with ELCIRC, we begin with the ELCIRC model itself. The underflow model is based on the ELCIRC code, and consists of a single vertical layer 2D solution of the ELCIRC algorithm. This use of the same basic code is done for simplicity; in this way, the underflow model can have the exact same horizontal grid as the larger 3D model to which it is coupled. In addition, maintaining the same solution methods between the two coupled models reduces the possibility of numerical error accumulation. To avoid confusion, the term "ELCIRC" will refer only to the pre-packaged model available from Oregon Health and Science University (http://www.ccalmr.ogi.edu/CORIE/modeling/elcirc/). The 3D portion of our coupled system will be referred to as the "ambient model" rather than ELCIRC, because for coupling purposes modifications must be made to it, as well. The gravity current model will be referred to as the "underflow model", and the ambient and underflow models operating as a cohesive model system will be referred to as the "coupled model system", or CMS.

To continue with the example basin depicted in Figure 3.1, the model domain for the coupled ELCIRC and underflow models is depicted in Figure 3.5. Figure 3.5a shows

that the space where the gravity current is flowing is actually *excluded* from the ambient model domain.

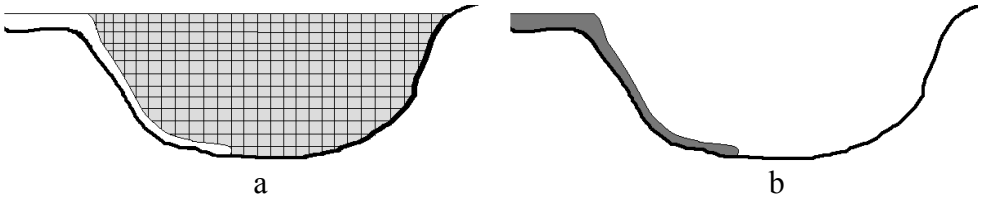

Figure 3.5: Coupled model domains: (a) the ambient model and (b) the underflow model.

The coupling scheme splits the modeled water column into an ambient portion and an underflow portion. The element column depicted in Figure 3.4 is split as shown in Figure 3.6.

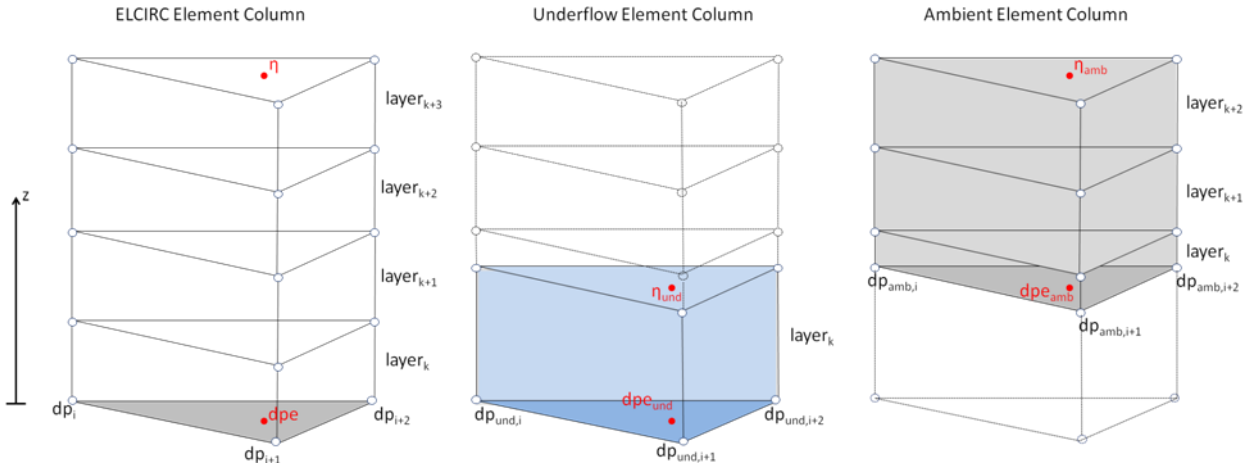

Figure 3.6: Element column representation in the ELCIRC model, the underflow model and the ambient model. A water column that would be modeled as a single vertical unit in 3D ELCIRC is split between the underflow and ambient models in the CMS.

The CMS created in this dissertation consists of two separate models with distinct computational domains that communicate at each time step to exchange boundary conditions and adjust surface elevations (for the underflow) and bottom boundary elevations (for the ambient) to be consistent. This is a distinction from other underflow models developed in the literature and summarized in Chapter 2, which do not allow a time-varying fluid displacement to alter the ambient model domain throughout a simulation (Dallimore et al 2003, Beckman and Doscher 1997, Killworth and Edwards 1999, Holland 2011, Danabasoglu et al 2010, e.g.).

The flow chart in Figure 3.7 represents the general CMS code structure. In the coupled model system, the ambient model serves as a shell that wraps around the underflow model. After the ambient model's setup algorithms (or the setup "routine") are complete, the model calls the setup routine for the underflow model. In the underflow setup routine, the initial underflow thickness is read in from input files. On completion of the underflow setup routine, the initial underflow thickness is used to modify the ambient model's initial vertical domain before timestepping begins.

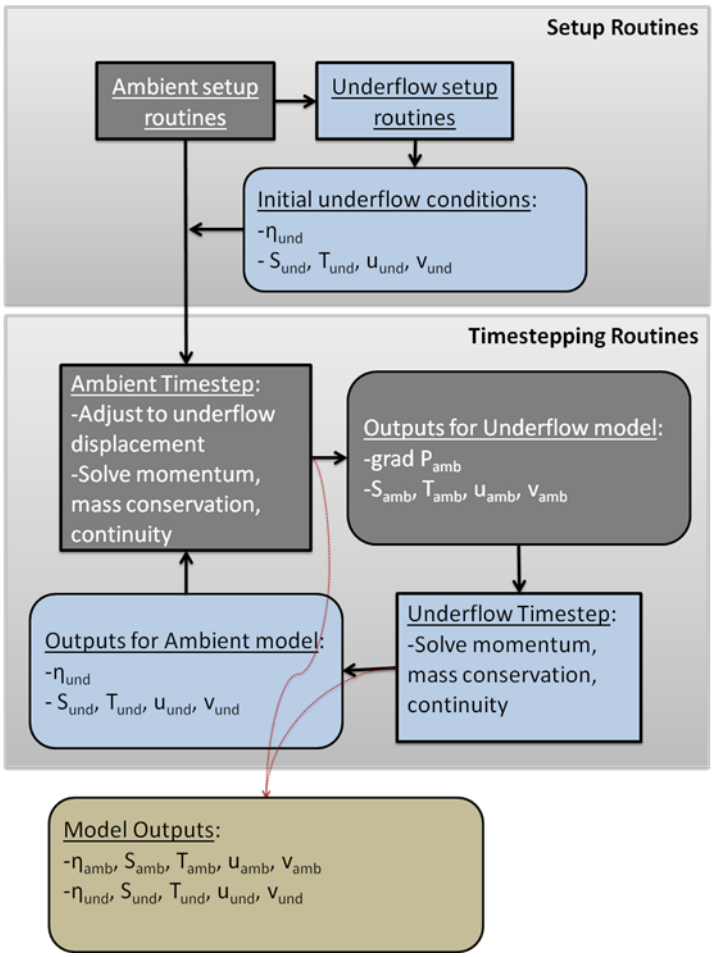

Figure 3.7: Coupled Model System Algorithm Architecture. Grey boxes indicate routines in the ambient model, blue boxes indicate routines in the underflow model and the brown box indicates model outputs. Boxes with sharp corners indicate algorithms, and boxes with curved corners indicate algorithm outputs. Black arrows represent information transfer from one routine to another, and red dashed arrows indicate data transfer for model outputs.

During the ambient model solution calculation, underflow model properties (velocities, temperature and salinity concentrations) are applied as boundary conditions for solving ambient momentum, mass and continuity equations. At the end of each ambient solution timestep, the ambient model calls the underflow model. During the

underflow model solution calculation, updated ambient model properties (density, barotropic pressure gradients, velocities, temperature and salinity concentrations) are applied as boundary conditions for solving underflow momentum, mass and continuity equations. After the underflow model time step is completed, the ambient model adjusts the bottom boundary location to account for displacement from the underflow model.

The interaction between models is first order explicit in time; the ambient and underflow models do not iterate between each other within a single time step. This coupling method is a limitation of the coupling algorithm.

The horizontal domain of both models extends to the entire basin's computational domain. Where the underflow is not present, the underflow model element is "dry", following the existing ELCIRC wetting and drying scheme. Similarly, where the ambient model is not present (upstream of an underflow plunge line, e.g.), the ambient model element is "dry".

3.4 ALGORITHMS

3.4.2 Ambient Model

To respond to the underflow model, the ambient model must be altered from its original ELCIRC code. Features must be included to account for a variable bed location and associated water column displacement, and also bed boundary conditions that allow viscous effects.

Displacement

Bed Displacement

Changes in bed elevation in the ambient model are dictated by shifts in η_{und} calculated in the underflow model. Underflow surface elevations are transferred to nodes using 3D ELCIRC's interpolation method, and are transferred to the ambient model. The

ambient model imports nodal underflow surface elevation changes, $\Delta\eta_{und}$, as a shift in ambient model bed elevation (see Figure 3.8).

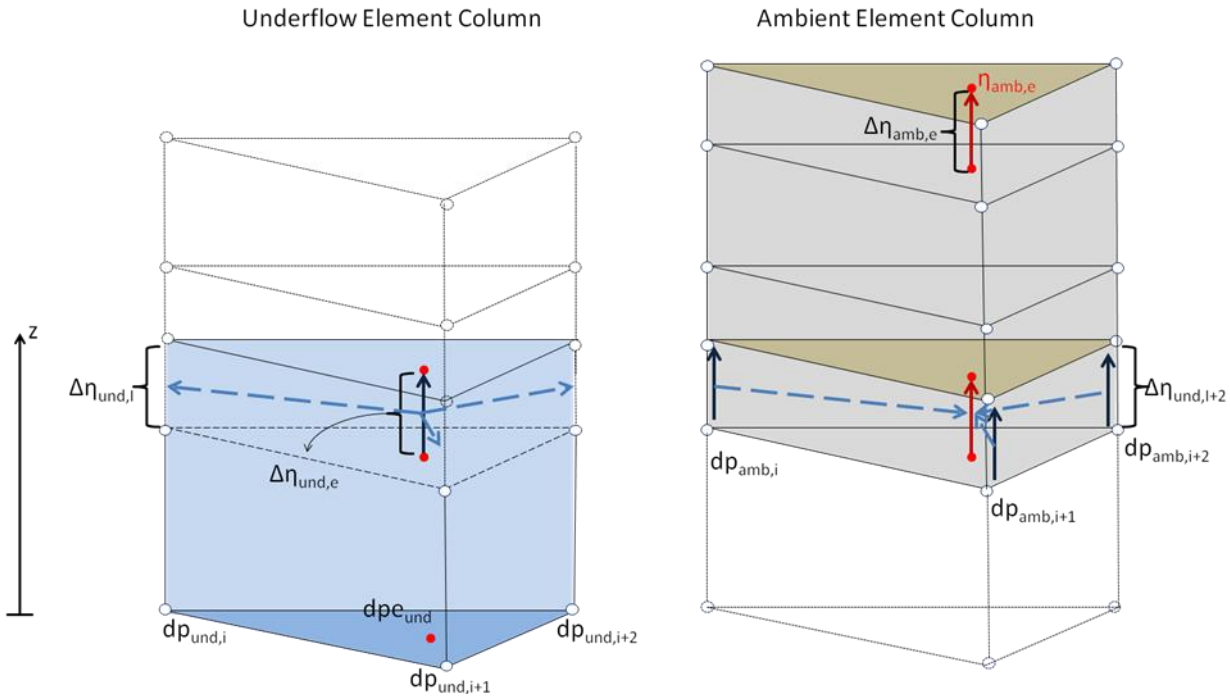

Figure 3.8: Element center bed displacement in the ambient model's bottom layer. $\Delta\eta_{und}$ is calculated at element centers in the underflow model (left) and translated to nodes. $\Delta\eta_{und}$ at nodes are read into the ambient model (right) and translated back to element centers, to calculate $\Delta\eta_{amb}$ for the displacement algorithm.

Free Surface Displacement

Bed displacement in the ambient model also translates to a displacement of the free surface, and a corresponding change in vertical velocity and flow properties throughout the water column. The free surface and vertical velocity variables are both stored at element centers (Figure 3.3). The ambient model interpolates bed elevation shifts ($\Delta\eta_{und}$) from nodes to element centers (Figure 3.8). When the bed is displaced in

the ambient model, the entire water column is pushed upwards. The free surface at the element center, η_{amb}, is moved up (or down) to exactly match the bed displacement.

Free surface displacement is applied as a forcing in the continuity equation. In this way, the displacement is included in the continuity and implicit portion of the momentum solutions. This method of incorporating displacement ensures that the horizontal velocity field reflects the displacement to the extent possible, and the resulting transport solutions do, as well.

Vertical Velocity Adjustment

Vertical velocity is stored in the element center, both vertically and horizontally. To account for motions associated with displacement, the displacement velocity is added to the velocity resulting from the governing equations in each layer of the water column to make the adjusted velocity, w*, at element m and layer n:

$$w_{m,n}^{*} = w_{m,n} + \frac{\Delta\eta_{amb,e}}{\Delta t}. \qquad 3\text{-}15$$

The vertical velocity is adjusted within the vertical velocity calculation at each time step. This allows the vertical velocity to be consistent with the continuity solution and horizontal velocity field. The velocity adjustment is also reflected in the transport equations.

Bottom Boundary Condition

Viscous effects are imposed on the interface between the underflow and ambient models as a corrector term after the momentum, continuity and transport equations have been solved. Exchange of diffusive temperature and salinity (and viscous momentum) between the underflow and ambient fluids is calculated as a diffusive (or viscous) mixing

length scale (consistent with process M_0 in Figure 3.1). The updated bed velocity $u_{amb,bot}$* is calculated as:

$$u^* = u + \frac{\partial}{\partial z}\left(\nu \Delta t \frac{\partial u}{\partial z_{av}} \right) \qquad 3\text{-}16$$

or in discretized form:

$$u_{amb,bot}{}^* = u_{amb,bot} + \frac{\frac{\nu \Delta t}{\Delta z_{av}}\left(u_{und} - u_{amb,bot}\right)}{\Delta z_{zmb,bot}} \qquad 3\text{-}17$$

where Δz_{av} is the average of the underflow thickness and the bottom ambient layer thickness, u is the "uncorrected" ambient bottom layer velocity, u_{und} is the underflow velocity and ν is molecular viscosity. In the above equation, the term $\frac{\nu \Delta t}{\Delta z_{av}}$ can be thought of a viscous mixing length. This algorithm is applied to normal and tangential velocities, and an analogous algorithm is also applied for temperature and salinity diffusivity at element sides and nodes.

As discussed in Chapter 4, molecular diffusion and viscous effects are only modeled in cases where other mixing processes (entrainment and wind mixing) do not take place. Because no mixing is included in the algorithms and test cases presented in Chapter 3, M_0 mixing is modeled for all test cases in this chapter.

3.4.1 Underflow Model

Because the underflow model uses the ELCIRC code as a basis, as does the ambient model, the basic solution method for solving the governing equations (3-7) through (3-11) are the same as 3D ELCIRC, with several modifications. Features of the underflow model include:

1. The coordinate system is terrain-following, so that terms involving gravitational acceleration must include the bed slope.

2. The 3D ELCIRC algorithm for calculating the free surface barotropic pressure gradient based on $\frac{\partial \eta_{amb}}{\partial x}$ is altered in the underflow model to calculate the underflow surface pressure gradient based on $\frac{\partial \eta_{und}}{\partial x}$; due to ambient fluid surrounding the underflow, g is replaced by g'.
3. The underflow momentum equation includes the barotropic pressure gradient from the ambient model.
4. An algorithm is included that accounts for viscous shear stresses across the interface with the ambient fluid.

These modifications highlight the physical differences between a gravity current flowing within a larger, less dense fluid system and a typical, unstratified fluid system being modeled in a 2D application of ELCIRC.

Terrain-following modifications

ELCIRC has a z-coordinate vertical grid. Vertical layers are fixed throughout the computational domain and do not vary with free surface oscillations. Layers are orthogonal and have bottom faces normal to the z-axis. The ELCIRC governing equations therefore do not include gravitational body forces. Gravity currents moving down slopes are impacted by along-slope components of body forces. Thus in the underflow model, the body force is included in the governing equations, so that along-slope acceleration is taken into account (as depicted in Figure 3.2). In addition, the underflow surface pressure term is rotated to account for the sloping bed (equations 3-7 and 3-8).

Underflow Surface Pressure Modifications

The 3D ELCIRC algorithm for calculating the free-surface barotropic pressure gradient is modified to calculate the pressure gradient at the underflow surface (rather than the free surface). In this transformation, the reduced gravity term g' replaces gravitational acceleration g in equations (3-7) and (3-8). Because the slab approximation represents the underflow as vertically uniform, baroclinic pressure gradients internal to the underflow itself can be neglected. Barotropic pressure gradients associated with the ambient fluid's free surface are captured separately and are discussed below.

Ambient Pressure Modifications

Some existing gravity current models treat the ambient fluid as sufficiently deep that barotopic pressure gradients can be neglected (Dallimore et al 2001, Bradford and Katapodes 1999). In cases of shallow ambient water, dynamics at the free surface can influence gravity current motion; an episodic gravity current exiting Oso Bay (Texas) has been observed to oscillate with the tidal signature (HFK11).

Considering a basin similar to that depicted in Figure 3.9, the coupled model system consists of a dense (dark blue in the figure) underflow contained in the domain of the "underflow" model, and a less dense (lighter blue in the figure) ambient water body contained in the 3D ELCIRC model.

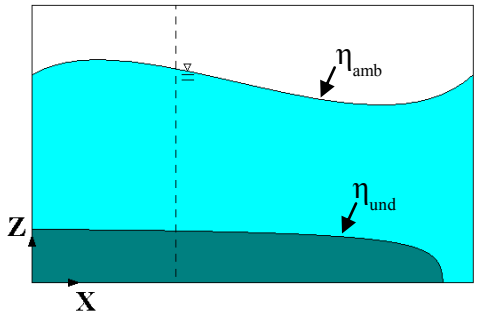

Figure 3.9: Sample basin depicting the domains of the coupled model system.

We make the approximation that barotropic pressure gradients are much larger than baroclinic pressure gradients withinin the ambient fluid, which are neglected in the underflow momentum equations.

Underflow Surface Boundary Conditions

The 3D ELCIRC surface boundary condition enforces wind shear, but otherwise allows a free-slip condition. In the case of an underflow, the underflow surface experiences shear at the interface with the ambient fluid (where ambient water is present above the underflow). Diffusive temperature and salinity, and viscous momentum, exchange between the underflow and ambient fluids is calculated as a diffusive (or viscous) mixing length scale $\frac{\nu\Delta t}{\Delta z_{av}}$ (consistent with process M_0 in Figure 3.1).

Like the ambient model, the underflow model reflects molecular kinematic viscosity at the underflow surface as a corrector term after the momentum equation has been solved. This is done for compatibility with the mixing algorithms discussed in Chapter 4. The updated underflow velocity u^*_{und} is calculated as:

$$u^*_{und} = u_{und} + \frac{\partial}{\partial z}\left(\nu\Delta t \frac{\partial u}{\partial z_{av}}\right) \qquad 3\text{-}18$$

or in discretized form:

$$u^*_{und} = u_{und} + \frac{\frac{\nu\Delta t}{\Delta z_{av}}\left(u_{amb} - u_{und}\right)}{\Delta z_{und}}. \qquad 3\text{-}19$$

This algorithm is applied to normal and tangential velocities, and an analogous algorithm is also applied for temperature and salinity diffusivity at element sides and nodes.

Front preservation

In order to prevent artificial diffusion of the gravity current front, ELCIRC's wetting and drying scheme is modified to limit flux out of elements at the underflow

front. This prevents the front from propagating from a partially filled element. All filling elements are designated as "frontal" elements. In addition to limiting flux out the front of frontal elements, the momentum and continuity equations are solved as though the frontal elements were all empty. This preserves the hydrostatic pressure gradient at the gravity current's front.

Plunging

Gravity currents in most physical systems result from dense fluids entering lighter fluids. In many cases, the dense fluid originates from a source in which it is not itself an underflow; this means that at some location there is a *plunge point* at which the dense fluid sinks below the lighter fluid (depicted in Figure 3.1). Before the dense fluid reaches this plunge line, it is at the free surface and is exposed to different forces than it is as an underflow. In cases where no ambient water is present above the underflow fluid, the model enforces wind boundary conditions on the underflow and applies a traditional barotropic pressure gradient calculation using the gravity term g, rather than g'.

3.5 DISPLACEMENT MODEL TEST CASES

Test cases are presented in this chapter to demonstrate CMS performance measured by both qualitative and quantitative metrics. Model results are compared with literature observations from the laboratory and the field. The test cases examine gravity current propagation, plunging, and displaced ambient fluid behavior.

3.5.1 Test Case 1: Inertial Flow Regime for a Deep Current

Test Case Configuration

This test case consists of a finite volume of dense fluid that is released into a rectangular channel with an ambient water depth much deeper than the initial dense fluid

depth. Theoretical analysis, corroborated by experimental results, indicates that this type of gravity current flow tends to have a constant initial velocity while the gravity current "slumps", followed by an inertial stage where buoyancy and inertial forces dominate. In this inertial stage, the current front propagates at a speed that scales on $t^{2/3}$ (Rottman and Linden 2002, Simpson 1997). The intertial stage can be characterized with a uniform-depth "slab" approximation, where the depth is fairly uniform throughout the gravity current. When viscous effects become large relative to other terms, the speed begins to scale on $t^{1/5}$ (Rottman and Linden 2002).

Although we compare model results with theory that is largely supported by laboratory scale experimentation, the basin simulated in Test Case 1 is designed to reflect scales observed in the environment, rather than the laboratory. The test basin is 50 km long, 250 m wide and 25 m deep. Initial dense fluid is 2.5 km long (x_0), 250 m wide and 2 m deep (h_0). Grid cells are 250 m long, 250 m wide and 0.75 m thick (in the ambient model). Time steps are set for a Courrant number of ~0.2. Figure 3.10 shows the dimensions of the model domain.

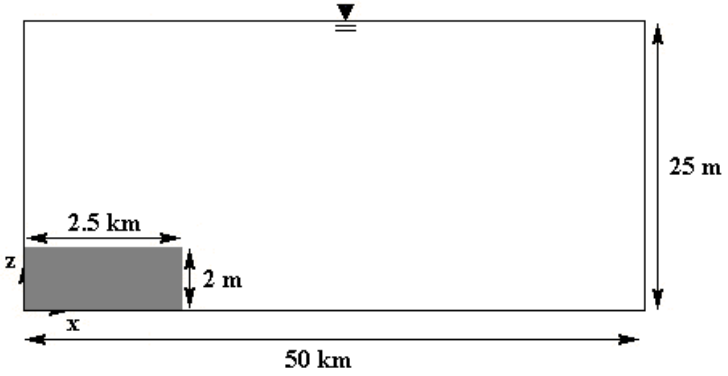

Figure 3.10: Initial conditions for the intertial phase test case. The grey rectangle is initial volume of dense fluid.

Because the horizontal scales of the initial conditions in Test Case 1 are so much larger than the vertical dimensions (1,250:1), the non-hydrostatic forces responsible for the slumping phase would not be expected. For Test Case 1 specifically, modeled viscosity has been turned **off**, preventing viscous effects from dominating front propagation. We therefore expect the underflow in Test Case 1 to propagate in the inertial phase.

Results

Figure 3.11 shows the profile of the gravity current at several time intervals. As demonstrated in the figure, rather than slumping, the current behaves as a uniform slab with fairly constant thickness. In this way, the CMS behaves as expected.

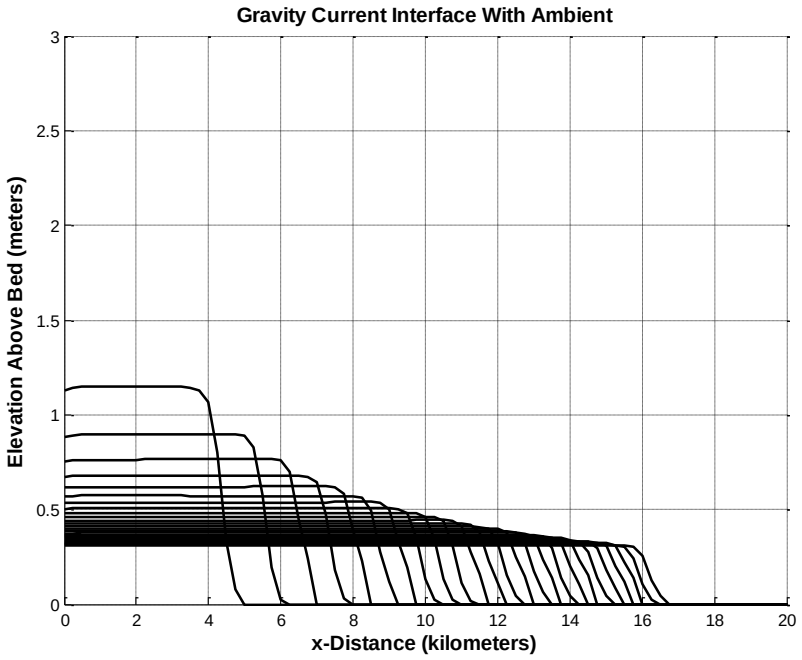

Figure 3.11: Gravity current propagation profiles at various time intervals.

Figure 3.12 contains a plot of the modeled gravity current front against elapsed time. The front follows a $t^{2/3}$ slope closely throughout the simulation. However, at later

times the slope begins to trail off from the 2/3 slope. It is possible that in the absence of modeled viscous effects, background numerical viscosity may be observable at slower velocities.

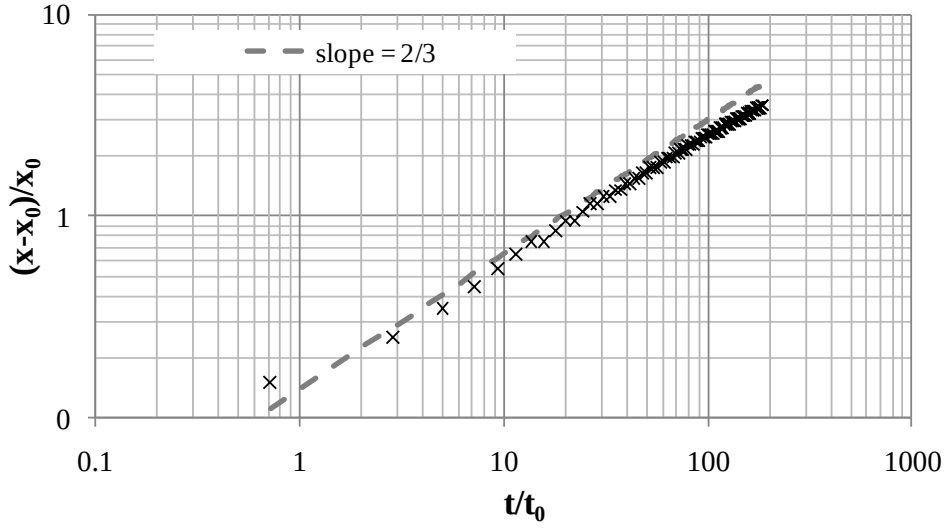

Figure 3.12: Gravity current front propagation compared with theoretical results. The dashed line represents a constant slope of 2/3 for comparison with model results. Time is normalized by t_0, which is x_0 divided by the initial wave speed.

For cases where bed roughness is increased, the slope decreases from 2/3 much more quickly, though it appears to converge to $t^{1/3}$ rather than the expected 1/5 for the viscous regime (Figure 3.13). For the simulation results presented in Figure 3.13, ν is 1 x 10^{-3} m^2/s, and C_D is 0.3. It is possible that if the simulation were allowed to run for longer, the slope would converge to $t^{1/5}$, but it is also likely that the absence of turbulent mixing (entrainment) in the model limits agreement with observations in the viscous regime.

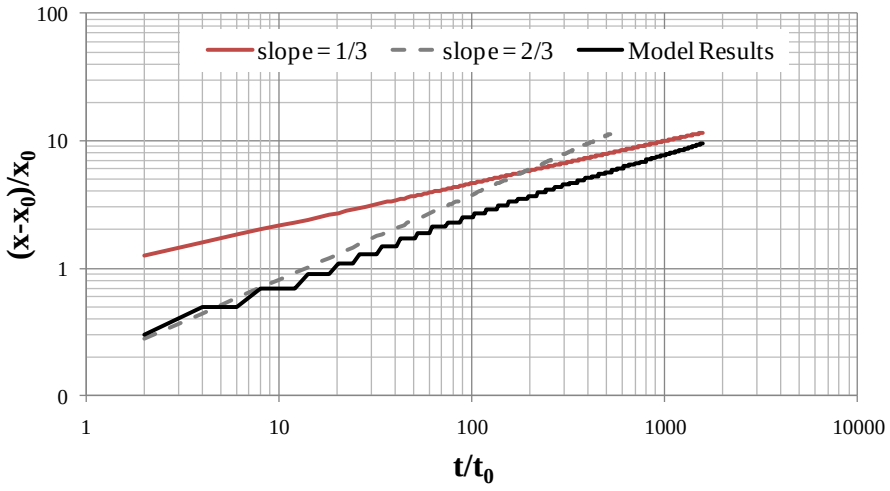

Figure 3.13: Gravity current front propagation compared with theoretical results. The dashed grey line represents a constant slope of 2/3, and the red line represents a slope of 1/3.

3.5.2 Test Case 2: Underflow Model Hydrostatic Limit

Configuration

Test Case 2 demonstrates the limitations of the underflow model in representing the non-hydrostatic nature of the slumping phase. Like the inertial phase test case, the hydrostatic limit test case consists of a finite volume of dense fluid that is released into a rectangular channel with an ambient water depth deeper than the initial dense fluid depth. Although the dimensions of Test Case 2 are also highly hydrostatic and would logically reflect flows in the inertial regime, the horizontal scale has been lowered by an order of magnitude compared with the inertial test case, and the vertical scale has been increased by a factor of 3 (Figure 3.14). This change in dimensions makes modeled initial stages of fluid flow (modeled representation of the slumping phase).

It is impossible to model a test case that is fully conducive to initial slumping using the underflow model discussed in this dissertation. The use of a single vertical layer for the underflow model makes capturing the bore-like phenomena that are

characteristic of the slumping phase impossible; by definition, vertical velocity gradients cannot be modeled with a depth-integrated model. This limitation of a slab approximation limits the initial dimensions of Text Case 2; higher initial dense water depths would not result in a converged numerical solution, because of the hydrostatic solution method in the underflow model. Coarsening the horizontal grid resolution results in poor resolution of the underflow-ambient interface.

The test basin is 5 km long, 25 m wide and 25 m deep. Initial dense fluid is 250 m long (x_0), 25 m wide and 6 m deep (h_0). Grid cells are 25 m long, 25 m wide and 0.75 m thick (in the ambient model). Figure 3.14 shows the dimensions of the model domain. The length:thickness ratio is 250:6.

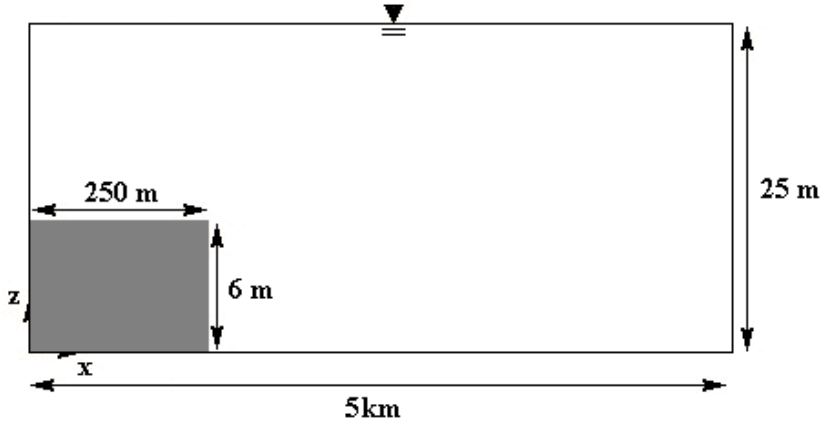

Figure 3.14: Initial conditions for Test Case 2. The grey rectangle is initial volume of dense fluid.

Results

Figure 3.15 shows the underflow surface profile at several time intervals. It is possible to see some non-uniformity in the underflow surface elevation. As the current propagates further (not shown), the profile approaches a slab shape similar to the profile associated with Test Case 1. It is also clear that, as expected, no bore is present in the

profile at any time. The dip in elevation close to the wall is the underflow model's closest approximation of a bore.

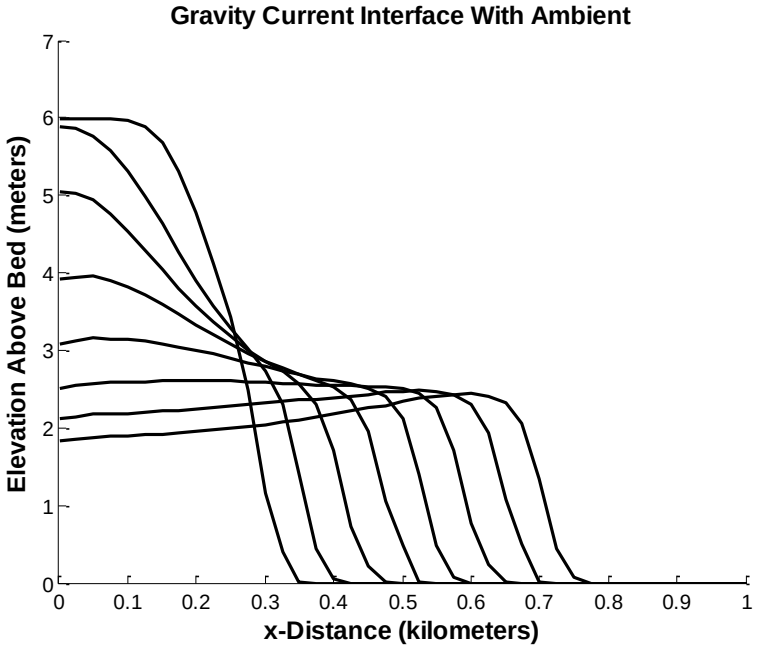

Figure 3.15: Gravity current propagation profiles at various time intervals.

3.5.3 Test Case 3: Plunging Underflow with Slight Bottom Slope

Test Case 3 demonstrates underflow propagation along a slope, modeled plunging, and fluid motions in the ambient model that result from fluid displacement. The test basin is 50 km long and 250 m wide. Using the coordinates in Figure 3.16 for orientation, basin depth is 2 m for almost 10 km, and thereafter slopes gently to 9.3 m over 40 km (slope is ~ 1:5,500). Initially, dense fluid occupies the shallow shelf, such that x_0 is 9.5 km, and h_0 is 2 m. Grid cells are 250 m long, 250 m wide and 0.75 m thick (in the ambient model). Figure 3.16 depicts the dimensions of the model domain.

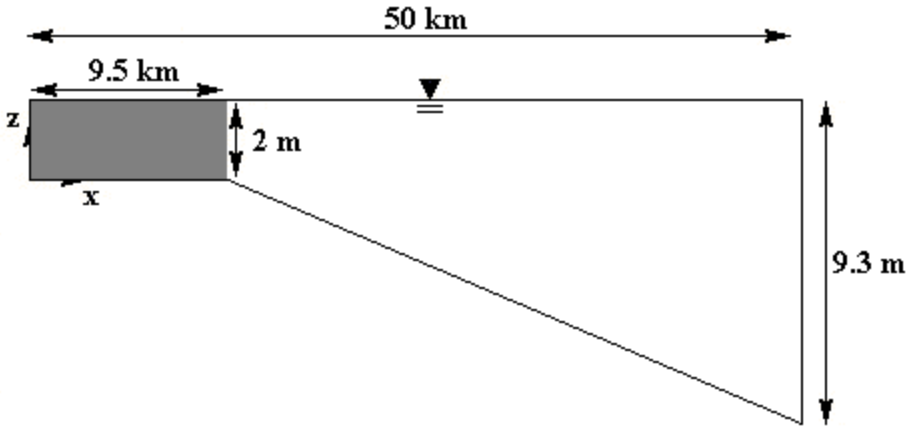

Figure 3.16: Initial conditions Test Case 3. Grey fluid is initial volume of dense fluid.

For the plunging test case, the left boundary in Figure 3.16 is an open boundary in the underflow model. The elevation is held constant at the boundary to maintain a 2 m depth in the underflow at the wall boundary. In the ambient model, the right boundary in Figure 3.16 is open and also has a fixed elevation, to prevent displaced ambient fluid from building up in the test basin. Viscosity is set to molecular levels in both models for this test case, and the friction coefficient C_D is 0.005. As with the other test cases in this chapter, g' is 0.13 m^2/s.

Results

Figure 3.17 shows the profile of the gravity current at several time intervals. As demonstrated in the figure, the current plunges approximately where the bed slope changes. At later time steps when the current reaches the wall, the underflow begins to fill the basin.

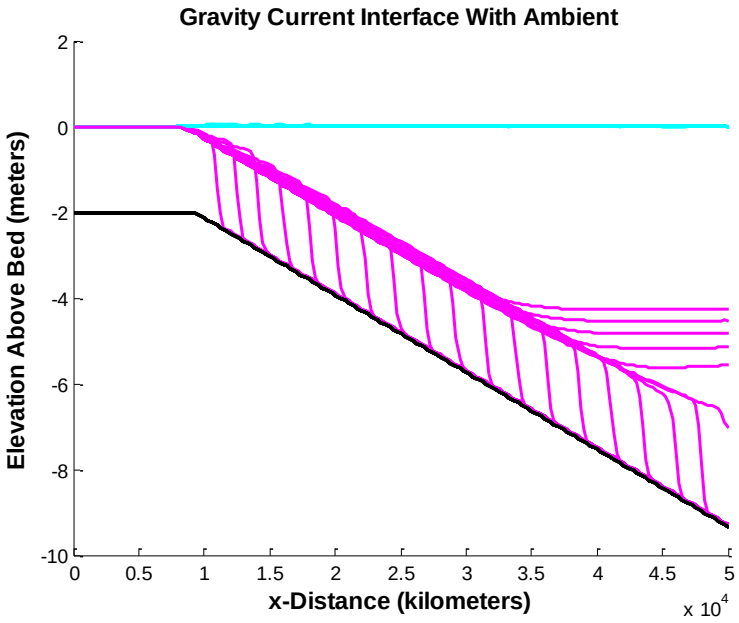

Figure 3.17: Underflow (magenta) and ambient (cyan) surface profiles at various time intervals.

The plunging test case is simulated with several variants of fixed flowrates per unit width (q). Results are compared with relationships for plunge depth developed by Singh & Shah (1971), Savage & Brimberg (1975) and Akiyama & Stefan (1984) in Figure 3.18. The figure shows that our underflow model is in fairly good agreement with Akiyama & Stefan, which is the relationship most specific to a mild slope. Akiyama and Stefan define a mild slope as less than 1/10, and compare their plunge depth formula with observations from a slope of 1/1,000. The slope in the plunging test case presented in the present work is 1/5,500. The increased mildness of the slope in the plunging test case compared with those on which Akiyama and Stefan's relationship is based may explain the slight discrepancy between the CMS results and the formula.

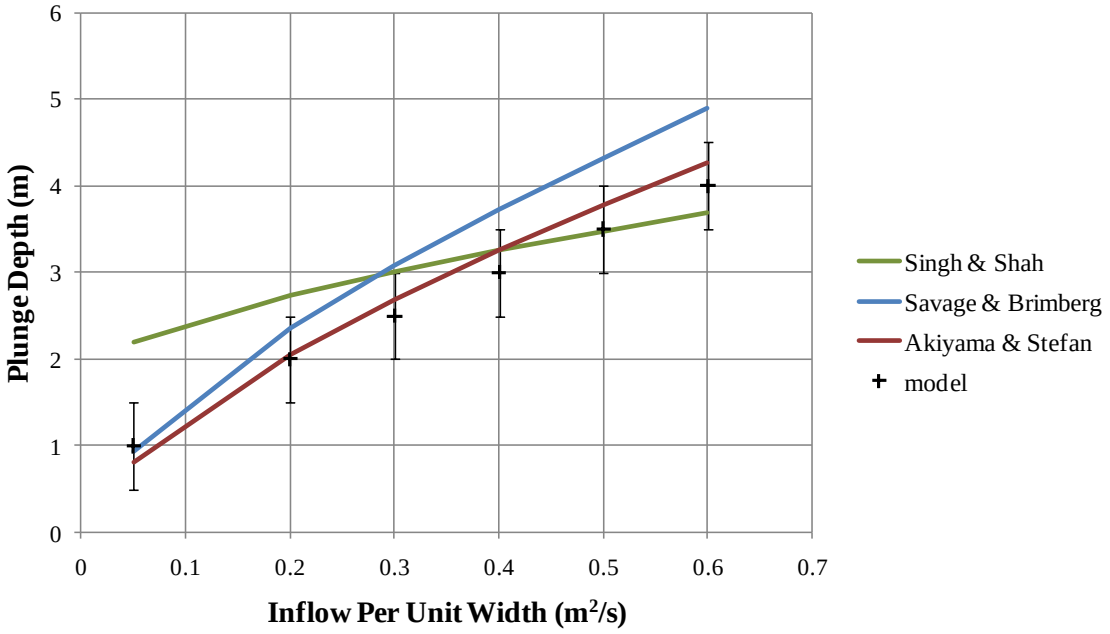

Figure 3.18: Modeled plunge depths compared with empirical relationships in the literature.

Displacement Influence on Ambient Velocity Field

The plunging test case can also be used to examine how the underflow model influences the ambient fluid's flow field. In basins where underflow fluxes are non-negligible compared with other fluxes, this feature is essential for accurately modeling the ambient flow field. Figure 3.19 shows the velocity field of the ambient fluid during a plunging simulation where $q_0 = 0.4$ m^2/s. The velocity field reflects ambient water leaving the area where the underflow is entering, with an upward and outward motion. Without the displacement feedback mechanism demonstrated in this model, the flow field would not be captured by the coupled model system. While displacement itself is a vertical process, the resulting barotropic pressure gradient induced a horizontal flow to compensate for the displacement.

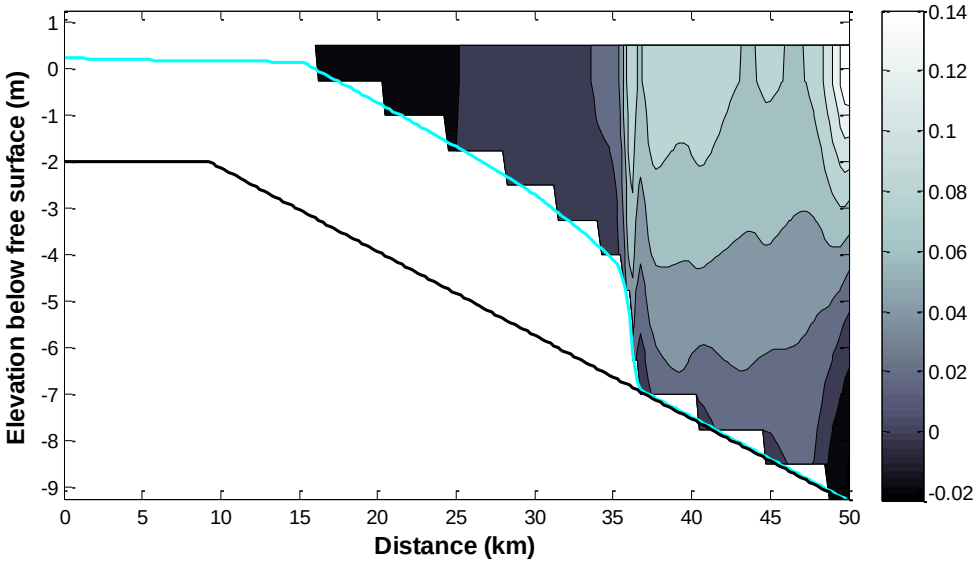

Figure 3.19: Ambient fluid velocity field during plunging. The scale to the right is of velocity (m/s). The cyan line in the plot is the underflow modeled surface. The black line is the bed elevation.

3.6 CONCLUSIONS

This chapter presents the CMS conceptual model and numerical model architecture. The model architecture is efficient in its use of the same basic code for both the underflow and ambient model; this facilitates model coupling. Coupling algorithms are also presented. Most coupled field-scale models in the literature do not represent ambient fluid displacement by an underflow; this is a contribution to science and engineering that facilitates modeling studies of shallow, stratified systems.

Test cases presented in this chapter show that the displacement model represents underflow in the inertial regime well when compared with theoretical and laboratory-based spreading rates. The model also represents the viscous regime fairly well on a field scale, though modeled momentum decay in the viscous regime is lower than expected. It is possible that including a better parameterization of shear in the absence of entrainment would increase momentum decay at lower Re. The CMS's spreading and displacement

mechanisms allow the underflow to respond to slope and hydrostatic pressure gradients, and also allow ambient fluid to respond appropriately.

Test cases presented in this chapter also examine the limits imposed by capturing a non-hydrostatic phenomena, a dense underflow, with a hydrostatic model. Initial slumping is not possible to model with the CMS. While plunging is also not a hydrostatic process, the CMS represents plunging well enough that in larger environmental, field scale applications, modeled plunging should not introduce large errors into the model.

Other limitations of the CMS displacement model are related to the explicit nature of the coupling method, and also to the simplistic pressure representation in the underflow model – ambient baroclinic pressure gradients and atmospheric pressure gradients are both considered negligible compared with other forces in the underflow model. While this may be appropriate for most shallow systems, it may be a limitation for some systems.

Chapter 4: Mixing Model

4.1 INTRODUCTION

The previous chapter presented the Coupled Model System (CMS) conceptual model and model architecture. This chapter presents the mixing algorithms used in the CMS. It presents the conceptual mixing model, discusses the algorithms for numerical implementation, and presents test cases demonstrating model performance.

The mixing model of the CMS reflects turbulent mixing in two directions: ambient fluid entrainment into the gravity current, and also underflow mixing into the ambient fluid due to wind mixing. Both mixing types are calculated independently, and mixing in either direction impacts both the ambient and underflow models. The amount of fluid entrained into the underflow model is a function of velocity shear and slope, while the amount of fluid mixed into the ambient fluid from the underflow is a function of wind magnitude and the level of stratification. Where turbulent mixing does not occur, the molecular diffusion and viscosity are imposed at the underflow-ambient model interface (described in Chapter 3).

The CMS is engineered to be flexible, so that it can be made compatible with a wide array of fluid systems. Both the wind mixing and entrainment algorithms are easily replaced by empirical relationships that have been calibrated to field data, or may be more representative of mixing in the basin being modeled. The algorithms presented in this dissertation are representative algorithms that demonstrate the capabilities of the CMS, and are also thought (based on preliminary field data) to be representative of the Corpus Christi Bay-Oso Bay system.

4.2 CONCEPTUAL MIXING MODEL AND GOVERNING EQUATIONS

The mixing model uses the conceptual model described in Chapter 3 as a basis. The model consists of a generic basin with a dense fluid at the basin's bed. Figure 4.1 shows a 2D example of a basin represented in the conceptual model.

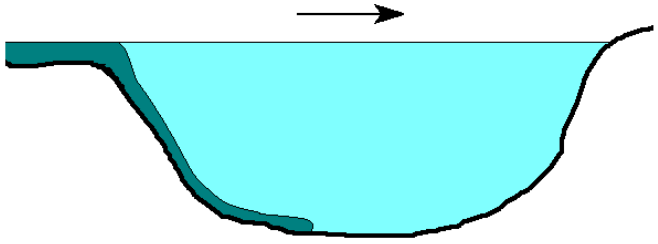

Figure 4.1: A typical basin represented by the conceptual model. Dense fluid is represented with darker blue.

4.2.1 Coupled Model System

If the underflow spreads, it may entrain ambient fluid into it. This will increase the volume of the underflow, decrease the volume of the ambient fluid, and it will also decrease the underflow's density. Where entrainment into the underflow does not occur, viscous and diffusive effects across the underflow-ambient model interface will impact transport variables and momentum. Where entrainment does occur, diffusion and viscous effects are likely negligible compared with turbulent mixing lengths associated with entrainment and are therefore neglected.

The conceptual model is designed for shallow systems where the wind mixed layer extends through the ambient water column. In the CMS conceptual model, energy transferred to the water body from the wind directly impacts mixing between the ambient and underflow fluids. This treatment of wind energy is an integral component of the shallow-water application for the model developed in this dissertation, and it is a major difference between the model developed in the present work and other models

using a uniform slab gravity current representation (Dallimore et al 2003, Beckman and Doscher1997, Killworth and Edwards 1999, Holland 2011, Danabasoglu et al 2010).

As wind blows across the conceptual basin's free surface, turbulence erodes the surface of the underflow following typical wind mixed layer deepening in water bodies (Spigel et al 1986, Kraus and Turner 1967). This will increase the ambient fluid's volume and salinity. It will also decrease the underflow volume. Where mixing into the ambient fluid does not occur, viscous and diffusive effects across the underflow-ambient model interface will impact transport variables and momentum. Where mixing does occur, diffusion and viscous effects are likely negligible compared with turbulent mixing lengths associated with wind mixing.

Mixing Direction and Leakage

Figure 4.2 shows the mixing model components, including entrainment, wind mixing and diffusion. The conceptual model's governing equations define the motions of the underflow and ambient fluid, and mixing between the two. Both mixing conceptualizations, entrainment into the underflow and into the ambient fluid, are based on the concept of defining a mixing length over which the turbulent kinetic energy (TKE) in the entraining model is capable of mixing fluids between models in a time step. The fluid that is the source of the mixing energy is assumed to engulf all fluid over the mixing length, as it is the model containing the TKE responsible for the mixing (as shown in Figure 4.2). This differs from traditional Reynolds-averaged turbulent mixing, where mixing is assumed to mutually influence both sides of a mixing interface, rather than being entirely engulfed by one side (as essentially a diffusion coefficient that represents turbulent mixing). In the CMS, mixing in both directions can occur simultaneously at the

same interface, because the two mixing forms are calculated completely independently of each other.

Where turbulent mixing does not occur, a mixing length equivalent to diffusive (in the case of scalars) and momentum fluxes is calculated, as discussed in Chapter 3. Where mixing only occurs in one direction, diffusion is applied to the non-mixing fluid only. For example, where there is no wind but the underflow is entraining ambient fluid, diffusion and viscous effects will be applied to the ambient fluid's bottom boundary.

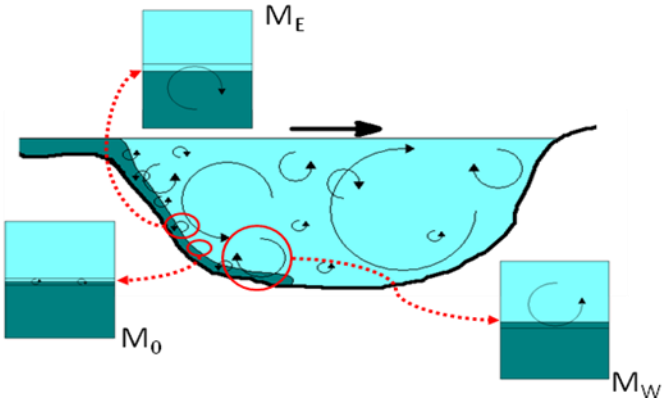

Figure 4.2: Conceptual mixing model. A 2D representation of the conceptual mixing model components, which include mixing into the underflow from entrainment (M_E), mixing into the ambient model due to wind mixing (M_W), and diffusion and friction across the model interface, where turbulent mixing does not occur (M_0, discussed in Chapter 3).

4.2.2 Underflow Entrainment

Entrainment into the underflow occurs where the underflow is moving quickly relative to the ambient fluid. Consistent with entrainment laws in the literature presented in Chapter 2, TKE leakage is treated as negligible, resulting in an entirely *one-way flux* of fluid (Dallimore et al 2001, Sherman et al 1978). A schematic of the entrainment represented in the conceptual model is presented in Figure 4.3, where ambient fluid

entrained into the underflow increases the volume of the underflow, and also alters the depth-averaged fluid properties.

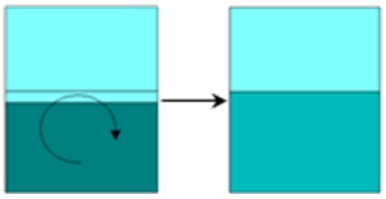

Figure 4.3: Entrainment (M_E) as represented in the conceptual model. Density is represented on a color gradient, where darker blue represents denser fluid. As the dense lower layer entrains lighter fluid, its density decreases. The upper, lighter fluid's density remains unchanged.

As discussed in Chapter 2, entrainment of ambient fluid into the underflow is governed by the TKE within the underflow. Many equations have been developed in the literature that describe the rate of this entrainment E, where

$$E = \frac{w_e}{U}. \qquad 4\text{-}1$$

In the above equation, w_e is the bulk vertical velocity of fluid into the underflow and U is the velocity difference between the ambient and underflow fluids. In Chapter 2 we demonstrate the similarity among various entrainment rate calculations in Corpus Christi Bay, which implies that increased sophistication does not necessarily result in increased model accuracy. For this reason, this dissertation uses a simple algorithm, developed by Bo Pedersen (1986):

$$E = 0.072\sin\theta \qquad 4\text{-}2$$

where θ is the bed slope. This formula relies on slope alone to calculate entrainment, and is based on empirical data on slopes ranging from close to 1:1 to $1:10^4$. This simplistic representation of entrainment may pose a model limitation, as it may not apply to all physical systems; where little or no bottom slope is present this algorithm may under-represent entrainment.

As ambient fluid is entrained into the underflow, the underflow volume per unit area can be expressed as a mixing length. The mixing length representative of entrainment over a time period δt is $w_e \delta t$, equivalent to $EU\delta t$ using equation (4-1). The underflow's salinity, temperature and momentum are affected by this entrained fluid. As entrained fluid enters the underflow conceptual model, it is simultaneously leaving the ambient fluid. The ambient-underflow interface moves accordingly.

4.2.3 Ambient Fluid Wind-Induced Mixing

Turbulent kinetic energy in the ambient fluid is supplied the wind, and as a result ambient fluid may engulf underflow fluid. The vertical mixing that takes place over a time period δt as a result of a wind speed U_W is limited by both the energy provided by the wind and the potential energy associated with lifting the dense underflow fluid. The conceptual model calculates wind mixing as a thickness of the underflow water column, δh, that is entirely mixed into a thickness H_{amb} of the ambient water column over a time period δt (Figure 4.4). The mixing length is calculated such that all energy transferred to the water column by the wind over δt is available for mixing the underflow. This calculation limits model applicability to shallow systems where the wind mixed layer extends vertically through the ambient water column. Following the parameterization established in Hodges et al 2011 and discussed in Chapter 2, mixing length δh is calculated as:

$$\delta h = -C_m C_N^3 \left(C_D \frac{\rho_{air}}{\rho_{amb}} \right)^{3/2} \frac{\rho_{amb}}{g\Delta\rho} \frac{U_w^{\ 3}}{H_{amb}} \delta t , \qquad 4\text{-}3$$

where C_m, C_N, and C_D are mixing coefficients, whose values are established as 0.2, 1.33 and 1.4×10^{-3}, respectively (Hodges et al 2011). The thickness of the ambient water column over which the underflow fluid fully mixes within δt is H_{amb}, the density of the ambient fluid is ρ_{amb}, and the density anomaly associated with the underflow is $\Delta\rho$.

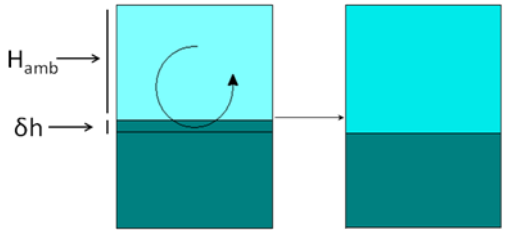

Figure 4.4: Wind mixing as represented in the conceptual model. Density is represented on a color gradient, where darker blue represents denser fluid.

4.3 NUMERICAL MIXING MODEL ARCHITECTURE

Mixing and diffusive fluxes are calculated after the momentum and continuity routines in both the underflow and ambient models. The underflow model both adjusts for underflow fluid lost to the ambient model, and also calculates ambient fluid entrained into the underflow. Likewise, the ambient model both adjusts for fluid lost into the underflow and also underflow fluid engulfed into the ambient model. A schematic showing how the mixing algorithms fit into the numerical model developed in Chapter 3 is shown in Figure 4.5.

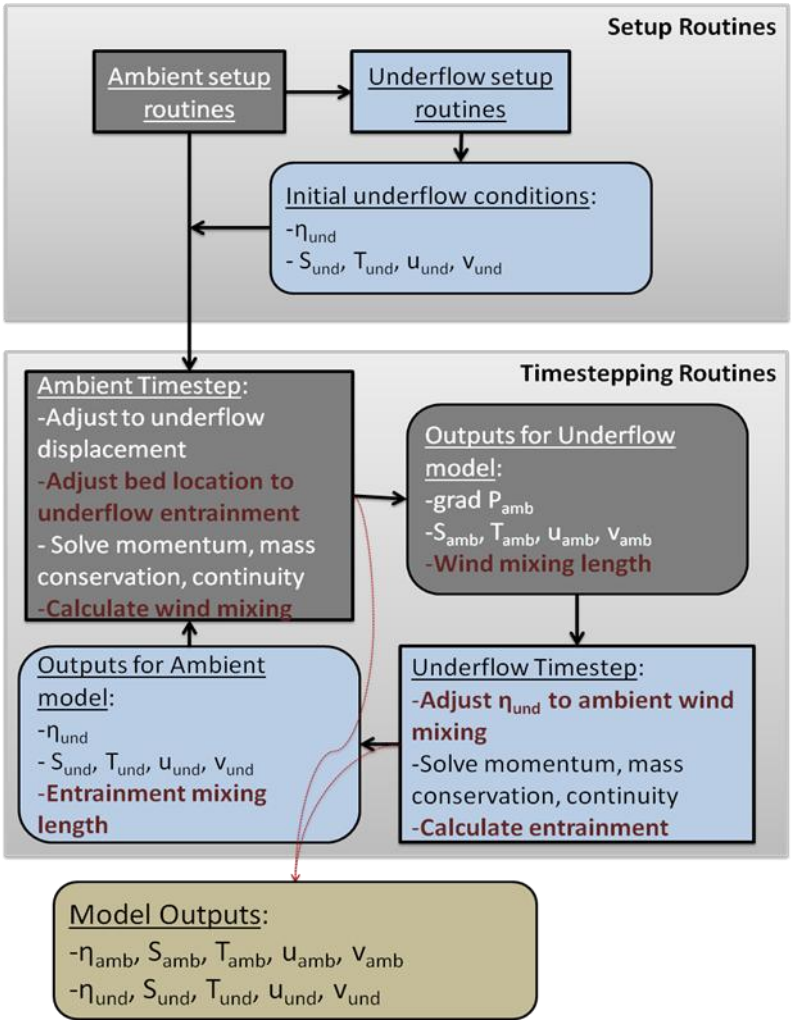

Figure 4.5: Coupled Model System Algorithm Architecture. Grey boxes indicate routines in the ambient model, blue boxes indicate routines in the underflow model and the brown box indicates model outputs. Boxes with sharp corners indicate algorithms, and boxes with curved corners indicate algorithm outputs. Black arrows represent information transfer from one routine to another, and red dashed arrows indicate data transfer for model outputs. Red text indicates algorithms and data transfers related to the mixing model.are Other parts of the schematic are described in Chapter 3.

4.4 ALGORITHMS FOR ENTRAINMENT INTO THE UNDERFLOW MODEL

4.4.1 Entrainment Algorithm

In the initial underflow model setup routine, entrainment rates E are calculated for each element side according to equation (4-2). Mixing lengths representing entrainment into the underflow are calculated after the underflow momentum and continuity equations have been solved for surface elevations η_{und} at element centers and normal and tangential velocities u_{und} and v_{und} at element sides (see Chapter 3). A vertical entrainment velocity of ambient fluid into the underflow is then at calculated at each side j of an element as:

$$w_{e,j} = E\sqrt{u_{und,j}^{\ 2} + v_{und,j}^{\ 2}} \qquad 4\text{-}4$$

The vertical entrainment velocity is used to calculate the change in underflow side depth due to entrainment into the gravity current: The mean of $w_{e,j}$ over all sides in model element m, $\overline{w_{e,j}}$, is multiplied by the model timestep Δt to determine the depth change at the element center (where η_{und} is stored). The updated surface elevation η_{und}' for element m is then:

$$\eta_{und,m}' = \eta_{und,m} + \Delta t\overline{w_{e,j}} \qquad 4\text{-}5$$

The schematic in Figure 4.6 depicts entrainment length calculation at element sides and the element center.

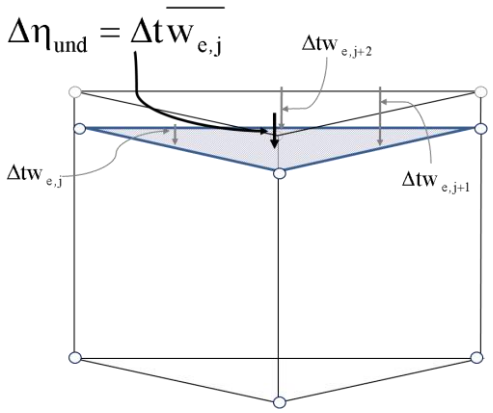

Figure 4.6: A sample underflow model element entraining ambient fluid of thickness $\Delta t\overline{w}_{e,j}$.

4.4.2 Mass Balance Algorithm

As entrainment incorporates ambient fluid into the underflow, momentum, salinity and temperature from the ambient fluid are also incorporated. The velocities, temperatures and salinities of the underflow sides and nodes are therefore updated by a simple mass balance equation reflecting the engulfed fluid. For a generic underflow variable β_{und} at element node i,

$$\beta_{und,i}' = \frac{\beta_{und,i} h_i + \beta_{amb,i,bot} \Delta tw_{e,i}}{h_i + \Delta tw_{e,i}} \qquad 4\text{-}6$$

where $\beta_{amb,i,bot}$ is the variable's value in the ambient model layer immediately above the underflow-ambient interface, and h_i is the underflow water column thickness before entrainment ($\eta_{und,i} + dp_{und,i}$). Equation (4-6) is solved at element sides for normal and tangential velocities, and at both element sides and nodes for salinity and temperature.

4.4.3 Impacts on the Ambient Model

We use 3D ELCIRC's area-weighted algorithm for interpolating elevation values from element centers to nodes (Zhang et al, 2004). Changes in bed elevation in the

ambient model are read in at nodes, and projected to sides and element centers (similar to the ambient model displacement from underflow spreading, discussed in Chapter 3). Ambient fluid entrained into the underflow is removed from the ambient model after the underflow timestep is completed (see Figure 4.5). Because the entrainment algorithm approximates leakage as negligible , the ambient model fluid properties do not change as a result of underflow entrainment. If future model revisions alter the leakage approximation, ambient flow properties may be impacted by underflow entrainment.

Entrainment into the underflow, and diffusive and viscous effects, is limited by the vertical thickness of the ambient and underflow model domains. The underflow mixing algorithm does not allow underflow entrainment to completely engulf the ambient model so that it disappears; a minimum depth of 5 mm of ambient water column is maintained in the ambient model from entrainment algorithms. In the event that a calculated entrainment mixing length reaches this limit, the ambient model element will be treated as dry.

4.5 ALGORITHMS FOR MIXING INTO THE AMBIENT MODEL

Wind-Induced mixing into the ambient model is limited to the thickness of the underflow. Full mixing of underflow fluid into the ambient model is allowed numerically, as the time scale for full mixing is of interest in many fluid systems, and is physically possible in a shallow system.

In modeled fluid systems where a very thin ambient fluid (on the order of a few centimeters, for example) propagates over an underflow that is an order of magnitude or more thicker than the ambient, the potential energy required to mix the water column may be low enough to mix the entire underflow into the thin ambient fluid. While this mixing may be representative of physical mixing, is would result in dense water entering

the ambient model. This phenomena defeats the purpose of the CMS, which is to retain density gradients by dseparating dense fluid and

The ambient model can only entrain underflow fluid if the ambient fluid is deeper than 10 cm. This arbitrary, unphysical threshold is necessary to prevent the underflow model from emptying into the ambient model in the event of a thin ambient overflow. A thin ambient fluid results in low wind requirements for full water column mixing. The CMS represents this mixing by removing the underflow fluid from the underflow model, and placing it into the ambient model. Where the ambient fluid is thin, little mixing will occur in this process. This transfer of underflow fluid into the ambient model with potentially negligible mixing undermines the purpose of the CMS, which is to keep dense fluid in the underflow model until it mixes with ambient fluid. This ad hoc mixing limit may limit CMS functionality in extremely shallow systems where the ambient fluid is on the order of 10 cm thick.

4.5.1 Wind Mixing Algorithm

The mixing model only represents mixing into the bottom layer of the ambient model; mixing among vertical layers in the ambient model is resolved by the ambient ELCIRC model. Mixing lengths Δh_{amb} are calculated at nodes in the ambient model (Figure 4.7) using equation (4-3). For node i, the mixing length Δh_{amb} is calculated as:

$$\Delta h_{amb,i} = -C_m C_N^3 \left(C_D \frac{\rho_{air}}{\rho_{amb,i,surf}} \right)^{3/2} \frac{\rho_{amb,i,bot}}{g\Delta\rho_i} \frac{U_{W,i}^3}{\Delta z_{amb,i,bot}} \Delta t \qquad 4\text{-}7$$

Where $\rho_{amb,i,surf}$ is the density at node i in the ambient model's top layer, $\rho_{amb,i,bot}$ is the density at node i in the ambient model's bottom layer, $U_{W,i}$ is the wind speed at node i, $\Delta\rho_i$ is $(\rho_{amb,i,bot} - \rho_{und,i})$, and $\Delta z_{amb,i,bot}$ is the vertical thickness of the ambient model's bottom layer at node i. After the mixing length $\Delta h_{amb,i}$ is projected to element centers, it

is in turn used to lower the volume of the underflow. TKE in the bottom layer of the ambient model is not lowered to account for TKE consumed in the mixing process – this is a model limitation that may impact the ambient model's turbulence closure.

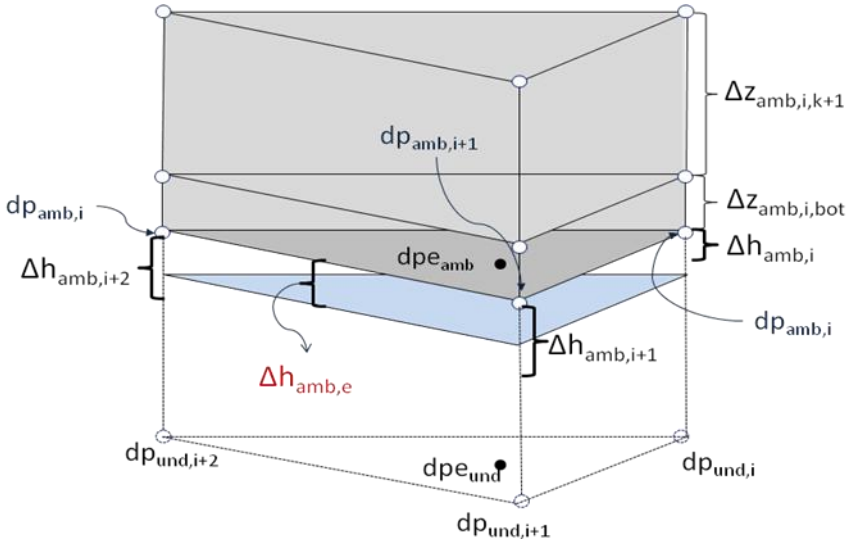

Figure 4.7: Wind mixing length Δh_{amb} calculation at ambient model nodes in a grid element column. The mixing length interpolated to the element center is $\Delta h_{amb,e}$. The shaded volume represents ambient modeled layers. The clear volume represents the underflow model layer. The blue plane represents the elevation to which the ambient bottom boundary (dpe_{amb} at the element center) will move as a result of mixing underflow fluid over a mixing length $\Delta h_{amb,e}$. The blue also represents the elevation to which the underflow surface η_{und} will move as a result of wind mixing.

4.5.2 Wind Mixing Mass Balance

The velocities, temperatures and salinities of the ambient model's bottom layer sides and nodes are updated by a simple mass balance equation reflecting the engulfed fluid. For a generic ambient variable $\beta_{amb,bot}$ at node i,

$$\beta_{amb,i}{}' = \frac{\beta_{amb,i,bot}\Delta z_{amb,i,bot} + \beta_{und,i}\Delta h_{amb,i}}{\Delta z_{amb,i,bot} + \Delta h_{amb,i}} \qquad 4\text{-}8$$

Equation (4-8) is solved at element sides for normal and tangential velocities, and at both element sides and nodes for salinity and temperature.

4.5.3 Impact of Wind Mixing on Underflow Model

The bed elevation change calculated in the ambient model is projected to ambient element centers $\Delta h_{amb,e}$. This mixing length at element centers is subtracted from underflow surface elevations η_{und} at the beginning of the underflow timestep (see flow chart, Figure 4.5). Because wind mixing is removing fluid from the underflow (rather than adding fluid to it), no adjustments are made for velocity, salinity or temperature changes.

4.6 TEST CASES

This Chapter includes two test cases, which demonstrate both wind-induced mixing and entrainment into the underflow. Both test cases compare CMS performance with a 3D ELCIRC simulation of the same configuration. The first test case consists of a dense fluid on a shallow shelf plunging down a gradual slope into lighter fluid. This first test case demonstrates modeled entrainment. The second test case consists of a flat, idealized basin with two distinct vertical layers (separated into the underflow and ambient models). Wind is blown across the surface, allowing a comparison of modeled wind mixing with expected mixing based on scaling arguments.

4.6.1 Gravity Current Propagating Down a Slope

Configuration

For the down-slope test case we compare the most finely resolved 3D ELCIRC application of the test case with the CMS representation of the same configuration. The test basin is 50 km long and 250 m wide. Using the coordinates in Figure 4.8 for orientation, the basin is 1 m deep for the first 9.5 km, and thereafter slopes gently to 8.3 m over 40 km (slope is ~ 1:5,500). Initially, dense fluid occupies the shallow shelf. Grid

cells are 250 m lon and 250 m wide. Vertical layers are 75 cm thick in the ambient model for the CMS simulation, and they are 5 cm thick in the 3D ELCIRC simulation.

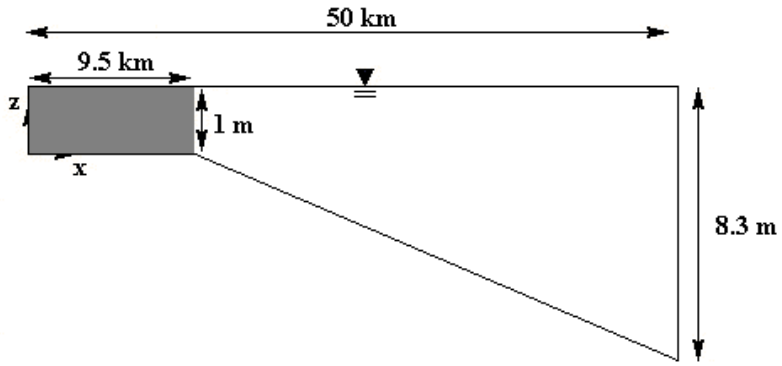

Figure 4.8: Test case basin profile. The gray area in the figure represents initial dense fluid.

For this test case, the left boundary in Figure 4.8 is an open boundary in the underflow, with elevation held constant to maintain a 1 m depth. In the ambient model, the right boundary in Figure 4.8 is open and also has a fixed elevation, to prevent displaced ambient fluid from building up in the test basin. Viscosity is set to molecular levels, the friction coefficient C_D is 0.005, and the initial g' is 0.13 m^2/s. Chapter 3 demonstrates the good agreement between the CMS modeled plunging and the relationship developed by Akiyama and Stefan (1984). For this configuration, the Akiyama and Stefan relationship estimates a plunging depth of about 1 m.

Results

CMS results for sloping test case are shown in Figure 4.9b, with color contours displaying salinity. The plunge line of the CMS underflow is consistent with Akiyama and Stefan (1 m, see discussion in Chapter 3), while the plunge depth modeled in 3D ELCIRC is deeper (2.8 m, see Figure 4.9a). The propagation speed of the underflow is

also faster in the underflow model, which can be seen by the location of the gravity current front in Figure 4.9.

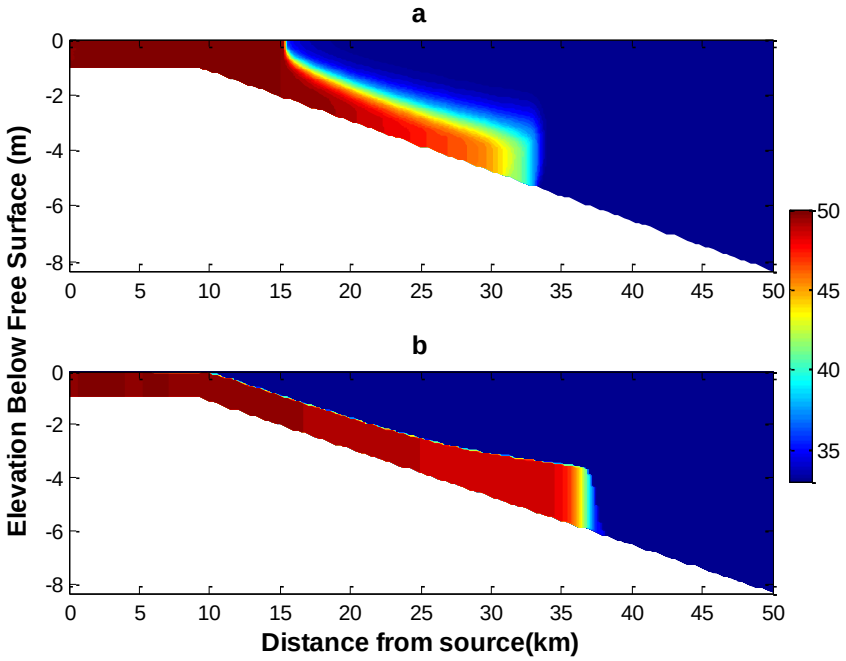

Figure 4.9: Salinity profile after 5 days of simulation time for (a) 3D ELCIRC with Δz = 5 cm, (b) CMS. The colorbar represents salinity in psu.

By calculating the vertical location of the maximum salinity gradient (ζ) from the 3D ELCIRC results, it is possible to more quantitatively compare underflow spreading modeled in the CMS and in 3D ELCIRC. Figure 4.10 contains a plot of ζ along the test basin after 5 days of simulation time, along with the CMS-modeled underflow surface η_{und}. Because the 3D ELCIRC plume plunges farther downstream than the underflow plume, ζ is not in the same vertical location as η_{und} near plunging locations for either model (10 to 20 km from the wall boundary). Farther downstream from the plunge lines (20 km from the wall), ζ and η_{und} are within centimeters of each other. This shows good agreement between the CMS and the finely resolved ELCIRC simulation. The ζ plot

shows that the 3D ELCIRC-modeled underflow is between 1 and 2 m thick, which translates to 20-40 grid cells vertically resolving the underflow.

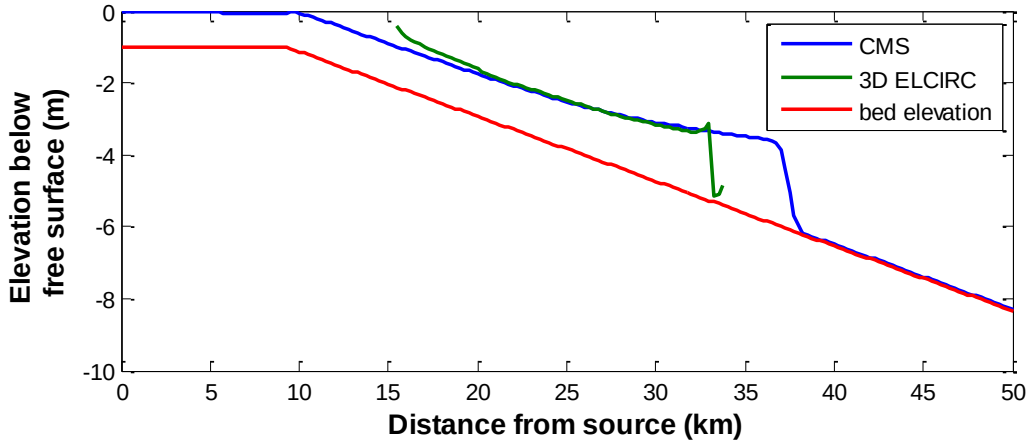

Figure 4.10: Gravity current interface location after 5 days of simulation time, modeled by the CMS (blue) and calculated as ζ in 3D ELCIRC (green).

Using the entrainment relationship established by Ellison and Turner (1959):

$$E = \frac{1}{U}\frac{\partial(Uh)}{\partial x} \qquad 4\text{-}9$$

where U is the depth-averaged along-slope velocity h is the underflow thickness and x is along-slope distance, entrainment can be measured in the underflow. Using model results from 17.5 km to 22.5 km (to avoid interferences from the unsteady gravity current head), the modeled entrainment rate is 1.23×10^{-5}. According to equation (4-2), the entrainment rate for this test case should be 1.48×10^{-5}. The 17% error between expected and modeled entrainment may in part be due to non-negligible modeled ambient currents; the underflow displaces a significant volume of fluid in this test case, producing ambient currents that are in the same direction as the underflow (discussed in Chapter 3). Ambient currents flowing with the underflow current reduce shear between the fluids, therefore reducing entrainment.

The CMS results show a less significant degree of diffusion at the gravity current front compared with 3D ELCIRC. This can be observed qualitatively in Figure 4.9, and more quantitatively in the underflow salinity anomaly plot in Figure 4.11. The salinity anomaly plot shows the fractional salinity decrease along the basin. Salinity anomalies are calculated in 3D ELCIRC by taking the mean salinity anomaly from the bed to ζ. The smooth curve of the 3D ELCIRC anomaly shows that more mixing is occurring in the ELCIRC model than in the CMS. Most of the underflow modeled in the CMS has retained at least 90% of the source salinity anomaly, and the 3D ELCIRC-modeled underflow salinity ranges between 60% and 90% of the source salinity anomaly for most of the basin length (downstream of the plungeline). This difference between models is expected, because front preservation schemes in the underflow model (discussed in Chapter 3) are designed to prevent horizontal diffusion.

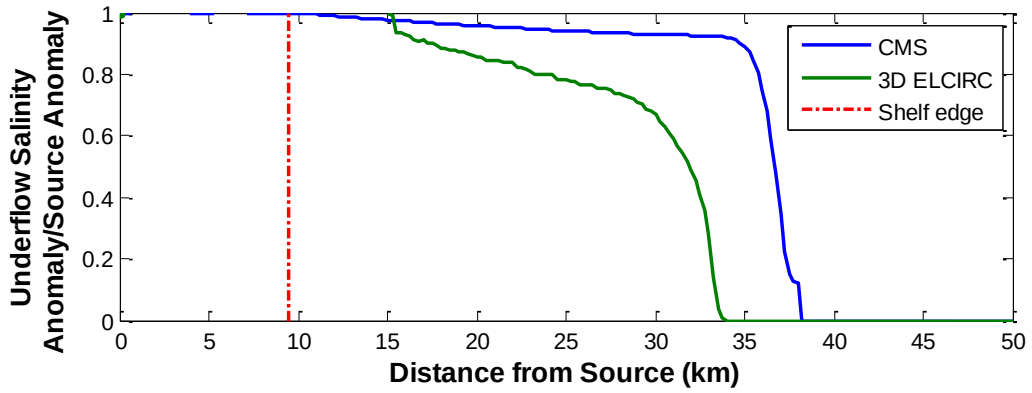

Figure 4.11: Underflow salinity anomaly with distance down-slope. Depth-averaged underflow salinity in the CMS (blue) and 3D ELCIRC (green) gravity currents after 5 days of simulation time. The "shelf edge", marked with a red dashed line, represents the location where the model domain transitions from a flat bed to a sloping bed.

4.6.2 Modeled Wind Mixing

Configuration

The wind mixing test case consists of a uniform 2D basin with a flat bottom. Dense water (40 psu) fills the bottom 3 m of the basin, and the upper 7 m is lighter, at 33 psu, such that g' = 0.005. The wind speed is 4 m/s. The dense and ambient fluids are initially quiescent, such that all motion is a result of the wind. Grid cells are 250 m long and 250 m wide. In the CMS vertical grid layers are 75 cm thick in the ambient model. CMS results are compared with 3D ELCIRC results at a vertical resolution of 15 cm, resulting in 20 grid cells in the initial dense layer. Figure 4.12 depicts the model domain used in the wind mixing test case.

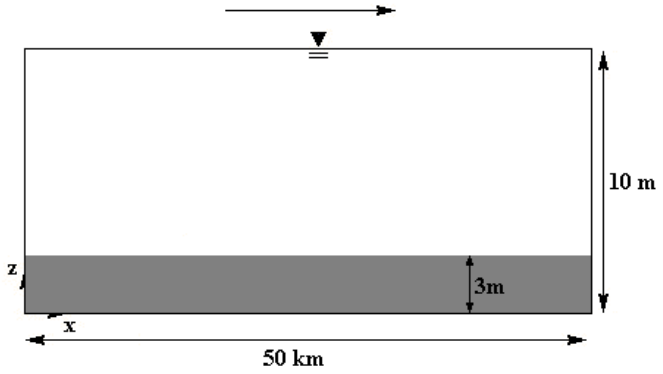

Figure 4.12: Initial conditions for the wind mixing test case. Gray shading represents initial location of dense fluid.

This basin configuration is designed to replicate wind mixed layer deepening. The wind blowing across the basin surface propagates down through the water column, and engulfs dense fluid as TKE permits. Because the dense fluid is quiescent, lighter fluid should not enter into the underflow beyond diffusive fluxes. As a constant wind on a basin will generally result in a surface seiche, we also expect to see a corresponding

internal seiche develop in the underflow-ambient fluid interface in response to hydrostatic pressure gradients.

Results

Figure 4.13 shows the salinity contours for both 3D ELCIRC simulations after 5 days of constant wind. Both the CMS (a) and the 3D ELCIRC simulation (b) result in an internal seiche, as expected. Visual inspection also demonstrates the contrast in modeled vertical density gradient between the CMS and 3D ELCIRC, though the bed salinity anomaly in 3D ELCIRC is mostly maintained; the bed salinity in the 3D ELCIRC simulation is at least 39 psu everywhere (retaining approximately 80% of the initial salinity anomaly at the bed). The bed salinity is 40 psu in the CMS model; some mixing has occurred to erode the underflow surface, but mixing has only brought dense fluid *out* of the underflow. The CMS calculates 8.7 cm of fluid mixing up into the ambient fluid during the simulation. According to scaling arguments, using equation (4-7), 8.6 cm of underflow fluid would be engulfed.

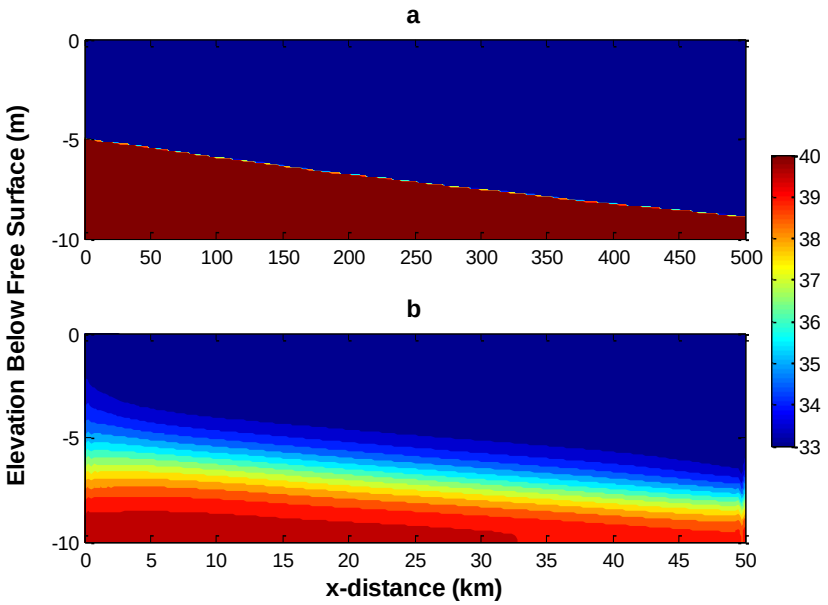

Figure 4.13: Salinity profile in the 3D model after 5 days of simulation time with vertical grid spacing of (a) 75 cm and (b) 15 cm. The colorbar represents salinity (psu).

Salinity anomaly profiles for both the CMS and 3D ELCIRC simulations are plotted in Figure 4.14. By definition, the CMS results are uniform throughout the underflow model. The vertical location of the maximum density gradient calculated from 3D ELCIRC results, δ, is also plotted for comparison. The underflow-ambient interface in the CMS model is within 25 cm of δ.

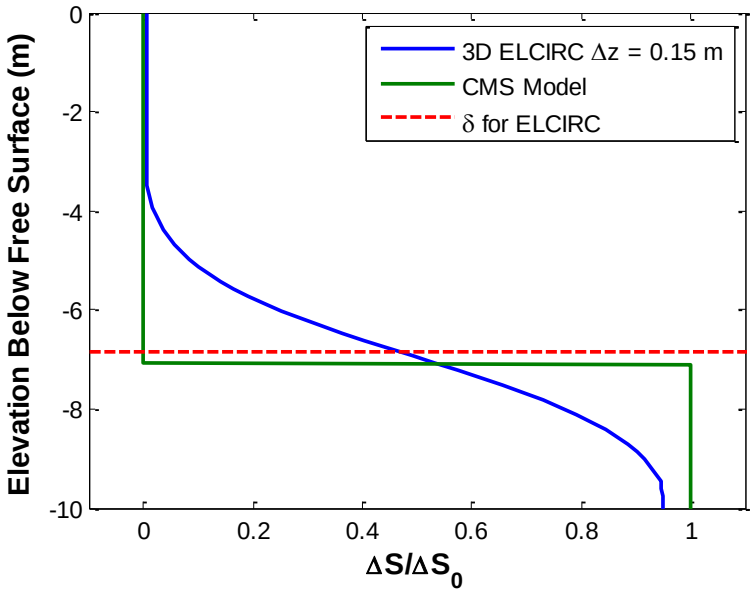

Figure 4.14: Salinity profile at basin centers after 5 days of simulation time. ΔS is the salinity anomaly from ambient, ΔS_0 is the initial salinity anomaly (7 psu). δ is the vertical location of the maximum density gradient modeled in 3D ELCIRC.

As wind mixes the water column, the anomalous salinity associated with the underflow leaves the "underflow" portion of the water column and enters the ambient fluid. Modeled wind mixing can be quantified by assessing the percentage of the initial anomalous salt (in total mass) that has left the underflow. This change in anomalous salt,

$\Delta S_{anomaly}$, after 5 days of simulation time is compared among scaling srguments, CMS results, and 3D ELCIRC in Figure 4.15. As the algorithms employed in the CMS are based on the scaling arguments, discrepancies between scaling and CMS results are due to numerical implementation errors. As can be seen from the figure, an order of magnitude more salt mixes into the ambient fluid in the 3D ELCIRC simulation than in the CMS simulation.

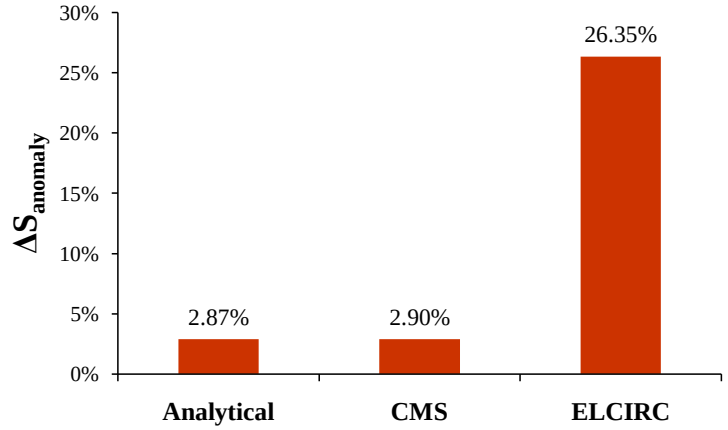

Figure 4.15: $\Delta S_{anomaly}$ after 5 days, calculated from an analytical solution, the CMS model results, and from 3D ELCIRC model results.

4.7 DISCUSSION

This chapter presents the mixing model component of the CMS, including entrainment and ambient wind mixing. The entrainment algorithms are tested by applying the CMS to a 2D test basin with a plunging underflow, and comparing results with a finely resolved ELCIRC model simulation and an expected entrainment rate. Results show that 3D ELCIRC and the CMS have good agreement in qualitative underflow shape, especially in terms of underflow thickness. However, the CMS modeled plunge line more closely matches expected values from the literature than 3D ELCIRC. Modeled entrainment agrees well with expected entrainment, though 3D

ELCIRC-modeled underflow salinities show more mixing than modeled in the CMS – this may be a result of modeled horizontal mixing in 3D ELCIRC at the gravity current front that, if physical, may need to be included in future revisions of the CMS.

Wind mixing algorithms in the CMS are evaluated by applying the CMS and 3D ELCIRC to a test case consisting of a uniform initial stratification and a spatially uniform and temporally constant wind field. Results are compared with a finely resolved 3D ELCIRC application, and also with expected analytical results. Results show that CMS modeled wind mixing is more limited than 3D ELCIRC mixing by an order of magnitude.

The concept of applying wind-mixed layer deepening energetic to a dense underflow has not been done in a dynamic model, and has not been investigated on a conceptual basis. This combination of two previously distinct conceptual mixing models, underflow models and wind mixing models, is a new contribution to coastal dynamics. Because this combination of conceptual models is a new concept, it is also not established as an appropriate scaling methodology. It is possible that wall effects from the bed influence wind mixing in a way not represented in the scaling applied here. It is also possible that the ambient turbulence from wind impacts entrainment in a way that is not represented by modeled entrainment laws applied in the CMS. Field investigations are needed to investigate turbulent mixing of the dense plumes observed in Corpus Christi Bay.

The high salinity anomaly maintained in the wind-mixing test case demonstrates the potential of the CMS in modeling bottom water isolation. Is salinity is considered an active tracer, the high salinity maintained in the underflow indicated little contact between underflow fluid and the ambient water column. Even though bulk properties resulting from the 3D ELCIRC application are similar to the CMS results, ELCIRC's

modeled bottom water salinities indicate more contact at the bed with ambient water than the CMS underflow model. This distinction of bottom water isolation becomes important when studying hypoxia, because for bottom waters in Corpus Christi Bay, contact with ambient water represents oxygen replenishment. Chapter 5 contains preliminary applications of the CMS to the Oso Bay gravity current observed in HFK11.

Chapter 5: Application to Corpus Christi Bay

5.1 INTRODUCTION

In this chapter we examine 3D ELCIRC and Coupled Model System (CMS) applications on Corpus Christi Bay. As discussed in Chapter 2, the HFK11 field study illustrates the presence of a dense underflow episodically entering Corpus Christi Bay from Oso Bay. Field data also indicates the importance of quantifying entrainment and wind mixing in order to understand hypoxia development in Corpus Christi Bay.

The simulations in this section examine two plume conditions. First, we discuss several simulations of a hypothetical lock exchange where Oso Bay is filled with dense fluid and Corpus Christi Bay is filled with less dense fluid. The lock exchange simulations examine modeled spreading and mixing as a plume migrates down-slope from Oso Bay into Corpus Christi Bay. Second, we examine the fate of a thin, finite, dense plume at the bottom of Corpus Christi Bay in the presence of a moderate wind field. The finite plume simulations examine modeled wind mixing on physical scales that are representative of observed field conditions. The simulations discussed in this chapter demonstrate potential uses of the CMS, some model limitations, and potential future work and data needs specific to Corpus Christi Bay.

5.2 MODEL GRID

All simulations presented in this chapter use the same model grid. The model grid includes the entirety of Corpus Christi Bay, Oso Bay and Nueces Bay, and extends several km into Redfish Bay and Laguna Madre to minimize open boundary condition effects in Corpus Christi Bay and the upper Laguna Madre. A portion of the Gulf of Mexico is also included in the model domain to serve a buffer for tidal boundary

conditions (though tidal forcings are not included in the test cases discussed here). The grid was generated to serve multiple modeling purposes, including an examination of the Laguna Madre outfall into Corpus Christi Bay (a dense underflow can enter Corpus Christi Bay from Laguna Madre in some cases, similar to the Oso Bay outflow; Hodges et al 2006). Where exchange flows occur, grid cells are smaller, shown by the dark blue patches in Figure 5.1. The distance between nodes varies from 15 m at the outlets of Oso Bay, Laguna Madre and in Packery Channel, to 2,000 m in the Gulf of Mexico.

The grid was generated using bathymetry obtained from NOAA (Taylor et al 2008), the Texas Water Development Board, the Texas A&M University Corpus Christi (TAMU CC) Division of Nearshore Research, and USACE (Packery Channel). Because this dissertation does not focus on circulation within Oso Bay, the bathymetry of Oso Bay is simplified to 0.2 meters deep (the mean depth of the bay). The grid was generated using the software xmgredit (Oregon Health and Science University [OHSU] 2003), and was orthogonalized by Yinglong Zhang at OHSU in order to minimize numerical errors. The resulting grid is shown in Figure 5.1.

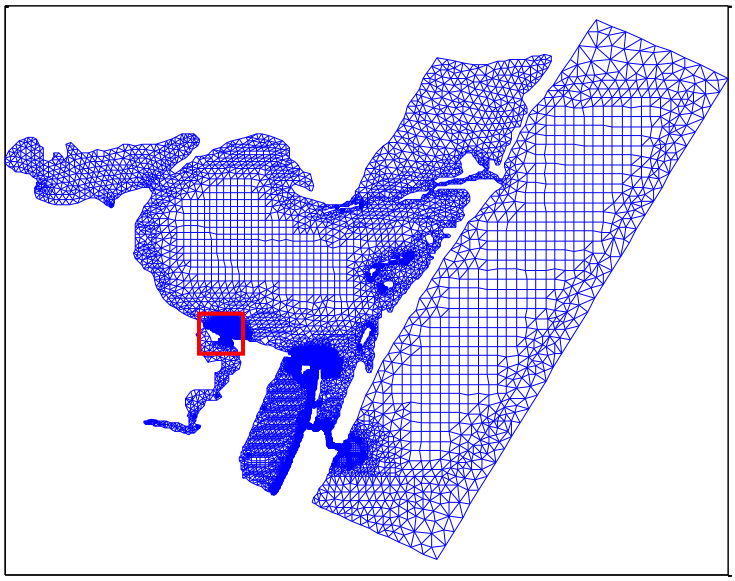

Figure 5.1: Model Grid for ELCIRC and CMS simulations. Portions of the grid with small grid spacing are dark blue. The area in the red box is magnified in Figure 5.2.

The focus of the simulations presented in this chapter is on the Oso Bay outlet into Corpus Christi Bay, which is an area of refined horizontal resolution in the model domain. Figure 5.2 shows the grid structure near the nexus of Oso Bay and Corpus Christi Bay. The sampling locations from HFK11 are included in Figure 5.2 for scale. Vertical grid spacing in the model is 10 cm for both 3D ELCIRC and the ambient model of the CMS.

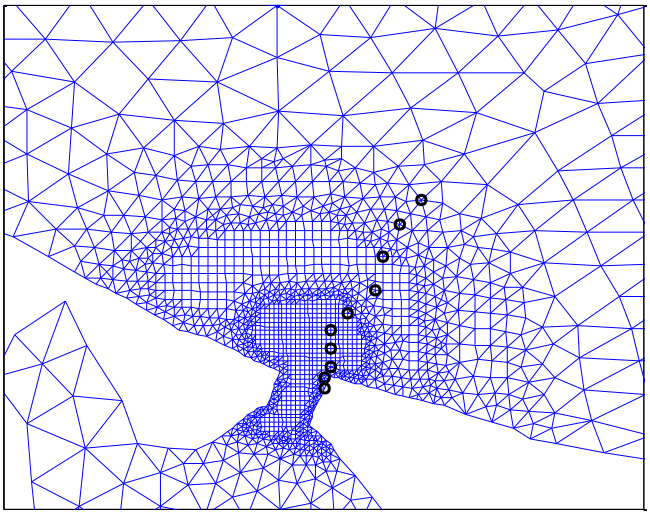

Figure 5.2: Model grid detail at the nexus of Oso Bay and Corpus Christi Bay. The field sampling locations from Hodges et al (2011) are shown in black circles for reference.

5.3 LOCK EXCHANGE SIMULATIONS

The lock exchange test cases consist of simulations at 3 different wind speeds modeled in both the CMS and 3D ECLIRC, for a total of 6 simulations. These simulations are summarized in Table 5.1.

Test Case Name	Model Used	Wind Speed (m/s)
C0	CMS	0
C4	CMS	4
C6	CMS	6
E0	3D ELCIRC	0
E4	3D ELCIRC	4
E6	3D ELCIRC	6

Table 5.1: Lock Exchange Test Cases.

The lock exchange simulations consist of an initially quiescent bay, with wind blown across the surface and Coriolis forces applied. This simplification of boundary

and initial conditions is done to evaluate CMS modeled mixing and spreading in comparison with 3D ELCIRC mixing and spreading.

5.3.1 Boundary Conditions and Initial Conditions

Open Boundaries

For all simulations, open boundary conditions are applied on the three edges of the buffer domain in the Gulf of Mexico, a northern boundary in Redfish Bay, the mouth of Nueces River in Nueces Bay, and a southern boundary in Laguna Madre. These boundaries are treated as radiation elevation boundaries with no flux. Tidal oscillations and Nueces River inflows impact Corpus Christi Bay's circulation (though wind may have a more dominant effect [Pothina 2009], and tidal oscillations during the HFK11 field study were minimal, ~10 cm), and the simplification of neglecting ambient currents neglects any drag on the underflow from tidal and river flow currents. Tidal oscillations are also thought to have a role in the pulsing effect observed in the Oso Bay outflows (HFK11); however, the time scales of simulation results that we discuss in this chapter (less than 12 hours) is less than a tidal cycle (which is longer than 24 hours in Corpus Christi Bay). Simulation times are long enough to be influenced by tidal oscillations, however, and impacts from this oscillation are not included in the model.

No flows are modeled entering Oso Bay; the bay is therefore treated as a finite supply of dense water for the simulations in this chapter. With a constant plume outflow rate into Corpus Christi Bay of 20 m^3/s (on the low end of flow rates observed in HFK11), the volume of Oso Bay would be exhausted after 27 hours. The results discussed here focus on the first 10 hours of outflow, and though modeled outflows should not exhaust Oso Bay's supply within the simulations, some tapering of flows is expected.

Wind

A constant wind from the south is applied uniformly over the model domain in all simulations. Wind speeds are applied at 0 m/s, 4 m/s and 6 m/s as shown in Table 5.1. and a no-wind test case is also examined. These wind speeds are representative of field conditions during the HFK11 field sampling event, where sustained high winds ranged from 4-6 m/s. This simplification is made to assess the modeled influence of wind on current spreading and mixing.

Coriolis and Bottom Drag

The Rossby number R, a balance of inertial and Coriolis forces, is defined as

$$R = \frac{U}{(2\Omega \sin\lambda)L} \qquad 5\text{-}1$$

where U is the characteristic velocity, L is the characteristic length scale, Ω is the earth's rotation rate (7.3×10^{-5}/s), and λ is the latitude (Kundu and Cohen 2002). Corpus Christi Bay is located at 27.7 degrees N, and HFK observations document a gravity current spreading over a distance of 2 km in 12 hours (approximately 5 cm/s). These characteristics result in an R value of 0.37, suggesting that Coriolis forces are on the same order as inertial effects. In model applications discussed in this chapter, Coriolis forces are included. The Coriolis frequency ($2\Omega\sin\lambda$) is treated as constant over the model domain, as it varies little (1%) over the modeled domain.

The bottom drag coefficient is set at a uniform constant value of C_D equal to 0.001.

Initial Conditions

The entirety of Oso Bay has an initial salinity of 50 psu. All other locations in the model domain have an initial salinity 35 psu. In the CMS simulation, at the simulation's

onset all 50 psu fluid is contained in the underflow model. All simulations are started from a quiescent bay.

5.3.2 Results

Outflows

Modeled outflows into Corpus Christi Bay from Oso Bay are plotted in Figure 5.3. In both the CMS and ELCIRC, flow into Corpus Christi Bay increases with wind speed. This result is consistent with the findings of To and Maidment (2009) that observed salinity stratification in Corpus Christi Bay is statistically related to wind speed. Outflows modeled in the CMS and ELCIRC are on the same order, though outflows are higher in the 6 m/s test case coming from ELCIRC than the CMS. Observed outflows in HFK11 were between 20 and 40 m^3/s, which is higher than all but the E6 simulation's outflow.

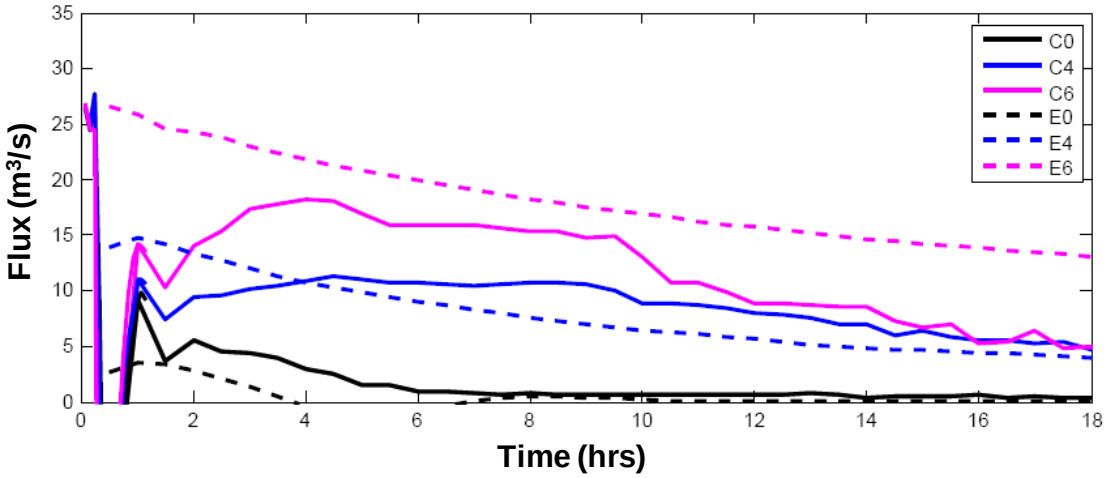

Figure 5.3: Modeled outflows from Oso Bay into Corpus Christi Bay with varied wind speeds using the CMS and ELCIRC models.

The CMS simulations are characterized by an initial surge of dense fluid exiting Oso Bay, followed by a sharp tapering off of the surge, and subsequently by a lower,

sustained flow. It is possible that this initial surge is a result of the (arguably unrealistically high) horizontal density gradient associated with the initial conditions for the lock exchange configuration. It is possible that this initial surge is not present in the ELCIRC simulations because horizontal diffusion mutes out the sharp initial density gradient.

Underflow Spreading

Figure 5.4 shows plan-view plume salinity plots of the CMS-modeled underflow after 6 hours of simulation time. Equivalent plots for 3D ELICRC results are shown in Figure 5.5. For the ELCIRC plots, modeled salinity in the bottom model layer is shown rather than calculating the depth-averaged salinity in the underflow. Depth-averaged underflow salinities are even lower in ELCIRC, and also tell us less about modeled conditions at the bed.

Plumes have larger footprints in simulations with higher wind speeds, consistent with the higher fluxes simulated at higher wind speeds (Figure 5.3). All ELCIRC simulations have smaller footprints with lower salinities than the CMS simulations at the same wind speed. This is even the case for the E6 simulation, which has a higher flux into Corpus Christi Bay than E6. The CMS simulations are all characterized by a band of high salinity fluid at the front of the plume. This band is consistent with, and is likely and artifact from, the initial surge of fluid leaving Oso Bay in all 3 CMS simulations (Figure 5.3).

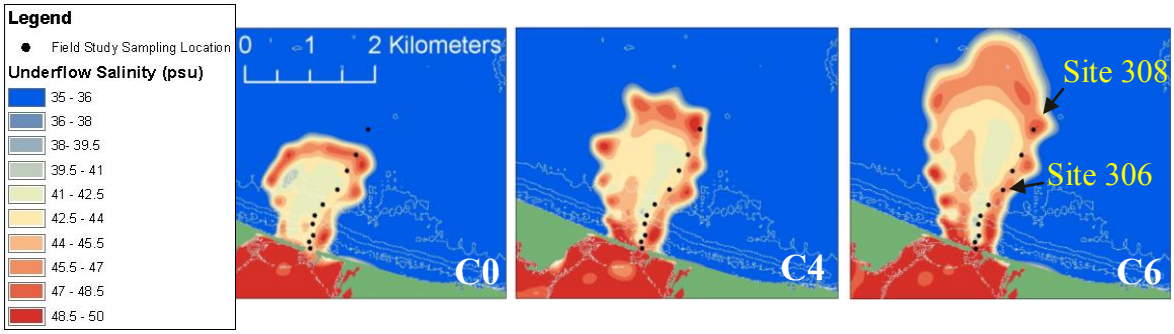

Figure 5.4: Plume salinity in CMS after 6 hours of simulation time. Black circles indicate HFK11 sampling locations. White dashed lines indicate 1 m contours.

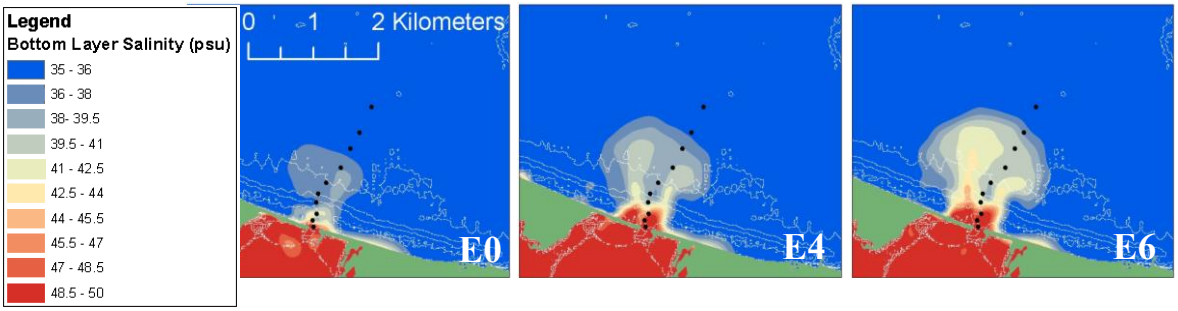

Figure 5.5: Plume salinity in 3D ELCIRC after 6 hours of simulation time Black circles indicate HFK11 sampling locations. White dashed lines indicate 1 m contours.

Vertical Salinity Profiles

Vertical salinity profiles after 10 hours of simulation time at HFK11 sampling sites 306 and 308 (see Figure 5.4 for sampling site locations) are plotted in Figure 5.6. All CMS profiles at site 306 (a) are less than 0.5 m thick, and all have an underflow salinity over 40 psu. In contrast, the ELCIRC salinity anomalies extend up to a thickness of 1 to 1.5 m above the bed, and salinities are between 35 and 40 psu. At site 308, CMS underflows are about 0.5 m thick and have salinities of approximately 45 psu, while the ELCIRC plumes are about 1 m thick, with salinity anomalies below 40 psu. The plume in E0 is only 35.1 psu, though it is also 1 m thick.

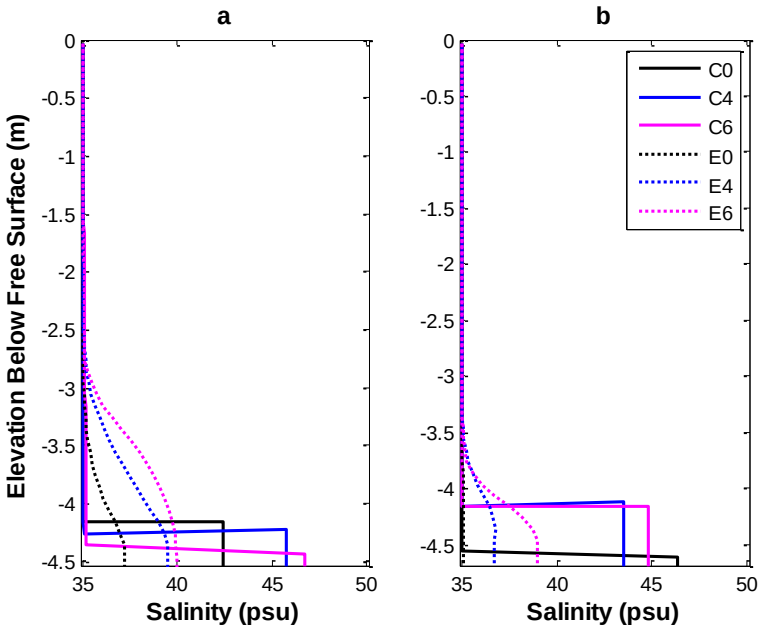

Figure 5.6: Vertical salinity profiles at HFK11 field sampling locations 306 (a) and 308 (b) after 10 hours of simulations time.

5.3.3 Discussion

The CMS model architecture clearly defines underflow plume extent and thickness, but 3D ELCIRC models the underflow as a part of a contiguous water body. For analysis purposes, we identify underflow presence in a local ELCIRC-simulated water column by a $\Delta\sigma_t$ greater than 1 (where σ_t is the density above 1,000 kg/m^3 [Fischer et al 1979], and $\Delta\sigma_t$ is the density difference between the top and bottom of the water column). Where an underflow is present, the underflow surface is identified as the elevation of the maximum vertical density gradient.

Plume Mixing

Decreases in plume salinity indicate modeled mixing of ambient (less saline) fluid into the underflow. Figure 5.7 contains a plot of underflow salinity over 10 hours of simulation time. Bottom salinity is averaged over the entire spatial extent of the

underflow plume (corresponding to the bottom model layer in ELCIRC and the underflow salinity in the CMS). Salinity is plotted as the fraction of the initial salinity anomaly ΔS_0 that remains in the underflow ($\Delta S/\Delta S_0$).

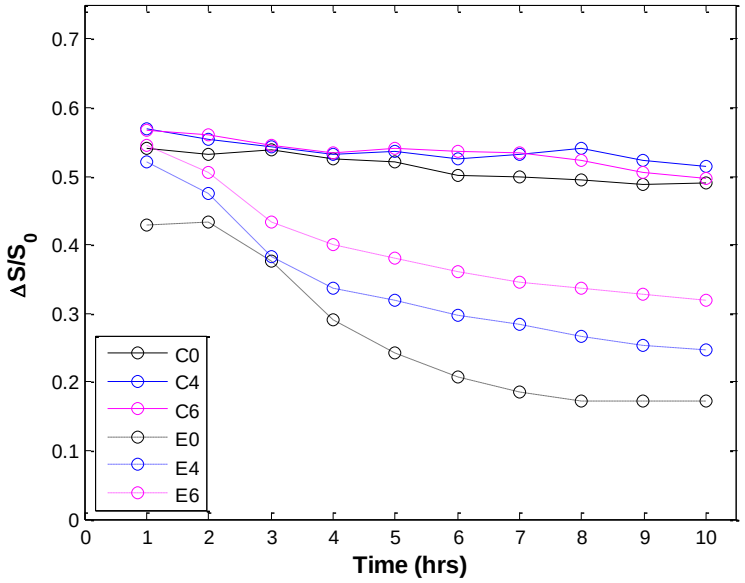

Figure 5.7: Mean underflow (for CMS) and bottom layer (for ELCIRC) salinities in the first 10 hours of simulation time.

There is little variation in the CMS-modeled underflow mixing over time. There is also little variation in underflow mixing among CMS simulations. This demonstrates the wind-independent nature of CMS-modeled underflow mixing; entrainment into the underflow is only a function of slope and underflow-ambient velocity shear.

ELCIRC-modeled $\Delta S/\Delta S_0$ is lower than in CMS results for all wind speeds, indicating more mixing in the ELCIRC model. Lower wind speeds in ELCIRC result in lower $\Delta S/\Delta S_0$. This result is counter intuitive; logically, one would expect higher wind speeds to result in more mixing. However, it is clear from Figure 5.3 that flow rates increase with wind. It is possible that inertia is smaller compared to modeled diffusion in

the ELCIRC simulations with lower wind, resulting in additional mixing in slower-moving gravity currents.

The along-slope $\Delta S/\Delta S_0$ (over the transect identified in Figure 5.8) is plotted in Figure 5.9 after 6 (a), 12 (b) and 18 (c) hours of simulation time. E0 and E4 salinities decrease nearly monotonically with distance from Oso Bay. However, all other simulations have a higher salinity anomaly at the plume front. This is consistent with data plotted in Figure 5.3, where a high flux of fluid exists Oso Bay at early timesteps in an initial "surge" of dense fluid. These spikes (which are all more than 1 km away from Oso Bay in [a], and are therefore beyond the steeply sloping portion of the transect) do not degrade in salinity significantly from 6 hours (a) to 18 hours (c), although they migrate away from Oso Bay. This retained salinity anomaly indicates that at distances greater than 1.5 km from Oso Bay, little modeled mixing occurs as fluid moves across the transect. This observation can be made for all ELCIRC and CMS simulations.

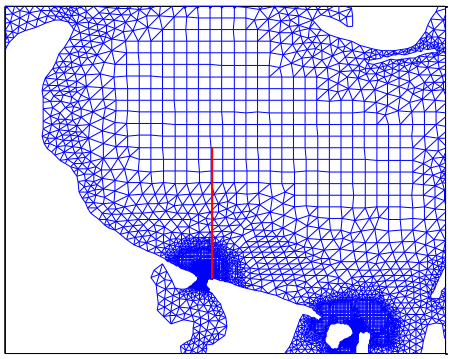

Figure 5.8: North-south line (red) of underflow transect plotted in Figure 5.9.

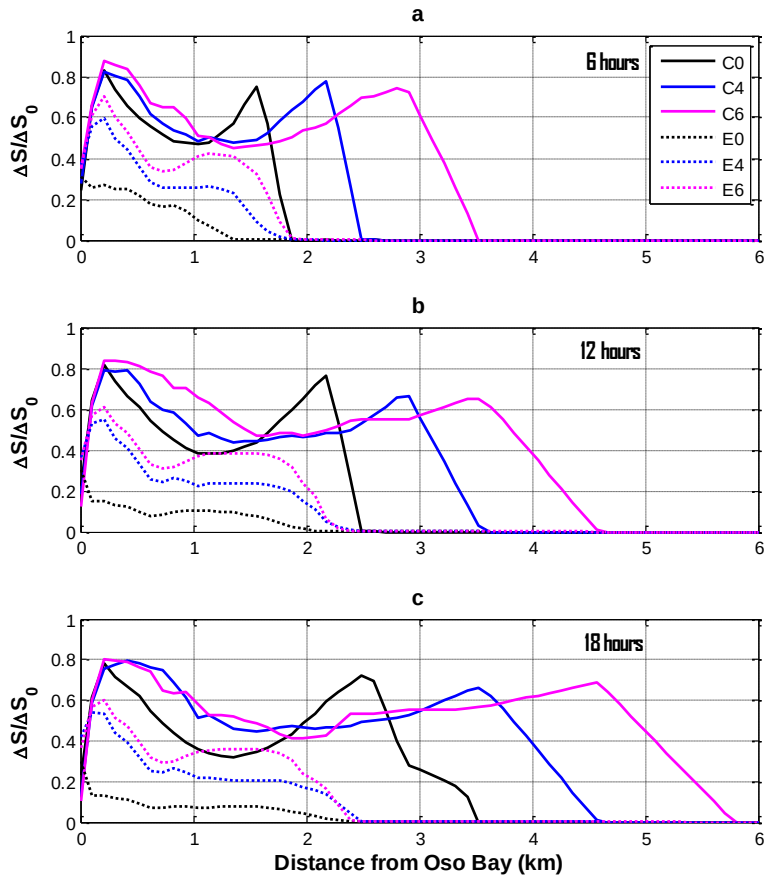

Figure 5.9: Bottom model layer (ELCIRC) and underflow (CMS) salinity anomaly along a north-south line after 6 (a), 12 (b) and 18 (c) hours of simulation time. Salinity is plotted as salinity anomaly divided by initial salinity anomaly, $\Delta S/\Delta S_0$.

Modeled mixing within the underflow (lateral diffusion and entrainment) can be estimated by examining underflow salinity as discussed above, but wind mixing can be discussed in terms of underflow loss into the ambient. In the absence of wind, the total buoyancy of the underflow should be equal to the cumulative buoyancy flux of underflow fluid into Corpus Christi Bay since the underflow initiation. Buoyancy flux is the flux of density anomaly from ambient ($\Delta\rho$). As $\Delta\rho$ in the lock exchange simulations is governed by salinity differences, we use salt flux as a proxy for buoyancy flux.

Figure 5.10 contains a plot of cumulative salt anomaly flux (in kg) into Corpus Christi Bay, compared with the total salt anomaly present in the integrated underflow volume. The overall cumulative salt anomaly contained in the underflow is increasing over time for C4, C6, E4 and E6 simulations, indicating that even though winds are high, bupyancy flux is strong enough to dominate over vertical mixing energy. The difference between cumulative buoyancy flux into the bay and total buoyancy flux in the bay is larger for ELCIRC simulations, indicating that the CMS limits the effect of wind mixing on the underflow more than ELCIRC.

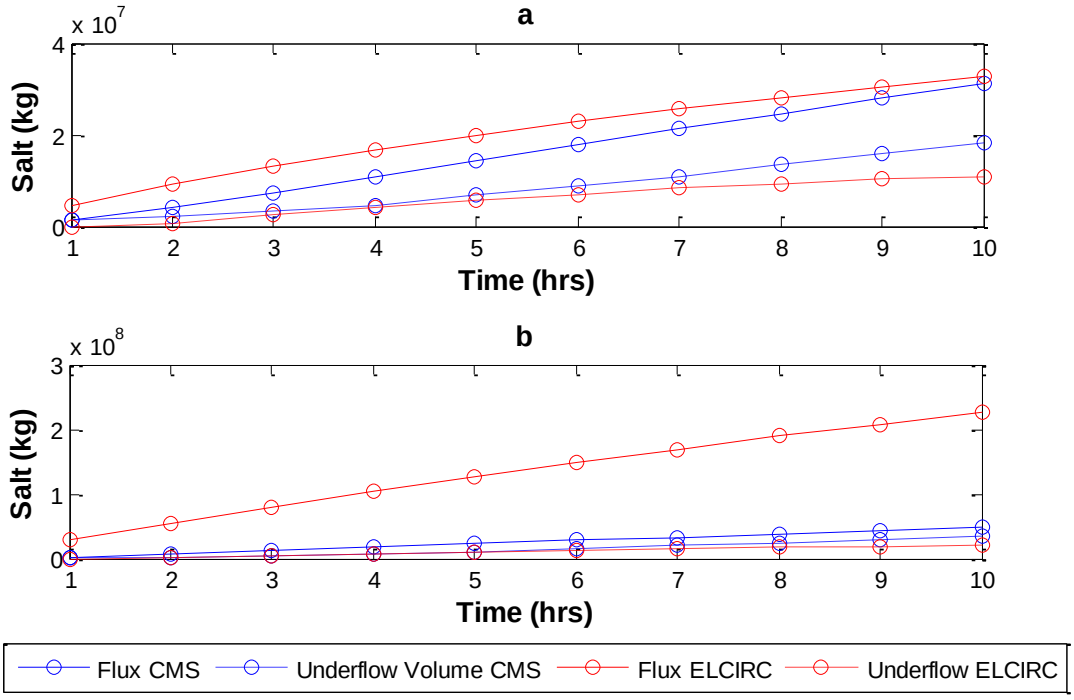

Figure 5.10: Total Salt anomaly flux into Corpus Christi Bay (solid lines) and total salt anomaly in the underflow volume (dashed lines) for (a) C4 and E4, and (b) C6 and E6.

Comparison with HFK11 Observations

Bulk characteristics. As discussed previously, observations from HFK11 indicate a dense underflow of hypersaline water exiting Oso Bay. The plume was observed to be

less than 0.5 m deep, and to contain salinities above 40 psu throughout the transect. TablesTable 5.2 andTable 5.3 list salinity (psu), thickness (H) and transport time (Δt) for field data and each simulation for both the steep transect portion (Oso Bay to Site 306) and the flatter portion (Site 306 to 308).

As can be seen in Figure 5.4, Figure 5.5 and Figure 5.6, the Modeled CMS plumes are 0.5 m thick or less, and range from 40 to 45 psu. Good agreement between CMS and field data also exists for propagation speed in the more steeply sloping portion of the transect. The underflow in simulation C6 reaches HFK11 sampling site 306 in 1.5 hours, compared with 1.3 to 2.6 hours in field observations. However, the plumes propagate faster than the plumes observed in the field in the more gradually sloping portion of the transect. The underflow reaches site 308 only 3 hours after reaching site 306, compared with about 10 hours in field observations.

It is possible that neglecting tidal influence on ambient current may reduce modeled ambient-underflow drag, which may contribute to faster modeled flow propagation. The initial conditions in the model simulations, where a sharp density gradient induces an initial surge of underflow, may also distort model propagation speeds. It is also possible, however, that the entrainment law included in the CMS is overly simplistic, and fails to accurately represent entrainment in more gradually sloping terrain.

wind speed	Field Data	C0	C4	C6	E0	E4	E6
Δt (hours)	1.5 – 2.5	1.5-2	1.5-2	1.5	5	4	3
H (m)	0.1-0.3	0.3-0.4	0.1-0.4	0.1-0.3	1.5-2	1.5-2	1.5
S (psu)	43-48	43	46	47	37	40	40

Table 5.2: Modeled and Observed underflow characteristics between Oso Bay and Site 306.

wind speed	Field Data	C0	C4	C6	E0	E4	E6
Δt (hours)	8-12	5.5-6	3.5-4	3	6	4	4
H (cm)	0.1-0.5	0.2-0.4	0.1-0.4	0.1	1.5-2	1.5-2	1-1.5
S (psu)	41-45	46	45	43	35	37	39

Table 5.3: Modeled and Observed underflow characteristics between Site 306 and Site 308.

Mixing. Analysis in HFK11 indicates that observed mixing was vertical entrainment-dominated in the first 1 km from Oso Bay, and that lateral mixing may dominate over convection at larger distances from Oso Bay. This analysis in HFK11 is consistent with the analyses in this Chapter, which indicate that modeled vertical mixing is lower at a farther distance from Oso Bay.

Model simplifications. Tidal oscillations; variable wind speed and direction (in space and time); variable stream, WWTP and power plant inflows into Oso Bay, circulation within Oso Bay; and atmospheric pressure gradients are not applied to the lock exchange simulations. Ambient currents are neglected (tidal, e.g.). The lockexchange simulations in this chapter also approximate Oso Bay as a finite water supply. During the HFK11 field sampling event, BDP flows into Oso Bay were 21 m^3/s, and measured outflows into Corpus Christi Bay were 20-50 m^3/s. The outflows modeled in the lock exchange tests is only on the order of 10-15 m^3/s (Figure 5.3). These differences all contribute to model divergence from HFK11 field conditions, and should be kept in mind when comparing field data with model results.

5.4 WIND MIXING SIMULATION

5.4.1 Model Configuration

The wind mixing simulation represents a case where plume exists at the bed of Corpus Christi Bay, but is no longer receiving a supply of dense water from Oso Bay. This scenario may occur in situations where the supply of dense water in Oso Bay has been exhausted. The simulation uses the same model grid as is used in the down-slope simulations. All open boundaries are treated with radiation boundaries (Nueces River, Oso Bay, Laguna Madre, Gulf of Mexico, Redfish Bay). A constant wind of 6 m/s due north is applied to the entire model domain (consistent with the E6 simulation from the lock exchange tests. An initial patch of dense fluid is placed in the gradually-sloping portion of Corpus Christi Bay (about 1 km north of Oso Bay). The patch is 0.25 m thick, with an initial salinity of 39 psu. These characteristics are applied uniformly across the patch as an initial condition for both the CMS and 3D simulations of the wind mixing test case. The location of the patch is shown in Figure 5.11. As for the lock-exchange simulations, the vertical grid resolution is 10 cm for both 3D ELCIRC and the ambient model in the CMS simulation. The simulation is run for 2 days.

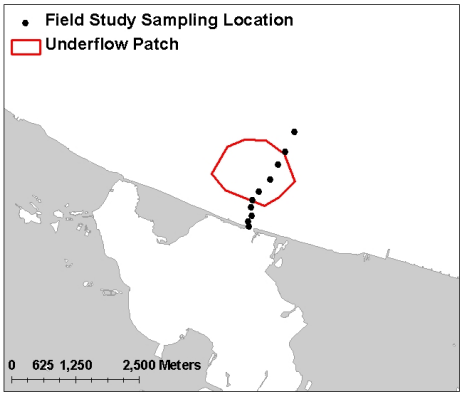

Figure 5.11: Initial patch of dense underflow fluid for the wind-mixing simulations in Corpus Christi Bay.

5.4.2 Results and Discussion

Figure 5.12 shows a comparison between the salinity in the bottom grid layer in ELCIRC and the CMS, and CMS plume thickness 1 hour after the simulation onset. In the ELCIRC simulation, the underflow has already almost completely mixed in the water column, while in the CMS much of the underflow is still approximately 20 cm thick. Using the scaling arguments presented in Chapter 2 on which the wind mixing algorithms in the CMS are based, for an average ambient fluid thickness of ~3.5 m and the wind speeds and initial plume conditions for the simulation, the underflow should be completely eroded after 30 hours. This longer time scale calculated by scaling arguments is qualitatively more consistent with field observations than the results observed in the ELCIRC model.

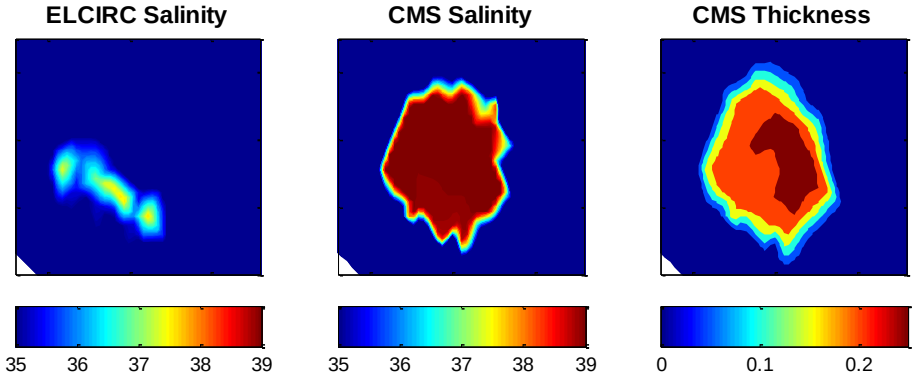

Figure 5.12: Bottom salinity (psu) in the ELCIRC and CMS underflow model simulations after 1 hour of simulation time, and CMS underflow thickness (m) after 1 hour of simulation time.

Figure 5.13 shows a comparison between the salinity in the underflow model and the bottom grid layer in ELCIRC 20 hours after the simulation onset. The dense fluid is gone in the ELCIRC model. The thickness of the plume is heavily eroded in the underflow model (down to ~10 cm), but the high salinity is maintained.

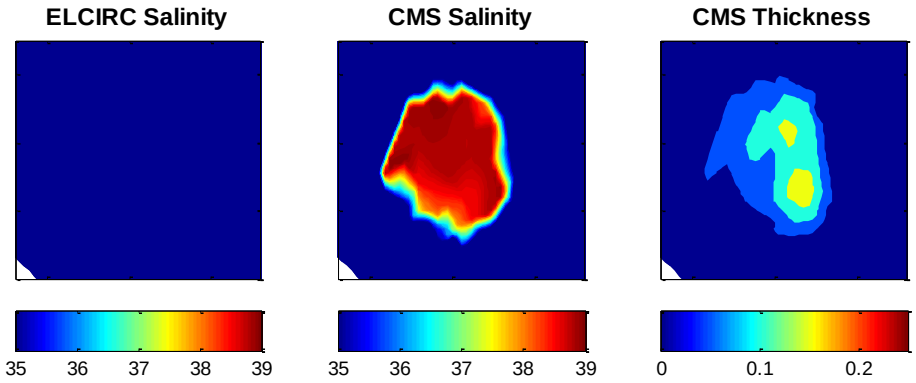

Figure 5.13: Bottom salinity (psu) in the ELCIRC and CMS underflow model simulations after 1 hour of simulation time, and CMS underflow thickness (m) after 20 hours of simulation time.

Figure 5.14 shows a comparison between the salinity in the underflow model and the bottom grid layer in ELCIRC 30 hours after the simulation onset. The dense fluid is gone in the ELCIRC model. While the salinity is still very high in the underflow model, the patch is only thicker than 5 cm in a very small area. The underflow model is essentially empty.

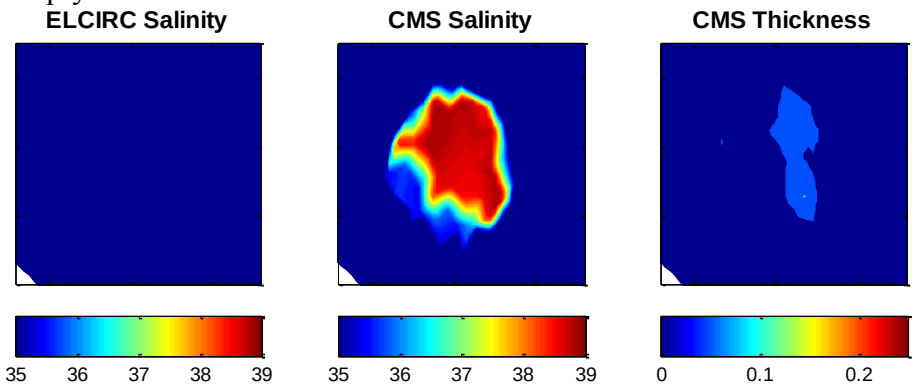

Figure 5.14: Bottom salinity (psu) in the ELCIRC and CMS underflow model simulations after 1 hour of simulation time, and CMS underflow thickness (m) after 30 hours of simulation time.

5.5 CONCLUSIONS

This chapter demonstrates an application of the Coupled Model System to a simplified version of Oso Bay's outfall into Corpus Christi Bay. It demonstrates the power of the CMS in capturing bottom-water isolation in a manner that is independent of the vertical grid used to model the rest of the bay, and it demonstrates the importance of wind in gravity current mixing and spreading in Corpus Christi Bay.

Lock exchange model simulations between Oso Bay and Corpus Christi Bay show that the CMS-modeled underflow tends to be denser, thinner and faster-moving than ELCIRC-simulated underflows. ELCIRC modeled entrainment and wind mixing are both higher than CMS-modeled mixing. In the absence of a continued source, the ELCIRC model mixes a thin underflow 25 cm thick almost completely within an hour, where scaling arguments suggest that the dense layer should persist on the order of 1 day.

Though field observations are qualitatively consistent with the thin, dense underflow modeled using the CMS, travel times are approximately two times faster in the CMS results that observations. It is possible that including a more representative set of ambient current forcings would improve CMS agreement with observations. Applying more representative initial salinities in Oso Bay and Corpus Christi Bay, may also improve model-observation agreement, and using a constant flux boundary into Oso Bay to represent high BDP flows would result in more representative fluxes into Corpus Christi Bay.

In addition to model configuration changes, model algorithm adjustments could also improve model-field agreement. As discussed in Chapter 3, the displacement model under-represents deceleration due to viscous effects at low Re. It is speculated that modeled entrainment might improve this model feature. However, the entrainment law used for the CMS is slope-dependent. The viscous flows in Corpus Christi Bay are over

a flat bed, and so it is possible that even with modeled entrainment included, the model may be under-representing turbulent viscous effects.

Wind Mixing and Dissolved Oxygen Modeling

Both the lock-exchange simulations and the wind mixing test case demonstrate the potential of the CMS to aid in DO and other water quality constituent transport studies. The high salinity maintained in the path of dense fluid throughout the CMS simulation demonstrates the ability of the CMS to reflect mixing appropriately. In the case of water quality modeling, the prevention of numerical mixing into the underflow also prevents numerical DO replenishment. This feature of DO conservation is a key aspect of understanding and modeling the relationship between the dense plume exiting Oso Bay and subsequent bottom water hypoxia.

As field data indicates the dominant role of sediment oxygen demand in hypoxia development, it would be most accurate to develop a second layer of the modeled underflow. This representation of dense plumes is consistent with observations and conceptual models such as that developed by Hogg et al (2005), where entrainment occurs mostly in an upper mixing zone, and a lower, denser layer at the bed is more isolated from the ambient fluid. A two-layer underflow representation may be necessary for representing the isolation of the bed from ambient fluid for DO modeling.

Chapter 6: Conclusions and Future Work

6.1 SUMMARY

6.1.1 Dissertation Summary

Field data and analysis imply that hypoxia in Corpus Christi Bay may be related to gravity currents that episodically enter the Bay from neighboring Oso Bay and Laguna Madre (HFK11, Islam 2011a,b,c, Montagna 2009). Representing the sharp density gradients associated with gravity currents is a well known challenge for hydrodynamic modeling (Legg et al 2009, Danabasoglu et al 2011). Most existing modeling solutions in the literature do not parameterize mixing in a way that represents wind-induced mixing, and do not have a mechanism for allowing the underflow to impact currents in the ambient fluid (Holland 2011, Dallimore et al 2003, Killworth and Edwards 1999, Beckman and Doscher 1997).

This dissertation develops a Coupled Model System (CMS) that couples a 3D application of the model ELCIRC with a specialized 2D application of ELCIRC. Coupling algorithms both exchange fluid between models, and also adjust boundary condition forcings within each model to reflect changing conditions in the other model. In this way, the CMS differs from existing field-scale gravity current models in two ways: 1) it provides a mechanism for an underflow to displace ambient fluid as it spreads, and 2) is parameterizes wind mixing of underflow fluid into the ambient water column.

Chapter 3 presents the general CMS conceptual model, governing equations and model structure. Test cases are presented that evaluate modeled underflow propagation speeds, modeled plunging and displacement. The CMS represents plunging and

displacement well, but underflow spreading at low Re does not decelerate as quickly as observed in some lab-scale experiments.

Chapter 4 presents the mixing conceptual model, governing equations and algorithms. Test cases evaluate modeled entrainment and wind mixing, and results are compared with high resolution 3D ELCIRC simulations (with at least 20 cells modeling the underflow vertically). Results compare well with 3D ELCIRC and with expected mixing rates, though propagating gravity current fronts maintain a sharper density gradient in the CMS than in 3D ELCIRC.

Chapter 5 discusses an application of the CMS to two test cases in Corpus Christi Bay. A lock-exchange test case is simulated with three different wind conditions, both in 3D ELCIRC and in the CMS. Test cases show that the CMS-modeled underflows are generally thinner, denser and faster-moving than the 3D ELCIRC-modeled plumes. The thickness and density anomaly in the CMS simulated plumes are similar to field observations; however, propagations speeds in field observations are much slower than in the CMS. It is possible that the entrainment law used in the CMS is too limiting, and may under-represent mixing at low slopes.

The differences between physical conditions and modeled boundary and initial conditions may also be the source of some discrepancy between modeled and observed underflow propagation speeds. The extreme (and arguably unrealistic) modeled initial horizontal salinity gradient between Oso Bay and Corpus Christi Bay, lack of inclusion of ambient current forcings (like wind and tide) in the model simulations, and treatment of Oso Bay as a finite underflow supply, could all influence CMS and ELCIRC model results. Incorporating these changes into the models would be a useful next step in CMS model evaluation.

6.1.2 Model Features

The model presented in this dissertation is novel in several ways: 1) it captures a dense underflow in a depth-integrated model that is completely separate from, but integrally coupled with, a larger 3D hydrodynamic model, 2) the coupled models use the same fundamental code (and therefore grid structure), which results in a smooth communication between models, 3) the structure of the model coupling is flexible, and could in theory be used to develop several coupled 2D models. Features of the CMS include:

1. The underflow model is terrain-following.
2. Full coupling enables displacement and mass transfer into (and out of) both the underflow and ambient models.
3. Mixing in both directions is calculated independently of the 3D model's vertical grid resolution.
4. Coupling structure could be easily applied to other 3D models, or be expanded to include multiple fluid layers.

Model Uses and Limitations

The model presented in this dissertation is designed to represent gravity current mixing and spreading in shallow, wind driven fluid systems. The algorithms are tailored to scaling representative of wind mixed layer deepening. Displacement algorithms allow the model to maintain an accurate mass balance for cases where an underflow's size may compete with the ambient fluid.

Although useful for a specific purpose, the CMS is not appropriate for every fluid system. The CMS does not represent gravity current slumping well, as this is a non-hydrostatic phenomenon. In deep systems where ambient displacement is not significant, the CMS may not be the most efficient use of resources, as the computational expense of

displacement may not be needed. For deep systems where wind does not penetrate to the vertical levels where an underflow is present, the mixing algorithms in the CMS may not be appropriate. The underflow model also does not initiate on its own; rather, the model user must know a priori that an underflow is present, where it is coming from and what its buoyancy flux is. Finally, the wind-mixing algorithm does not include TKE production from ambient currents (such as tides). This source of TKE is likely to be of secondary importance in Corpus Christi Bay, but may be more significant in other locations, and therefore should be included in the mixing algorithm in the future.

The CMS is also specifically designed to represent stratification in shallow basins. Therefore, the mixing algorithms may not be appropriate for deep fluid systems where the underflow may not be exposed to wind-induced turbulence.

6.1.3 Review of Research Objectives

The goal of this dissertation is to develop a methodology for quantifying wind mixing effects on gravity current spreading in shallow water. This dissertation develops and applies a conceptual and numerical methodology for quantifying wind mixing. The objectives of this dissertation, which were developed to accomplish the dissertation goal, are accomplished as follows:

Objective 1: Develop a methodology capturing dense underflow spreading within a 3D hydrodynamic model. In this dissertation, a new methodology is presented and demonstrated that builds on existing numerical underflow spreading models. The methodology developed in this dissertation represents ambient fluid displacement resulting from gravity current propagation in a water body, and this numerical methodology is applied to Corpus Christi Bay to examine lateral gravity current spreading.

Objective 2: Develop a set of numerical algorithms that represent dense underflow mixing in shallow fluid systems. This dissertation develops a new conceptual mixing model that combines traditional gravity current entrainment concepts with traditional wind mixed layer deepening conceptual models. This new mixing model is applied numerically to the gravity current model developed for this dissertation, and is used to evaluate mixing in Corpus Christi Bay.

Objective 3: Demonstrate model performance through model application on a gravity current entering Corpus Christi Bay from Oso Bay. Simulations of a lock exchange between Oso Bay and Corpus Christi Bay are used to demonstrate the performance of the CMS relative to 3D ELCIRC and field data. Though many differences are present between field conditions and simulated forcings, relatively good agreement between field observations and simulations results is achieved. Where good agreement is not achieved (propagation speed in mildly sloping areas), hypotheses are discussed that might explain differences, and may guide future work.

6.2 RESEARCH QUESTIONS

There are two main research questions that motivate this dissertation:

- Question 1: "What are the physical processes governing vertical mixing and plume spreading in Corpus Christi Bay?"
- Question 2: "How can the mass exchange and displacement associated with a gravity current in a shallow fluid system be represented in a numerical model?"

Although field observations provided some insight into the answers to these questions, this dissertation further contributes to answering these research questions.

Question 1: This dissertation develops a model that incorporates many processes into gravity current fate and transport. Although further study is still needed to determine relative strength of various forcings on gravity currents in Corpus Christi Bay, this dissertation indicates that ambient currents may be significant in determining underflow spreading rates. It also indicates that although entrainment is non-negligible in gravity currents in Corpus Christi Bay, wind mixing may ultimately determine plume mixing rates. This dissertation also demonstrates the usefulness of the CMS in representing mixing processes, as 3D ELCIRC (and most 3D numerical models) can easily over-represent vertical mixing due to both gravity current entrainment and wind mixing.

Question 2: Existing gravity current numerical models do not include ambient fluid displacement, mass balance between ambient and underflow fluids, or mixing of underflow fluid out into an ambient fluid. This dissertation presents a new numerical model that incorporates full mass balance, including fluid exchange and displacement between an underflow and the surrounding ambient fluid. Most existing field-scale numerical gravity current representations do not include this level of model coupling. The coupling method employed by the CMS is also a unique, simple method that is transferrable to other models, and also serves as a starting point for including multiple coupled models. The CMS mixing algorithm also combines the previously distinct mixing concepts of wind mixed layer deepening and underflow entrainment. The fluid exchange represented in the CMS demonstrates a conceptual and numerical implementation of displacement, mixing and mass exchange between two distinct models that reflects physics in shallow water bodies, and has not previously been developed numerically or conceptually.

6.3 CONTRIBUTIONS

The ***contributions to science and engineering*** from this dissertation include:

4. A conceptual model describing vertical gravity current mixing in the presence of significant ambient turbulence. Existing gravity current conceptual models do not include ambient turbulence and resulting underflow mixing out into the ambient fluid. The inclusion of ambient turbulence in a conceptual underflow model is a contribution to gravity current conceptual representation.
5. A new numerical method for developing coupled model systems. The inclusion is mass balance and displacement of ambient fluid on a field-scale model application is unique, and improves model representation of physical processes in shallow water bodies.
6. Developing an underflow model as a 2D representation of a 3D model is a technique that facilitates numerical issues associated with model grid coupling, and also sets the foundation for coupling multiple 2D layered models together. This technique can be applied to other numerical models.

6.4 FUTURE WORK

This research opens many questions that lead to future work for both field/lab studies, model alterations and potential future applications.

Field and Laboratory Studies

1. Additional laboratory and field investigations are needed to assess appropriateness of the scaling arguments used in the conceptual mixing model.
2. More field studies are needed to verify initial and boundary conditions for the Corpus Christi Bay model application. Conditions for which data is needed include a detailed salinity distribution within Oso Bay, salinity distribution in Corpus Christi Bay, and longer dataset of fluxes associated with outfall events for model calibration. Tides should also be included as an ambient forcing in future applications of the model to Corpus Christi Bay.

Model Alterations

1. It is possible that the entrainment algorithm under-represents entrainment at low slopes. It is possible that a Ri_b-based entrainment law would better represent underflow mixing, especially at low slopes.
2. The CMS could be improved by including algorithms allowing the underflow model to initiate when stratification is present in the 3D model; this would increase CMS flexibility and applicability.
3. The CMS wind mixing algorithm could be improved to include TKE production due to ambient currents. This would also increase the model's flexibility and applicability. The mixing algorithm should also be altered to reduce ambient TKE in proportion to underflow wind mixing.
4. The CMS could be used to evaluate dissolved oxygen transport. This model use may necessitate the addition of a second model layer at the bed to further isolate water in contact with the sediment from ambient water.

Future Model Applications

1. Additional application to Corpus Christi Bay. As additional data becomes available and additional model refinements are made, the CMS may continue to provide insight into gravity current mixing and spreading in Corpus Christi Bay.
2. Other Shallow Hypoxic Bays. Along the southeastern United States Atlantic Coast, other shallow bays experience bottom water hypoxia (Verity et al 2006, Lin et al 2006, Hagy and Murrell 2007). This coupled model system could be used to examine physical processes occurring in other shallow fluid systems.
3. Desalination Brine Disposal in Shallow Systems. As desalination becomes more integral in water resources world-wide, brine disposal becomes more of a concern. The CMS could be used to evaluate dense brine mixing in cases where pre-disposal and near-field mixing are low.

References

Altinakar, M. S., W. H. Graf and E. J. Hopfinger. (1996). Flow structure in turbidity currents. Journal of Hydraulic Research, 34(5): 713-719.

Applebaum, S., P. A. Montagna and C. Ritter. (2005). Status and trends of Dissolved Oxygen in Corpus Christi Bay, Texas, U.S.A. Environmental Monitoring and Assessment, 107: 297-311.

Atkinson, J. F. and Harleman D. R. F. (1987). Wind-mixing experiments for solar ponds. Solar Energy, 38(6): 389-403.

Baines, P. G. (2005). Mixing regimes for the flow of dense fluid down slopes into stratified environments. Journal of Fluid Mechanics, 538: 245-267.

Baptista, A. M., Y. Zhang, A. Chawla, M. Zulauf, C. Seaton, E. P. Myers III, J. Kindle, M. Wilkin, M. Burla, and P. J. Turner (2005). A cross-scale model for 3D baroclinic circulation in estuary-plume-shelf systems: II. Application to the Columbia River. Continental Shelf Research, 25(7-8): 935-972.

Beckmann, A. and Döscher, R., 1997, "A Method for Improved Representation of Dense Water Spreading over Topography in Geopotential-Coordinate Methods," Journal of Physical Oceanography, 27(4): 581-591.

Benjamin, T. B. (1968). Gravity currents and related phenomena. Journal of Fluid Mechanics, 31: 209-248.

Bernard, P. S. and Wallace, J. M. (2002). "Turbulent Flow." John Whiley and Sons, Inc., Hoboken, New Jersey.

bo Pedersen, F. (1986). "Environmental Hydraulics: Stratified Flows". Springer-Verlag, New York.

Bradford, S. F. and N. D. Katopodes. (1999). Hydrodynamics of turbid underflows I: formulation and numerical analysis. Journal of Hydraulic Engineering, 125(10): 1006-1015.

Bleninger, T. and G.H. Jirka. (2007) First Steps in Modeling and Design of Coastal Brine Discharges. International Desalination & Water Reuse Quarterly, International Desalination Association. 17(2):48-55. Aug/Sep 2007.

Choi, S. and Garcia, M. H. (2002). k-ε Turbulence Modeling of Density Currents Developing Two Dimensionally on a Slope. Journal of Hydraulic Engineering. 128(1): 55-63.

Coopersmith., E. J., B. Minsker and P. Montagna. (2011). Understanding and forecasting hypoxia using machine learning algorithms. Journal of Hydroinformatics. 13(1): 64-80.

Dallimore, C. J., Imberger, J., and Ishikawa, T. (2001). Entrainment and Turbulence in Saline Underflow in Lake Ogawara. Journal of Hydraulic Engineering. 127(11): 937-948.

Dallimore, C. J., Hodges, B. R. and Imberger, J. (2003). Coupling an underflow model to a three-dimensional hydrodynamic model. Journal of Hydraulic Engineering, 129(10): 748-757.

Danabasoglu, G., W. G. Large, and B. P. Briegleb. (2010). Climate impacts of parameterized Nordic Sea overflows. Journal of Geophysical Research. 115: C11005.

Ellison, T. H., and Turner, J. S. (1959). Turbulent entrainment in stratified flows. Journal of Fluid Mechanics, 6(3): 423–448.

J. S. Turner (1973). "Buoyancy effects in fluids." Cambridge University Press, New York.

Ezer, T. and Mellor, G. L. (2004). A generalized coordinate ocean model and a comparison of the bottom layer dynamics in terrain-following and in z-level grids. Ocean Modeling, 6: 379-403.

Felix, M. (2001). A Two-Dimensional Numerical Model for a Turbidity Current. In: McCaffery, W. D., B. C. Kneller and J. Peakall (editors), "Particulate Gravity Currents". IAS Special Publication, 31:71-81.

Furnans, J.E. (2005). Unpublished ADCP data of field experiment, Oso Bay outflow into Corpus Christi Bay, August 22-24, 2005. Texas Water Development Board.

Gale, E., C. Pattiaratchi, and R. Roshanka. 2006. Vertical mixing processes in Intermittently Closed and Open Lakes, and Lagoons, and the dissolved oxygen response. Estuarine, Coastal and Shelf Science. 69: 205-216.

Galperin, B., Kantha, L. H., Hassid, S., and Rosati, A. (1988). A Quasi-Equilibrium Turbulent Kinetic Energy Model for Geophysical Flows. Journal of Atmospheric Sciences. 45(1): 55-62.

Garcia, M. H. (1993). Hydraulic Jumps in Sediment-Driven Bottom Currents. Journal of Hydraulic Engineering. 119(10): 1094-1117.

Garcia, M. H. (1994). Depositional Turbidity Currents Laden With Poorly Sorted Sediment. Journal of Hydraulic Engineering. 120(11): 1240-1263.

Hagy, J. D., and Murrell, M. C. (2007). Susceptibility of a northern Gulf of Mexico estuary to hypoxia: An analysis using box models. Estuarine Coastal Shelf Science. 74(1-2): 239–253.

Hamrick, J. (1992). A Three-dimensional Environmental Fluid Dynamics Computer Code: Theoretical and Computational Aspects, The College of William and Mary, Virginia Institute of Marine Science, Special Report 317.

Hebbert, B., Patterson, J., Loh, I., and Imberger, J. (1979). Collie River overflow into the Wellington reservoir. J. Hydr. Div., ASCE, 105(5), 533-545.

Hodges, B. R., J. E. Furnans and P. S. Kulis. (2011). Thin-layer gravity current with Implications for Desalination Brine Disposal. Journal of Hydraulic Engineering stuaries and Coasts.

Hodges, B.R. and J.E. Furnans (2007), "Thin-layer gravity currents in a shallow estuary", Proceedings of the 18th ASCE Engineering Mechanics Division Conference, June 3-6, 2007, Blacksburg, VA. Electronic Proceedings (CD-ROM), 6 pgs.

Hodges, B. R., P. S. Kulis and C. H. David. (2006). Desalination Brine Discharge Model Final Report. Submitted to the Texas Water Development Board, Interagency Cooperation Contract 2005-001-059.

Hodges, B. R., Imberger, J., Saggio, A., and Winters, B. (2000). Modeling basin-scale internal waves in a stratified lake. Limnology and Oceanography 45(7): 1603-1620.

Hogg, A. J., M. A. Hallworth and H. E. Huppert. (2005). On gravity currents driven by constant fluxes of saline and particle-laiden fluid in the presence of a uniform flow. Journal of Fluid Mechanics, 539: 349-385.

Holland, P. R. (2011). Oscillating Dense Plumes. American Meteorological Society. 41: 1465-1483.

Huppert, H. E. and J. E. Simpson. (1980). The slumping of gravity currents. Journal of Fluid Mechanics, 99(4): 785-799.

Ilicak, M., T. M. Ogokmen and W. E. Johns. (2011). How does the Red Sea outflow water interact with Gulf of Aden Eddies? Ocean Modeling. 36(2011): 133-148.

Islam, M. S., J. S. Bonner, T. Ojo, and C. Page. (2011a). A mobile monitoring system to understand the process controlling episodic events in Corpus Christi Bay. Environmental Monitoring and Assessment. 175: 349-366.

Islam, M. S., J. S. Bonner, C. Page and T. Ojo. (2011b). Integrated real-time monitoring system to investigate the hypoxia in a shallow wind-driven bay. Environmental Monitoring and Assessment. 172: 33-50.

Islam, M. S., J. S. Bonner, and C. A. Page. (2010). A fixed Robotic Profiler System to Sense Real-Time Episodic Pulses in Corpus Christi Bay. Envrionmental Engineering Science. 27(5): 431-440.

Islam, M. S., J. S. Bonner, T. Ojo, and C. Page. (2006). Using Numerical Modeling and Direct Observation to Investigate Hypoxia in a Shallow Wind-Driven Bay. In Oceans 2006, September 18-21, Boston, MA.

Killworth, P.D. and Edwards, N. R. (1999). A turbulent bottom boundary layer code for ude in numerical ocean models. Journal of Physical Oceanography, 29(6): 1221-1238.

Kneller B. C., S. J. Bennett and W. D. McCaffery. (1999). Velocity structure, turbulence and fluid stresses in experimental gravity currents. Journal of Geophysical Research-Oceans 104 (C3): 5381-5391.

Kraus, E. B. and Turner, J. S. (1967). A one-dimensional model of the seasonal thermocline II. The general theory and its consequences. Tellus. XIX, 1: 98-105.

Kulis, P. and Hodges, B. R. (2005). Improved techniques for gravity current modeling. Proc., 2005 Mechanics and Materials Conference (McMat 2005), Luisiana State University, Baton Rouge.

Kulis, P. and Hodges, B. R. (2006). Modeling gravity currents in a shallow bay using a sigma coordinate model. Proc., 7th International Conference on Hydroscience and Engineering (ICHE-2006) Sept 10-13, Philadelphia, USA.

Kundu, P. K. and I. M. Cohen. (2002). "Fluid Mechanics". 2nd Edition, Academinc Press, New York.

Legg, S., B. Briegleb, Y. Chang, E. P. Chassignet, G. Danabasoglu, T. Ezer, A. L. Gordon, S. Griffies, R. Hallberg, L. Jackson, W. Large, T. M. Ozgokmen, H. Peters, J. Price, U. Riemenschneider, W. Wu, X. Xu, and J. Yang. (2009). Improving oceanic overflow representation in climate models. The Gravity Current Entrainment Process Team. American Meteorological Society. May 2009: 657-670.

Legg, S., R. W. Hallberg and J. B. Girton. (2006). Comparison of entrainment in overflows simulated by z-coordinate, isopycnal and non-hydrostatic models. Ocean Modelling, 11:69-97.

Lin, J., Xie, L., Pietrafesa, L. J., Shen, J., Mallin, M. A., and Durako, M. J. (2006). "Dissolved oxygen stratification in two micro-tidal partially mixed estuaries." Estuarine Coastal Shelf Sci., 70(3), 423–437.

Matsumoto, J., W. L. Longley and D. A. Brock. Effects of Structures and Practices on the Circulation and Salinity Patterns of the Corpus Christi Bay National Estuary Program Area, Texas. Corpus Christi Bay National Estuary Program Report Number CCBNEP-19. A Texas Natural Resources Conservation Commission Publication.

Mellor, G. L., and Yamada, T. (1982). Development of a Turbulence Closure Model for Geophysical Fluid Problems. Rev. Geophys. Space. Phys. 20(4): 851-875.

Melrose, D. C., Oviatt, C. A., and Berman, M. S. (2007). "Hypoxic events in Narragansett Bay, Rhode Island, during the summer of 2001." Estuaries Coasts, 30(1), 47–53.

Minsker, B. E. Coopersmith, B. Hodges, D. Maidment, J. Bonner, P. Montagna (2007) "An Environmental Information System for Hypoxia in Corpus Christi Bay: A WATERS Network Testbed." American Geophysical Union Fall Meeting, December 10-14, 2007, San Francisco, CA.

Monismith, S. G. and D. A. Fong. (1996). A simple model of mixing in stratified tidal flows. Journal of Geophysical Research, 101(C12): 28583-28595.

Montagna, P. A. and C. Ritter. (2006). Direct and indirect effects of Hypoxia on benthos in Corpus Christi Bay in Texas, U.S.A. Journal of Experimental Marine Biology and Ecology. 330: 119-131.

Montagna, P. A. and J. Froeschke. (2009). Long-term biological effects of coastal hypoxia on Corpus Christi Bay, Texas, USA. Journal of Experimental Marine Biology and Ecology. 381: S21-S30.

Montagna, P. A., and Kalke, R. D. (1992). "The effect of fresh-water inflow on microfaunal and macrofaunal populations in the Guadalupe and Nueces Estuaries, Texas." Estuaries, 15(3), 307–326.

Nielsen , M. H., B. Ramussen and F. Gertz. (2005). A simple model for water level and stratification in Ringkobing Fjord, a shallow, artificial estuary. Estuarine, Coastal and Shelf Science. 62(2005): 235-248.

Ojo, T. O., J. S. Bonner, and C. Page. (2006). Observation of shear-augmented diffusion processes and evaluation of effective diffusivity from current measurements in Corpus Christi Bay. Continental Shelf Research. 26(2006): 788-803.

Ozgokmen T. M., W. E. Johns, H. Peters, and S. Matt. (2003). Turbulent Mixing in the Red Sea Outflow Plume from a High-Resolution Nonhydrostatic Model. Journal of Physical Oceanography. 33:1846-1869.

Parker, G., Garcia, M., Fukushima, Y., and Yu, W. (1987). Experiments on turbidity currents over an erodible bed. J. Hydr. Res., 25(1), 123– 147.

Peters, T. and D. Pinto. (2008). Seawater intake and pre-treatment/brine discharge – environmental issues. Desalination. 221: 576-584.

Pond, G. and Pickard, G. (1983). "Introductory Dynamical Oceanography, 2nd Edition". Pergamon Press, New York. pp. 310-311.

Pothina, D. (2009). A multimodel approach to modeling bay circulation in shallow bay - ship channel systems (Doctoral Dissertation).

Purnama A. and H. H. Al-Barwani. (2006). Sreading of brine waste discharges into the Gulf of Oman. Desalination. 195: 26-31.

Rabalais, N.N. 2011. Twelfth Annual Roger Revelle Commemorative Lecture: Troubled waters of the Gulf of Mexico. Oceanography 24(2):200–211, doi: 10.5670/oceanog.2011.44.

Ritter, C. and Montagna, P. A. (1999). Seasonal Hypoxia and Models of Benthic Response in a Texas Bay. Estuaries, 22(1): 7-20.

Roache, P. J., (2002). Code verification by the method of manufactured solutions. Journal of Fluids Engineering, 124(1):4-10.

Roe, P. L. (1981). "Approximate Riemann solvers, parameter vectors, and difference schemes." Journal of Computational Physics, 43, 357-372.

Rottman, F. R. and J. E. Simpson. (1983). Gravity currents produced by instantaneous releases of a heavy fluid in a rectangular channel. Journal of Fluid Mechanics, 135: 95-110.

Sherman, F. S., Imberger, J., and Corcos, G. M. (1978). Turbulence and mixing in stably stratified waters. Annual Review of Fluid Mechanics, 10, 267– 288.

Spigel, R. H., Imberger, J. and Rayner, K.N. (1986). Modeling the diurnal mixed layer. Limnology and Oceanography. 31(3): 533-556.

Srinivasan, S. (2007). Stochastiv Methods for Reservoir Modeling, lecture notes. Texas Parks and Wildlife Department (TPWD), 2002. Marin Resource Monitoring Opertations Manual. Available on request from TPWD.

Tanny, J., Chai, A., and Kit, E. (1995). On the law of turbulent entrainment across a density interface. Fluid Dynamics Research. 15: 69-74.

Texas Water Development Board (TWDB). (2007). Final Draft State Water Plan. Available: http://www.twdb.state.tx.us/publications/reports/State_Water_Plan/2007/2007%20final%20draft%20SWP/Final_Draft_2007SWP1.htm

To, S. C. and D. R. Maidment. (2009). Hypoxia modeling in Corpus Christi Bay using a hydrologic information system. Center for Research in Water Resources, Bureau of Engineering Research. The University of Texas at Austin. CRWR Online Report 09-02.

Tseng, Y. and Dietrich, D. E. (2006). Entrainment and Transport in Idealized Three-Dimensional Gravity Current Simulation. Journal of Atmospheric and Oceanic Technology. 23: 1249-1269.

Verity, P. G., Alber, M., and Bricker, S. B. (2006). "Development of hypoxia in well-mixed subtropical estuaries in the southeastern USA." Estuaries Coasts, 29(4), 665–673.

Voutchkov, N. (2005). Alternatives for ocean discharge of seawater desalination plant concentrate. WateReuse Association, Denver, CO 2005.

Voutchkov, N. (2011). Overview of seawater concentrate disposal alternatives. Desalination. 273: 205-219.

Ward, G. H. (1997). Processes and Trends of Circulation Within the Corpus Christi Bay National Estuary Program Study Area, Corpus Christi Bay National Estuary Program Report Number CCBNEP-21. A Texas Natural Resources Conservation Commission Publication.

Wells, M. G., and Wettlaufer, J. S. (2005). "Two-dimensional density currents in a confined basin." Geophys. Astrophys. Fluid Dyn., 99(3), 199–218.

Winton M., Hallberg R., Gnanadesikan A., 1998, "Simulation of density-driven frictional downslope flow in z-coordinate ocean models," Journal of Physical Oceanography. 28(11): 2163-2174.

Zhang, Y. L., A. M. Baptista and E. P. Myers III. (2004). A cross-scale model for 3D baroclinic circulation in estuary-plume-shelf systems: I. Formulation and skill assessment. Continental Shelf research. 24(18): 2187-2214.